An Experimental Investigation into the Joining of Bulk High Temperature Superconductors

Marlini Pillay

This thesis was submitted to the University of KwaZulu Natal in fulfillment of the requirements for a Master's degree in Electronic Engineering.

Declaration

I hereby declare that this thesis is a result of my own original work and contains nothing that is a result of collaboration, except where specifically stated in the text. The work included in this thesis has not been submitted in part or whole to any university for a degree, diploma or other qualification.

Marlini Pillay

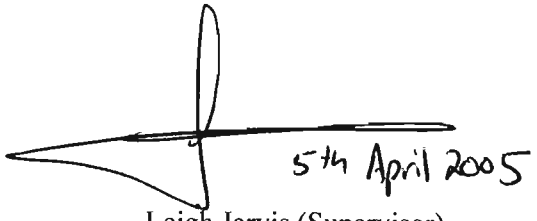

Leigh Jarvis (Supervisor)

To my loving parents and my Master Bhagawan Sri Sathya Sai Baba

Acknowledgements

I would like to express my thanks to the following people who assisted during this research:

- Mr Leigh Jarvis, for his supervision.
- The late Dr Fiona Graham from the Electron Microscope Department, for the many hours that she sacrificed in helping me obtain the SEM images. May God bless her soul.
- Mr Roos, Mr Swanepoel and Mr Basil, for their assistance in the construction of the experimental apparatus.
- Other technical staff at the University of Kwazulu Natal, for their assistance in making this study possible.
- Aroon Sukhnandan, for his friendship, support and help. I appreciate all his effort to make this a success.
- My parents, for their constant love and support.

Abstract

Current melt texturing processes can only produce high-quality High Temperature Superconducting (HTSC) domains of a few centimetres in size. Increasing the size of the domain by a joining technique is investigated.

The parent HTSC melt textured domains of $YBa_2Cu_3O_{7-\delta}$ (Y123), were used in this research to investigate the joining technique. The solder powders used to form the seam were HTSC $YbBa_2Cu_3O_{7-\delta}$ (Yb123), which has a peritectic temperature of approximately 925 °C, $Yb_2Ba_1Cu_1O_{7-\delta}$ (Yb211), Silver Oxide (Ag_2O) and Y123. A total of 8 different superconducting 'solders' were manufactured using these powders. Microstructural analyses using a scanning electron microscope (SEM) and an optical microscope were conducted on each sample. It was found that mechanisms occurring during the growth of the seam affect the performance of the join. During the growth, three interfaces are formed. The interface between the parent and the growth front produced an excellent join whereas most of the microstructural defects were present at the intersection of the two growth fronts also known as the impingement boundary.

The effect of the addition of Yb211 and silver particles to the join were investigated. It was found that although Yb211 particles improve the flux pinning and viscosity of the solder and the silver improves the intergranular critical current density (J_c) [1], they also reduce the effective cross-sectional area of the joined sample. Thus, the amount of non-superconducting particles added needs to be optimised.

Transport measurements were taken to evaluate the current carrying capacity of each sample. It was found that Sample 2-A (Yb123 + 5%Ag_2O) has the highest J_c of approximately 142 A/cm^2 at 80 K while Sample 3-A (Y123 + 5%Ag_2O) has the poorest J_c of about 37 A/cm^2 at 80 K. Resistivity vs. Temperature graphs show that all joined samples were superconducting implying that the joining process was successful in establishing a superconducting join. Magnetic field maps of the parent and joined samples were captured using a Hall Probe. It was found that the joined sample could trap almost 95 % of the field that could be trapped by the parent. From these results, it was concluded that joining HTSC bulk pieces is possible using an external 'soldering' agent.

Contents

Appendices

List of Figures

List of Tables

Nomenclature

HTSC	HIGH TEMPERATURE SUPERCONDUCTING
HTS	HIGH TEMPERATURE SUPERCONDUCTORS
T_C	CRITICAL TEMPERATURE
H_C	CRITICAL MAGNETIC FIELD
J_C	CRITICAL CURRENT DENSITY
Y123	$YBa_2Cu_3O_{7-\delta}$
Y211	Y_2BaCuO_5
Yb123	$YbBa_2Cu_3O_{7-\delta}$
Yb211	Yb_2BaCuO_5
SEM	SCANNING ELECTRON MICROSCOPE
RSFQ	RAPID SINGLE FLUX QUANTUM
RABiTS	ROLLED ASSISTED BIAXILLY TEXTURED SUBSTRATES
IBAD	ION BEAM ASSISTED DEPOSITION
dc	DIRECT CURRENT

Chapter 1

Introduction

1.1 History of Superconductivity

In 1911, Heike Kamerlingh Onnes discovered that the dc resistivity of mercury dropped to absolute zero below a temperature of 4 K [2]. Many other metallic elements were found to exhibit this phenomenon called superconductivity. Interestingly, good room temperature conductors such as gold, silver and copper do not superconduct. As time progressed, many characteristics of these superconducting materials were discovered. In 1933, Meissner and Ochsenfeld [3] noticed that a superconductor acts like a perfect diamagnet when cooled below its critical temperature T_c in the presence of a weak magnetic field. This effect is called the Meissner Effect. Several theories and models were proposed to explain how and why this phenomenon of superconductivity occurs. Some of these important theories are:

- London Model (1934) [4] – explains the Meissner effect and predicts the magnetic penetration depth (λ)
- Ginzburg-Landau Theory (1950) [5] – quantum phenomenological theory
- Bardeen Cooper Schrieffer (BCS) Theory (1957) [6] – discovered by John Bardeen, Leon Cooper and Robert Schrieffer. This microscopic theory explains the formation of the Cooper pairs and how zero resistivity is attainable in the superconductive state. In its current form, this theory cannot explain the phenomenon of superconductivity in HTSC materials

The first superconductors, so called conventional superconductors, all have critical temperature (T_c) less than 25 K and thus require liquid helium which has a boiling point of 4.2 K, to cool them below its critical temperature. Initially, these superconductors were not used in many applications due to the complexity and high costs associated with keeping them at a temperature below their critical point.

In 1986, High Temperature Superconductors (HTS) were discovered in Ba-La-Cu-O systems by Alex Muller and Georg Bednorz [7]. This ignited a new flame in superconductivity research. When Yttrium was substituted for Lanthanum in 1987, a superconductor $YBa_2Cu_3O_{7-\delta}$ (Y123) with a T_c of approximately 92 K was discovered [8]. This 'new' superconducting material could superconduct at much higher temperatures and thus liquid nitrogen could be used to cool Y123 to a temperature below their critical point. Liquid nitrogen boils at 77 K and is much cheaper than liquid helium and the cryogenic systems are also much less complex than those designed for liquid helium. This greatly improved the potential use of superconductors in many applications. Some of these applications include magnetic levitation, energy storage, magnetic resonance imaging and superconducting conductors/cables.

Figure 1.1 plots the dates of discovery of different superconducting compounds as well as their critical temperatures.

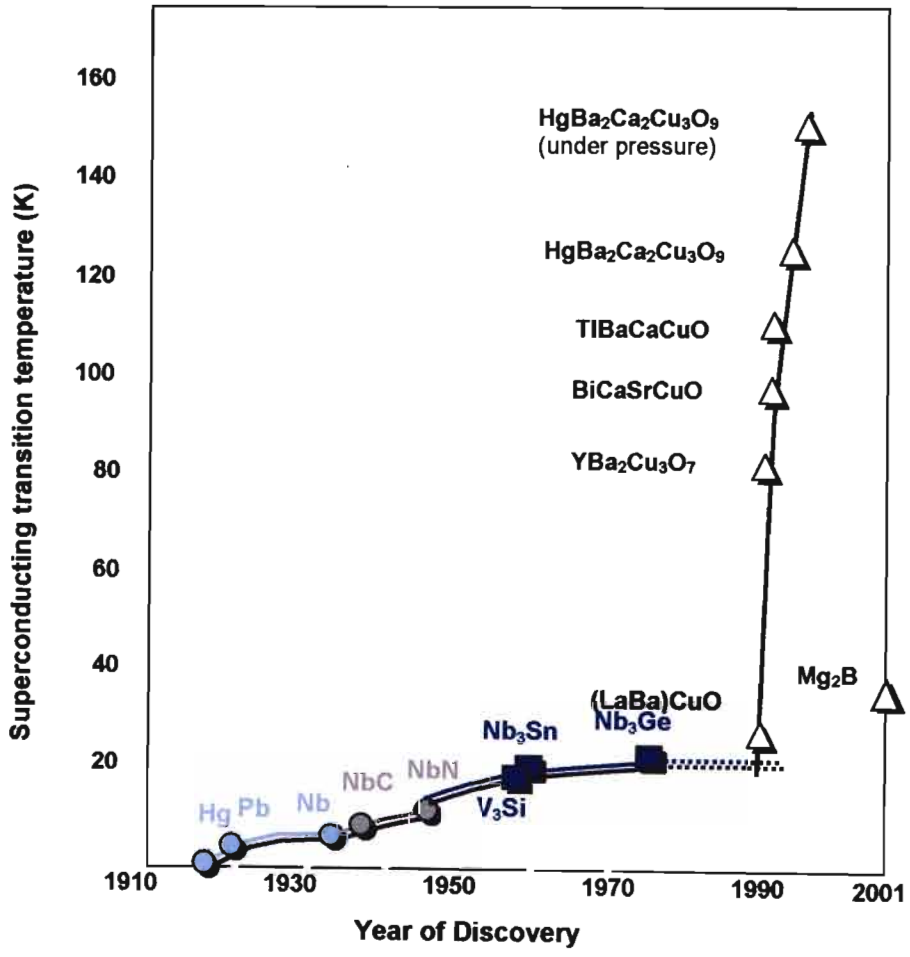

Figure 1.1: **Graph showing discovery date of different superconductors and their T_c.**

1.2 Drawbacks of High Temperature Superconductors

HTS are ceramic materials that are relatively very hard and brittle. They are also highly anisotropic and that means the degree of superconductivity differs in each plane of the material. Melt texturing processes has helped overcome this constraint by producing samples that are highly aligned [9].

The size of the superconducting bearing can greatly enhance the performance of certain applications for example flywheel storage systems. The problem experienced in developing HTSC bearings is that current melt texturing processes can only produce samples of a maximum diameter of approximately 100 mm [10]. Any attempt to increase the size results in a sample with a large amount of crystal defects such as twinning and weak link boundaries causing poor transport properties.

1.3 Current Research

Some researchers have concentrated their efforts on trying to improve the texturing process to get samples of relatively large diameters while others looked into developing techniques of joining small textured pieces to create larger samples.

Many joining techniques have been developed. One such method uses a superconducting solder made up of superconducting powders that have lower peritectic temperatures than the parent material [11-21]. Another technique utilises the liquid trapped in the platelet boundaries of the parent material as the bonding substance [22-25]. Other researchers have joined samples by multiseed texturing [26]. The common aim of these techniques is to produce a superconducting seam that has mechanical, microstructural and transport properties similar to that of the parent material.

All the techniques mentioned above have produced promising results. However, it was found that although the joined sample is superconducting a reduction in the superconducting properties such as critical current density (J_c) is experienced.

1.4 Objective of Thesis

In this thesis, a method of using superconducting powders to join the samples was investigated. Different solders were developed to identify their effects on the quality of the join. $YBa_2Cu_3O_{7-\delta}$ (Y123) was used as the parent material while $YbBa_2Cu_3O_{7-\delta}$ (Yb123), $Yb_2Ba_1Cu_1O_{7-\delta}$ (Yb211), $YBa_2Cu_3O_{7-\delta}$ (Y123) and Silver Oxide (Ag_2O) powders were used to manufacture 8 different types of solders.

Microstructural analyses were conducted using a Scanning Electron Microscope (SEM) and an optical microscope. Magnetic measurements were carried out using a Hall probe. HTS have relatively high critical current densities ($J_c > 10^4$ Acm^{-2}). Thus, one requires a current source that can supply very high currents for relatively large samples to measure J_c. A current source of this nature was not available thus the area of the joined samples had to be reduced considerably to measure the critical current.

Chapter 2

Theory of Superconductivity

2.1 Overview

This chapter briefly discusses theory associated with the phenomenon of superconductivity. The characteristic properties such as zero resistivity and zero magnetic flux density are explained. The BCS theory focuses on 'conventional' superconductors and details of this theory are presented.

Superconductors are broadly divided into two categories which are Type I and Type II. Characteristics of each category are discussed. The phenomenon of superconductivity occurs when current density (J), magnetic field (H) and temperature (T) are less than some critical values. These are called critical parameters and are discussed in this chapter.

Attributes of Y123 are discussed in Section 2.4. The Critical State Model (CSM) derived by C P Bean is presented. Concepts such as irreversibility and the weak link effect are also explained.

2.2 Characteristic Properties

Superconductors have two very distinct features i.e.

- zero resistivity and
- zero magnetic flux density within the superconductor (diamagnetic effect)

2.2.1 Zero Resistivity

Once a superconductor is cooled below its critical temperature (T_c), its resistivity reduces to zero at lower temperatures as shown in Figure 2.1.

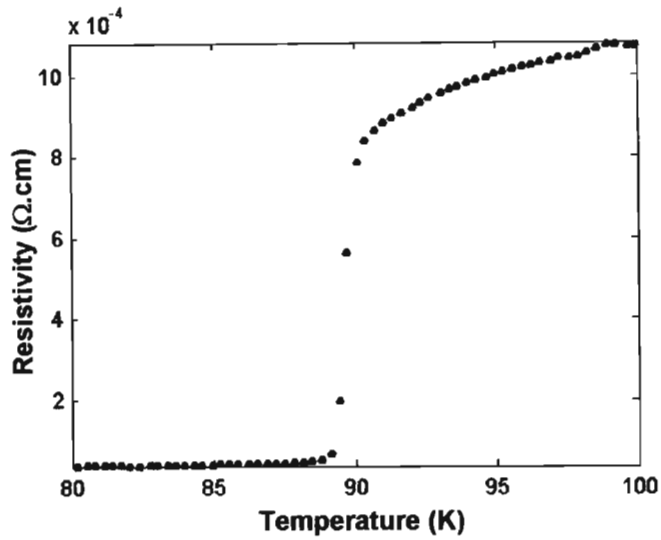

Figure 2.1: Graph of Resistance vs Temperature of a Y123 superconductor.

To explain basically why superconductors have zero resistivity, one must first consider how resistivity is caused in normal materials. In metals, there exists a set of delocalised electrons that are current carriers in the material. These free electrons are obtained when metal atoms dislodge their electrons to form a lattice that consists of positively charged ions as indicated in Figure 2.2.

This system is in a state of equilibrium since the total charge is balanced, thus making the metal electrically neutral. These ions are not stationary and vibrate around their equilibrium positions. These vibrations, which are called phonons, are caused by thermal energy in the system. Application of an electric field to the system results in acceleration of the free electrons.

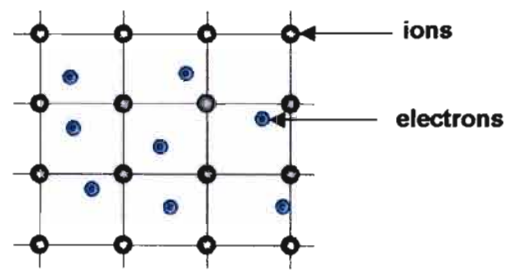

Figure 2.2: Metal lattice with delocalised electrons [27].

Scattering of electrons occurs due to the presence of impurities and dislocations which affect the ideal periodic potential. In superconductors, a very different phenomenon occurs as compared to the one just explained. The charge carriers are Cooper pairs i.e. coupled electrons, which are formed by electron-phonon interactions. As an electron moves through the lattice, it forms a distortion within the lattice as seen in Figure 2.3 (a). This creates a greater local positive charge density around the electron and thus attracts another electron within the material (Figure 2.3(b)).

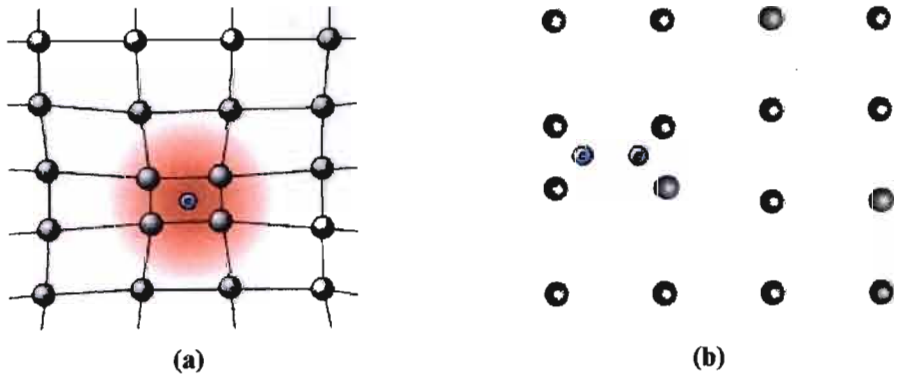

(a) (b)

Figure 2.3: **(a) Distortion of the lattice caused by an electron passing through it [27].**
(b) Formation of Cooper pairs due to lattice distortion [27].

These electrons that have opposite momentum and spin become weakly coupled forming a Cooper pair. This Cooper pair has a net momentum of zero. Thus from De Broglie's relation

$$P_F = \frac{h}{\lambda} \tag{2.1}$$

where P_F is the Fermi momentum, h is Planck's constant and λ is wavelength, one can see that the wave formed by these pairs has a wavelength of infinity. A wave is diffused when there is a "change in the number of scatter centres in a volume, the size of the wavelength" [28] thus, from this it can be seen that these Cooper pairs cannot be scattered and hence no resistivity is present in superconductors.

Since a Cooper pair has two electrons, it possesses double the charge i.e. 2e of a free electron. Electrons are fermions and are governed by Fermi-Dirac characteristics as well as Pauli's exclusion principle. Pauli's exclusion principle states that only one electron can occupy a given quantum state. Cooper pairs on the other hand are quasi bosons and obey

Bose-Einstein statistics which state that all Cooper pairs can occupy the same quantum state. This implies that all Cooper pairs can be described by a single wave function.

2.2.2 Zero Magnetic Flux Density

Figure 2.4 shows the difference between a perfect conductor and a superconductor in the presence of a magnetic field.

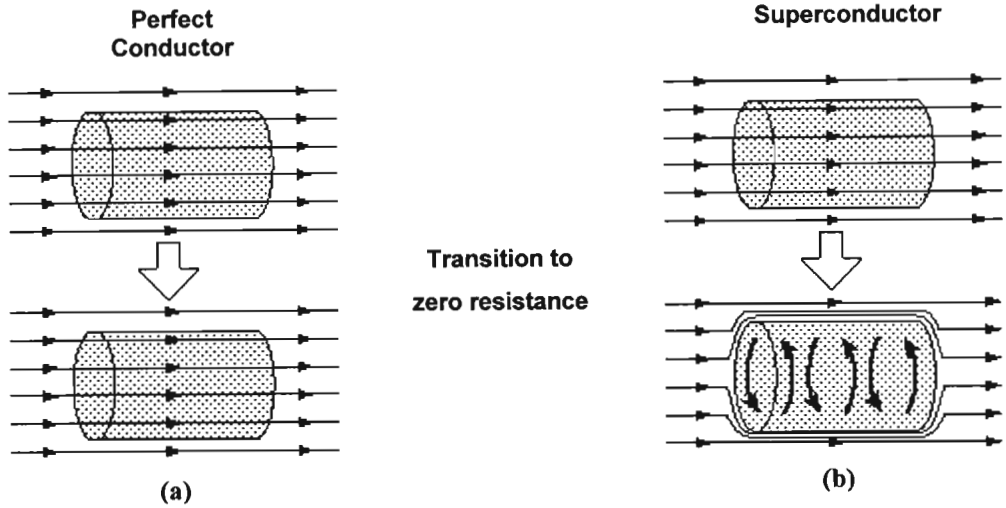

Figure 2.4: (a) Behaviour of a perfect conductor in a magnetic field. (b) Behaviour of a superconductor in a magnetic field [29].

When a perfect conductor in the presence of a magnetic field is cooled below T_c, the magnetic field still remains within the conductor as indicated in Figure 2.4 (a). However, when a superconductor is cooled below its critical temperature, it will exclude the magnetic flux from its interior (Figure 2.4 (a)). This is known as the Meissner effect. This is the fundamental difference between a perfect conductor and a superconductor, the latter is a flux expeller whereas the former is a flux conserver.

2.3 Superconducting Critical Parameters

Three critical parameters of superconductivity are critical temperature (T_c), critical magnetic field (H_c) and critical current density (J_c). The critical value of one parameter depends on the presence of the other two in a system. The graph shown in Figure 2.5 displays this relationship. Cooper pairs unlike electrons are described by the same quantum wave function thus the superconducting state is at a lower energy state than the normal state. The critical parameters are values at which it becomes energetically favourable for electron pairs to break apart and thus destroy the superconductivity state of the material.

An increase in temperature causes a greater agitation within the lattice until collisions in the lattice break up the Cooper pairs. In the presence of an external magnetic field, the critical field is reached when magnetic energy created due to the expulsion of flux exceeds the condensation energy. Condensation energy is defined as the difference between the energy level of the normal state and energy level of the superconducting state. An electric current will break up the Cooper pairs when the magnetic self-field created by the current exceeds H_c.

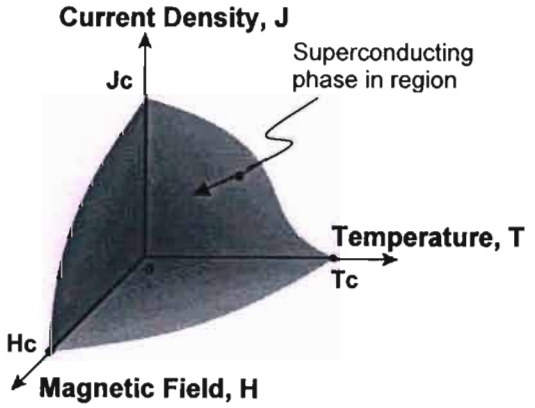

Figure 2.5: 3D phase diagram showing the operating region of a superconductor [30].

2.4 Characteristic Parameters

2.4.1 Penetration Depth

To achieve zero magnetic flux in the interior of the superconductor, screening currents created at the surface of the material produces a magnetisation value (M). The relationship between the applied magnetic flux density (B_a) and the magnetisation of the material which creates the zero magnetic flux at the interior of the superconductor is given by:

$$B_a + \mu_o M = 0 \tag{2.2}$$

where μ_0 is the magnetic permeability of space.

These supercurrents do not dissipate any energy. The penetration depth (λ) is a measure of the depth from the surface of the sample through which these supercurrents flow as indicated in Figure 2.6. This slight penetration of the magnetic field within the superconductor allows a lower energy state to be reached.

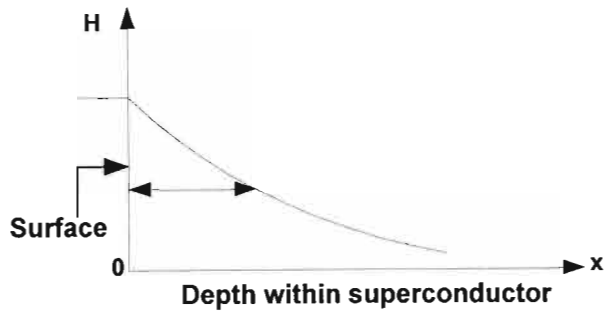

Figure 2.6: **Graph showing the decay of the magnetic field within a superconductor [28].**

2.4.2 Coherence Length

Coherence length (ξ) is a measure of the distance between two electrons of a Cooper pair. The ratio of penetration depth (λ) and (ξ) i.e.

$$\kappa = \frac{\lambda}{\xi} \tag{2.3}$$

is known as the Ginzburg-Landau constant which characterizes the superconducting material.

For $\kappa < 0.7$ it is energetically favourable for the material to exclude all the flux [28]. This will occur for $H_a < H_c$ as presented in Figure 2.7. This occurs in Type I superconductors e.g. Pb, Hg and Sn. The negative sign for magnetisation in Figure 2.7 shows that the sample becomes a perfect diamagnet. For $\kappa > 0.7$ complete flux exclusion is no longer achieved after some critical field (H_{cl}). After $H_a > H_{cl}$ it becomes energetically favourable for flux to penetrate the material through a number of cylindrical pores called vortices (Figure 2.8).

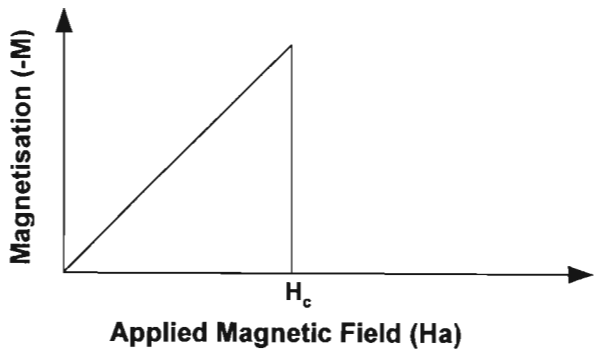

Figure 2.7: **Magnetisation graph of a Type I superconductor.**

Currents swirling around these vortices generate magnetic fields parallel to the applied magnetic field. They also screen out the field from the bulk of the superconductor.

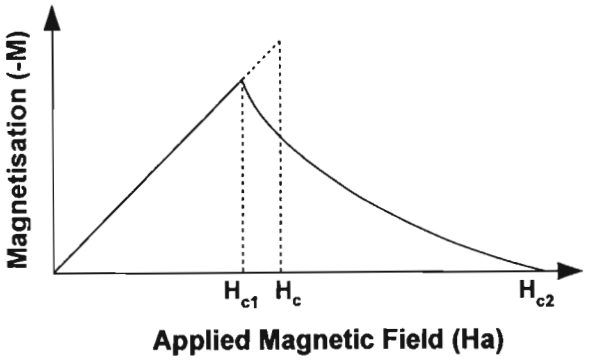

Figure 2.8: Magnetisation graph of a Type II superconductor (zero flux pinning).

These magnetic moments repel each other and move about to arrange themselves into a structure called a fluxon lattice. This region between H_{c1} and H_{c2} is known as the vortex phase or *mixed state*. Superconductors that exhibit this behaviour are called Type II superconductors.

A force known as the Lorentz Force as shown in Equation 2.5 acts on each vortex in the material in the presence of a current. This is shown in Figure 2.9.

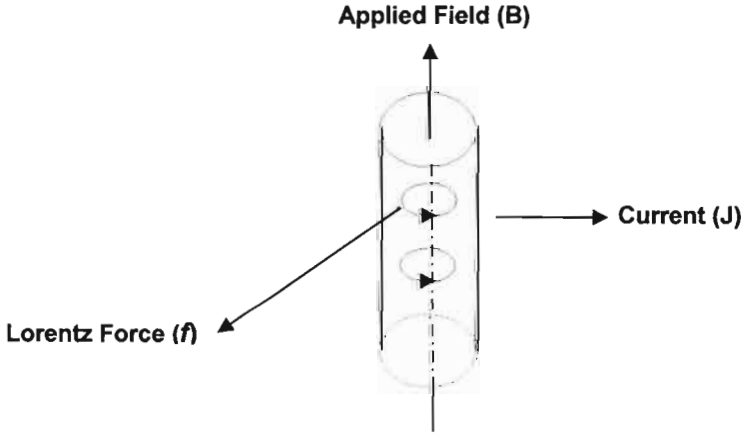

Figure 2.9: Representation of the Lorentz force ($f = J$ x ϕ_0) on a vortex [28].

The force on the lattice is thus

$$\boldsymbol{F} = \boldsymbol{J} \times n\phi_0 \tag{2.4}$$

$$\boldsymbol{F} = \boldsymbol{J} \times \boldsymbol{B} \tag{2.5}$$

where ϕ_0 is a magnetic flux quantum, n is the number of flux quanta, $\boldsymbol{F}$ is the Lorentz force and $\boldsymbol{B}$ is the magnetic flux density.

This force is responsible for the displacement of these vortices which result in undesirable energy dissipation. To prevent the motion of the vortices, a phenomenon called flux pinning occurs. This is achieved by sites in the material in which the vortex would require a large amount of energy to escape from. The force required to pin the vortex is called the pinning force (F_p). For $F < F_p$, the vortices will remain fixed and for $F > F_p$ the vortices will move.

For $F = F_p$ a critical regime is reached where,

$$\boldsymbol{F}_p = \boldsymbol{J}_c \boldsymbol{B} \tag{2.6}$$

2.4.3 Critical State Model (CSM)

The Bean model or Critical State Model (CSM) developed by C P Bean [31] is a non contact method of determining critical current density from the magnetisation of the sample. The critical current density is given by:

$$J_c = 2\frac{\Delta M}{d} \tag{2.7}$$

where ΔM is the difference in the magnetisations measured in increasing and decreasing fields and d is the sample thickness.

Figure 2.10 shows the magnetisation profile of a superconducting sample. ΔM is also indicated on this graph.

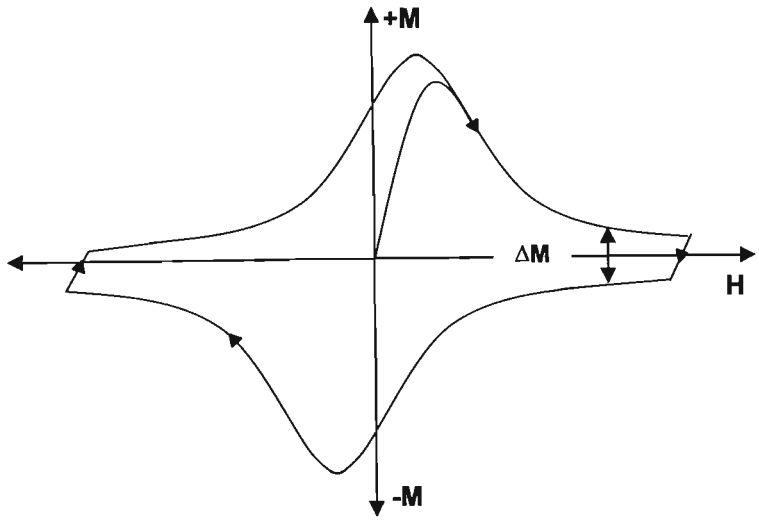

Figure 2.10: Typical magnetisation curve of Type II materials. The Bean model uses ΔM indicated in the magnetisation profile to estimate J_c.

2.5 High Temperature Superconductor Theory

Y123 was chosen as the parent superconducting material in this research. The reasons why Y123 was chosen are:

- it is a type II superconductor thus it can sustain large critical currents
- it has a high critical temperature of approximately 92 K
- it has good irreversibility properties (to be discussed in Section 2.5.3)

Although $Bi_2Sr_2Ca_2Cu_3O_x$ (BSSCO) has a higher critical temperature than Y123 (i.e.110K), it cannot sustain high critical currents and it has poor irreversibility properties which are important in magnetic levitation applications.

2.5.1 Structure of Y123

HTS have complex crystalline structures. Y123 is described as having a pseudo perovskite structure. The chemical formula for an ideal perovskite is ABX_3. In this formulae, A and B are metals and are positively charged atoms while X is a non-metal and is negatively charged. X is either an oxygen or a constituent of the halogen family i.e. fluorine, bromine etc. The unit cell of this perovskite is cubic in nature and is shown in Figure 2.11. The unit cell of Y123 consists of 3 tetragonal perovskite unit cells and copper oxide layers.

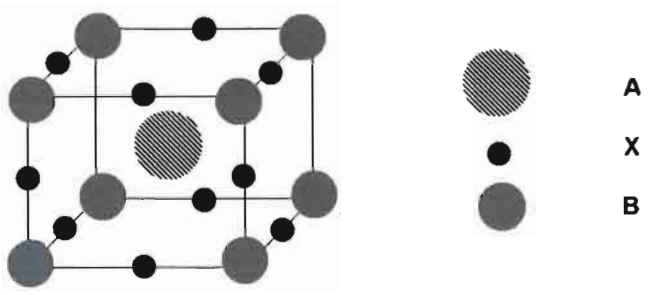

Figure 2.11: Cubic Structure of Perovskite Cell.

Figure 2.12 shows the unit cells of two compounds which are $YBa_2Cu_3O_6$ and $YBa_2Cu_3O_{7-\delta}$. $YBa_2Cu_3O_6$ is actually an insulator and to achieve the superconducting state ($YBa_2Cu_3O_{7-\delta}$), oxygen annealing is required. Typical values of δ are presented graphically in Figure 4.3 (Chapter 4).

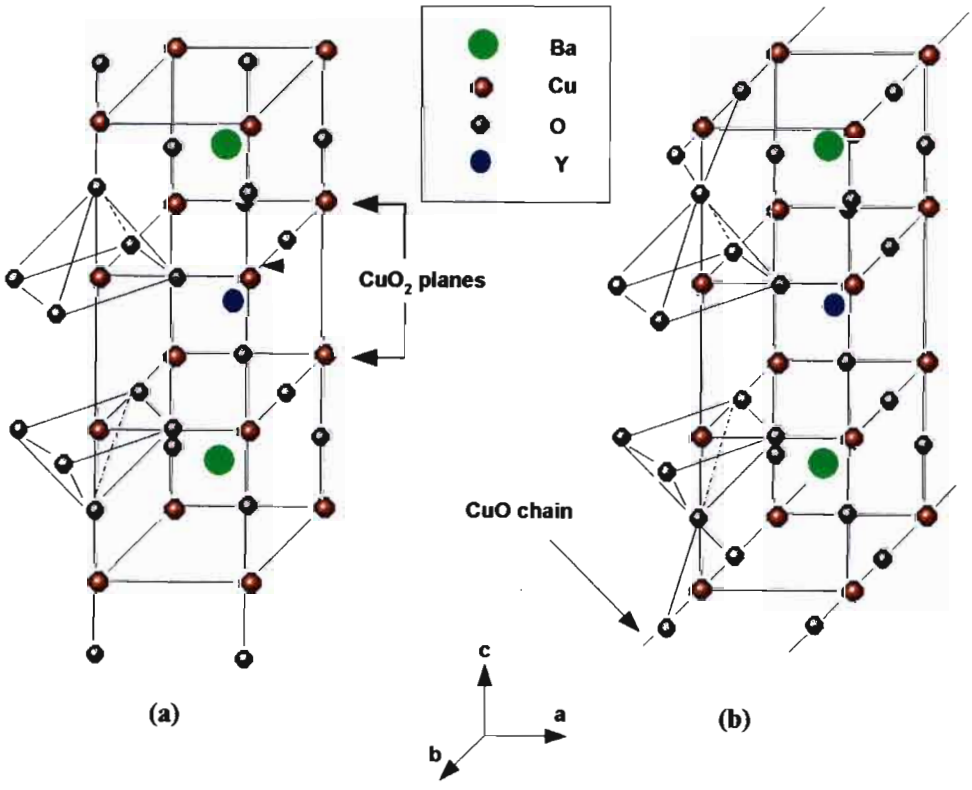

Figure 2.12: Unit Cell of (a) $YBa_2Cu_3O_6$ (insulator) and (b) $YBa_2Cu_3O_{7-\delta}$ (superconductor) [28].

The unit cell of $YBa_2Cu_3O_{7-\delta}$ (Y123) consists of a sequence of layers which are:

- CuO layer - this plane is made up of CuO chains. It has two oxygen vacancies as compared to the fully oxidised $YBa_2Cu_3O_7$ compound.
- BaO layer

- CuO_2 layer - the Cu atom in this plane is surrounded by 5 oxygen ions which form a polyhedral structure. Superconductivity occurs in this layer
- Yttrium layer - This layer has 4 oxygen vacancies. It can be replaced with certain other rare earth atoms while still maintaining its superconducting properties.

The Y123 compound can be represented by the layered structure as shown in Figure 2.13. From the explanation of the layers given above one can see that copper is present in two different sites in the unit cell which are the CuO chains and the CuO_2 planes. It has been found that most of the oxygen vacancies in the material occur in the CuO chains (a-b plane) rather than within the planes.

The CuO chains can be seen as a charge reservoir which is needed to transfer charge into the CuO_2 planes. The oxygen in the chains acts as "acceptor sites" for electrons from the CuO planes. This results in the formation of holes in the CuO_2 planes. Thus, Y123 has holes as its charge carriers.

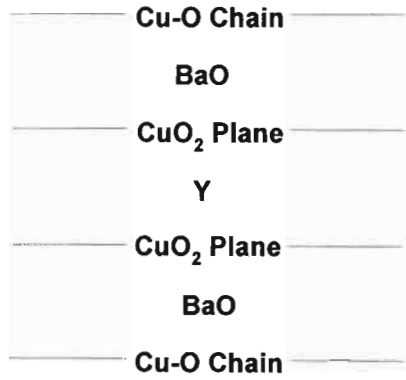

Figure 2.13: Layered structure of Y123 emphasising the different constituents [28].

As the number of charge carriers increases, superconductivity of the material increases. However, this will only happen until an optimum number of charge carriers are reached and once this occurs, any further increase in charge carriers will result in a decrease in the superconductivity as illustrated in Figure 2.14.

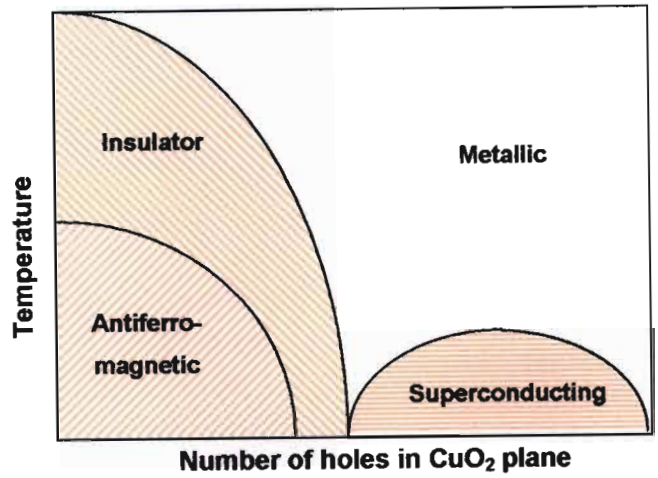

Figure 2.14: Phase diagram showing how the number of holes affects the material.

The $YBa_2Cu_3O_6$ compound has a tetragonal structure while $YBa_2Cu_3O_7$ is orthorhombic. Heating of the superconductor in a non-oxygen environment results in the loss of oxygen atoms from the material which results a reduction in the hole concentration. This leads to a reduction in T_c and finally leads to a complete loss in superconductivity which is the tetragonal phase of the material. Thus, oxygen annealing of superconducting material after heating is a critical step in the processing of good quality superconductors. This is discussed further in Chapter 4.

2.5.2 The Coherence Length Problem

According to the BCS theory:

$$\xi = \frac{V_F}{k_B T_c} \tag{2.8}$$

where ξ is the coherence length, k_B is Boltzman's constant ,V_F is the Fermi Voltage and T_c is the critical temperature.

As we know, the critical temperature for a HTS is relatively high and the Fermi energy (V_F) is much lower than in normal metals. Thus, this results in a relatively short coherence length in the material (approximately 10 Å) which is actually comparable to the size of the unit cell and is magnitudes smaller than conventional superconductors. It is important to note that the coherence length differs according to crystal direction i.e. ξ_{ab} is approximately 4 Å and ξ_c is about 15 Å implying that this is an anisotropic material. This anisotropy is due to the two

dimensional nature of the CuO_2 planes. Short coherence lengths in superconducting materials result in a highly complex mixed state, making them more sensitive to grain boundaries.

2.5.3 Irreversibility line

For $H > H_{c1}$, a Type II material enters the mixed state. As mentioned in Section 2.3.2, the flux penetrates the material in the form of vortices. The ability of the vortices to move into and out of the material is inhibited due to the irreversibility nature which results in a hysteretic magnetic profile as illustrated in Figure 2.15 (a) and (b).

These magnetic profiles were obtained from experiments conducted on $Bi_{1.8}Pb_{0.3}Sr_2Ca_2Cu_3O_{10+\delta}$ ($T_c \sim 106$ K) at 5 K and 85 K [32]. When current flows through a material that has a strong magnetic hysteresis i.e. strong irreversibility, the force created by it is not strong enough to overcome the pinning force of the vortices. Consequently, no dissipation of this current occurs. Thus, the J_c of a material is directly related to the strength of irreversibility. When there is no effective pinning of the vortices, the magnetic profile is reversible (Figure 2.15 (c)).

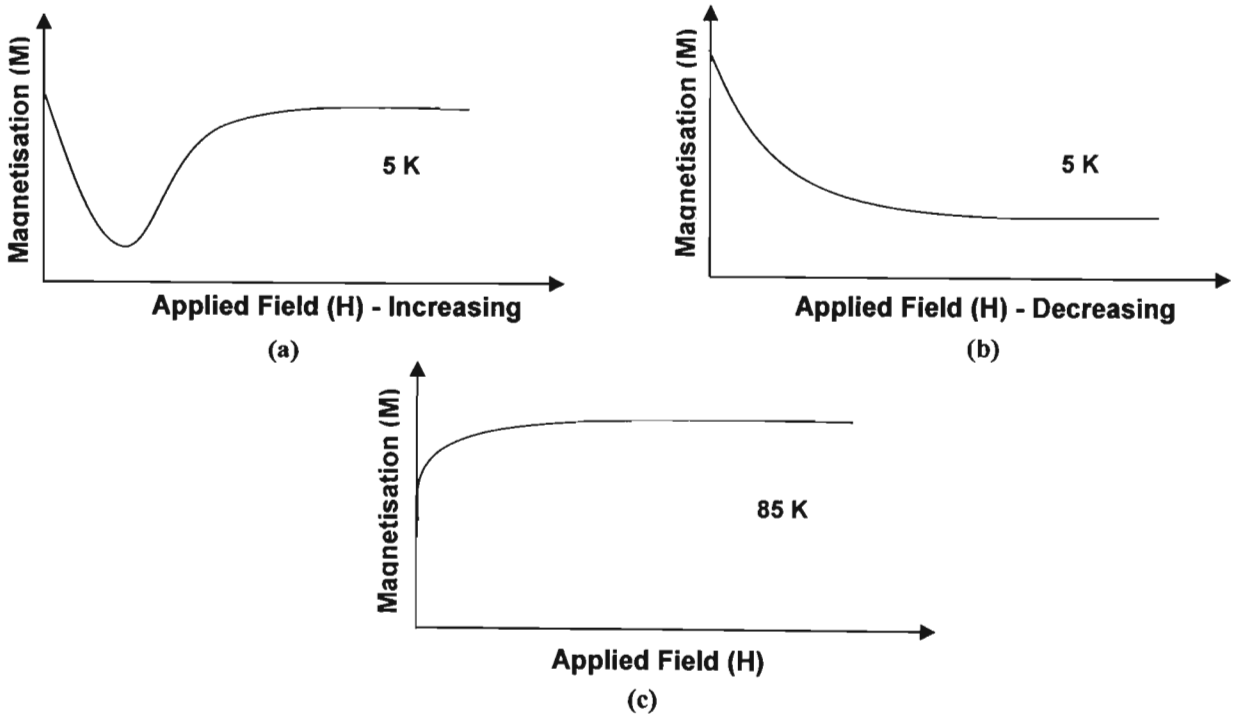

Figure 2.15: **Diagram showing the irreversibility nature of HTS ((a) and (b)). No pinning of vortices results in a reversible magnetic profile as shown in (c) [32].**

2.5.4 Weak Links and the Josephson Effect

2.5.4.1 Josephson Junctions

The Josephson junction was discovered by Brian D Josephson in 1962 [33]. A Josephson junction is basically two layers of superconductor separated by a thin insulating barrier as shown in Figure 2.16.

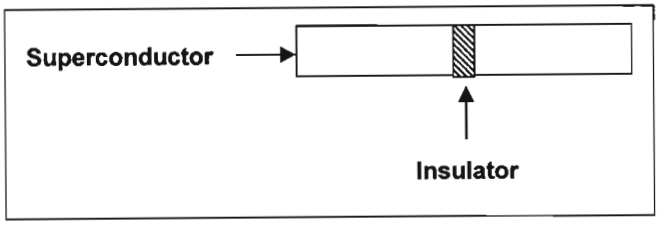

Figure 2.16: Diagram of a Josephson junction.

The Cooper pairs in the superconductors on either side of the insulating layer can be described by a single wave function. These two waves overlap at the barrier implying that the tunneling phenomenon occurs resulting in the presence of Cooper pairs in the barrier region. The junction can only sustain a certain current beyond which results in the breaking up of the Cooper pairs.

2.5.4.2 Weak Links

On an atomic level, a grain boundary is an interface consisting of two joined grains as shown in Figure 2.17. It is a planar defect separating two adjacent grains which have been rotated i.e. twisted or tilted with respect to one another. These grain boundaries in a HTSC structure act like Josephson junctions and are known as weak links since depression of J_c usually occurs at these points in the structure.

An accumulation or migration of impurities and secondary phases occurs at this boundary which hampers the transport properties of the material. The strain energy between the two grains determines the egression or migration of impurity or secondary phase atoms. According to Salama et al [34] the two crystals will take up a position whereby the strain energy is minimised.

HTSC materials have transport current characteristics that differ significantly from those of conventional superconductors. This is attributed mainly to weakly coupled grains, which

behave as magnetically sensitive Josephson junctions. This is the so-called 'weak link' effect.

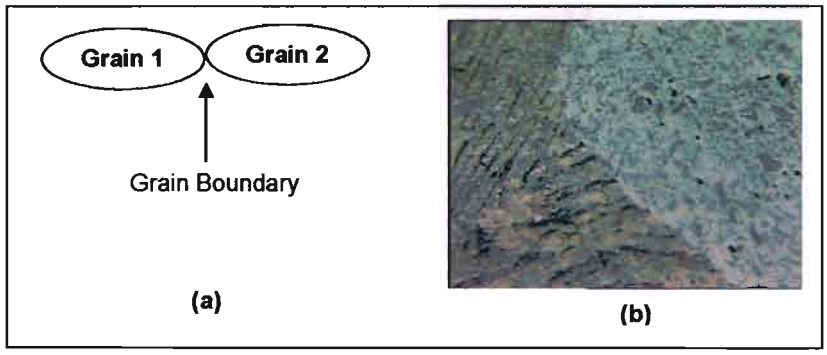

Figure 2.17: **(a) Schematic Representation of a grain boundary.**
(b) Optical image of a grain boundary found in Y123 structure [35].

Chapter 3

Superconductor Applications

3.1 Overview

Applications of superconductors can be broken up into low power and high power applications. In low power applications the superconducting material is processed as a thin film which is mounted on a dielectric substrate. In most low power applications, a phenomenon known as the Josephson Effect is utilised. High power applications refer to bulk type uses for example, wire, magnets, motors etc. In Table 3.1 typical magnetic fields and critical current densities required for different applications are shown.

Table 3.1: Typical magnetic fields and critical current densities required for some applications [36].

APPLICATION	H(T)	J(A/cm^2)
Interconnects	0.1	5×10^6
AC transmission lines	0.2	$10^5 - 10^6$
Power Transformers	0.3 – 3	10^5
DC transmission lines	0.2	2×10^4
SQUIDS	0.1	2×10^2
Motors, Generators	2.5 – 5	$4 \times 10^4 - 10^5$
Magnetic Levitation	5 – 6	4×10^4
Fault current limiters	> 5	$> 10^5$

3.2 Low Power Applications

3.2.1 Squids

A Superconducting Quantum Interference Device (SQUID) consists of a superconducting ring with two Josephson junctions as presented in Figure 3.1. The operation of a SQUID is based on flux quantization. Quantum theory states that a magnetic field in a superconducting

ring has a number of discrete levels of magnetic field strength and each step is called a *fluxon* of a *flux quantum* ($\phi_0 = 2.07 \times 10^{-15} Wb$).

A SQUID is the most sensitive device for measuring magnetic fields. They are used in the following applications

- voltmeters with sensitivities of the order of 10^{-15} V
- sensitive magnetometers
- computer switching applications

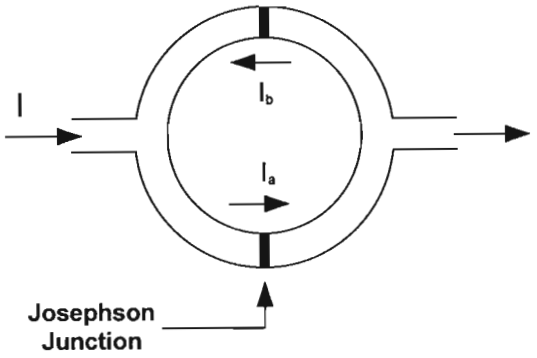

Figure 3.1: Representation of a SQUID.

3.2.2 Rapid Single Flux Quantum Devices

Around 1960, researchers began investigating the use of superconductors in the Integrated Circuit (IC) industry. The semiconductor technology that is currently used experiences high power dissipation as well as a high degree of dispersion of the signal. Superconductors were investigated in order to overcome these problems and thus maximise the clock speed that could be attained.

At first, a clock speed of only 1 GHz could be achieved and this was only slightly higher than that of semiconductor technology. It was found that the main limiting factor was the "latching circuitry". In semiconductor technology, transistors are used as voltage latching devices. In superconductor technology Josephson junctions were used to mimic transistors in the latching circuitry by using voltage levels [37].

Rapid Single Flux Quantum (RSFQ) logic uses the presence/absence of a single flux quantum to indicate a zero (0) or a one (1). The presence of a fluxon is indicated by a

voltage. RSFQ logic can be clocked at speeds of up to 300GHz in low temperature superconductors, and theoretical speeds approaching 1THz in high temperature superconductors whereas current semiconductor circuits are limited to 4GHz.

The advantages of superconducting technology in IC's are:

- availability of active devices (Josephson junctions)
- low power consumption
- superconducting microstrip lines allow ballistic transfer of pico-second waveforms with minimal attenuation, dispersion and cross talk

The disadvantage is the high cost incurred to maintain the temperature below the critical temperature of the superconducting material.

3.3 High Power Applications

3.3.1 Manufacture of High Temperature Superconducting Wire

Researchers have been investigating the use of HTSC materials in the production of electrical conductor. There are many advantages of using HTS. One of which is increased current carrying capacity which is approximately 100 times greater than conventional wire [38]. Another advantage is the reduction in the size of electrical equipment such as in transformers and motors due to the reduced wire thickness of the superconducting wire as illustrated in Figure 3.2.

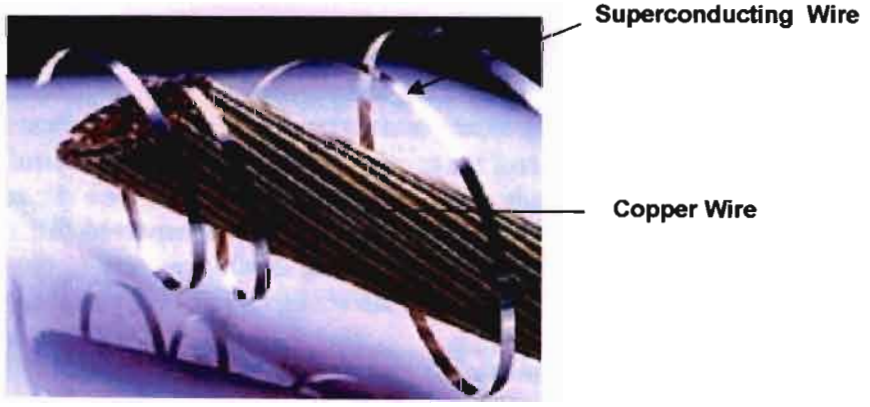

Figure 3.2: HTS wire and Copper Wire depicting the relative physical size difference [39].

The difficulty that researches are faced with is the design of a process that results in HTS wire that has a high current capability as well as high durability. HTS are highly anisotropic and brittle. There are two ways of producing superconducting wire. One method uses BSSCO to manufacture 1st generation wire. Powder in Tube (PIT), dip coating and bulk processing are popular techniques used to fabricate this wire.

The PIT method was one of the first methods developed to make HTSC wires/conductors [40]. $Bi_2Sr_2Ca_2Cu_3O_x$ (BSSCO) is the high temperature superconducting material that is most commonly used in this process. The HTS powder is first placed in a silver tube. Silver is used because it is permeable to oxygen and it does not contaminate the superconducting materials. It also assists processing of the conductors since it lowers the melting point of the superconducting material [41]. Once the material is placed in the tube, it is then extruded to form a wire about 1-2 mm in diameter. This wire is then rolled into a flat tape and it is subjected to a heat treatment. Since HTS are anisotropic materials, it is very important to align the a-b planes which are highly superconductive as compared to other planes, in the direction of the current flow in the wire. This is achieved during the heat treatment.

The Dip Coating Method coats HTSC material that is mixed into a slurry with an organic binder and a solvent onto a substrate which is usually silver [40].

There are two different techniques employed for bulk processing HTSC wires. When conductors are made with $Bi_2Sr_2Ca_1Cu_2O_x$ (Bi-2212) and BSSCO, the HTSC material is cast into a rod or cylinder and is then exposed to a heat treatment which partially melts the material. The resultant material is not as highly textured when compared to the conductor processed using the PIT method. [40].

Second generation wire was developed around 1996. The processes to make this type of wire use Y123 as the superconducting medium of choice. There are essentially two processes namely Ion Beam Assisted Deposition (IBAD) and Rolled Assisted Biaxially Textured Substrate (RABiTS) [42].

RABiTS is a method of manufacturing HTSC wire developed by Oak Ride National Laboratory (ORNL - USA) in 1996. The first step in this process is to condition a substrate or template upon which the superconductor could be formed. It was found that if a metal is rolled out into a flat sheet, it acquires a high degree of texture, thus, nickel is rolled out into a

sheet and is used as the substrate. Y123 is used as the superconducting material. In order to attain high critical current densities, it is important that much of the a-b planes are aligned. This is achieved using a highly textured metal substrate onto which the superconductor is formed.

The IBAD process was first designed by Fujikura Ltd and then was improved by Los Alamos National Laboratory (LANL – New Mexico). The metal substrate used is called Hastelloy nickel alloy which is not as aligned as the pure nickel substrate used in the RABiTS process. Alignment of the Y123 atoms is achieved by the use of an Ion Beam. Figure 3.3 shows the performance of first and second generation wire.

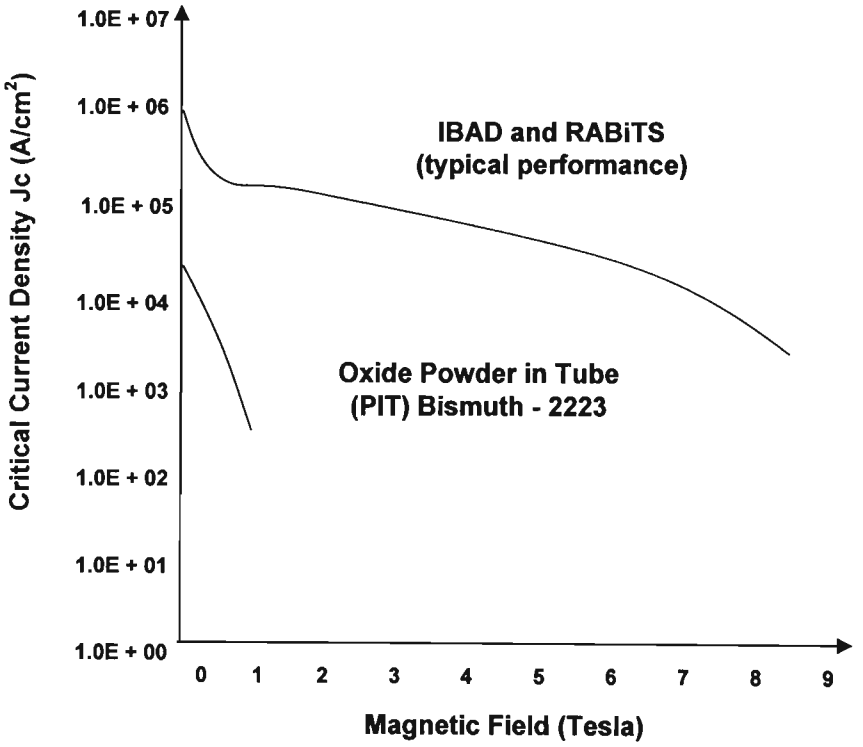

Figure 3.3: **Graph representing the performance of 1st and 2nd generation wire [43]. The performance of second generation wire is far superior to first generation wire.**

The advantages of second generation wire compared to first generation wire are:

- it is much cheaper to process
- cooling of 2nd generation is attained using liquid nitrogen so the cooling system is much cheaper and less complex
- it has much better transport properties (Figure 3.3)

3.3.2 Fault Current Limiters (FCL)

Fault current limiters are used for managing current faults on utility distribution and transmission networks. Because of the properties of a superconductor, it has the ability to provide varying impedance to the system which is dependant on the operating conditions.

In the normal operation of the system, the superconducting fault limiter has very low impedance and thus does not load the system. When a fault occurs, the fault current pushes the superconductor into its resistive state and thus inserts impedance into the system. This is a promising application for the power industry [40].

3.4 Other Applications

Magnetic levitation is used for suspension of trains (MAGLEV). Since the train does not touch the track, the friction experienced is minimal and considerable speeds are attained (~581 km/hr) [43].

Magnetic Resonance Imaging (MRI) is used to obtain images of soft tissue without the need of exposure to radiation. Magnets used in MRI have to provide very uniform magnetic fields over large volumes. Superconductors have been employed in MRI equipment because they can provide much higher magnetic fields per volume as compared to normal copper electromagnets.

3.5 Energy Storage

Energy storage is a mechanism that is used to increase the performance of power networks. Table 3.2 shows the different applications of energy storage. On the generator side, it has the

ability to increase the efficiency and on load side of the network, it can improve the quality of power to the consumer. Some energy storage technologies are explained below.

Pumped hydro storage is very dependent on the availability of sites that have an upper and lower reservoir that has a large vertical and a small horizontal distance between them. During peak demand, water is released from the upper reservoir and drops downwards through high pressure shafts. Once it passes through the turbines, it collects in the lower reservoir. During low demand times, the water from the lower reservoir is pumped back up to the upper reservoir.

Superconducting Magnetic Electric Storage (SMES) stores electrical energy using an electromagnetic coil that is made up of superconducting wire.

3.5.1 Flywheel Storage Systems

The findings of this research have a direct impact on flywheel storage applications since their performance is directly related to the dimensions of the magnetic bearing.

A flywheel is in essence a mechanical battery that consists of a rotating cylinder (which is connected to a motor/generator) and magnetic bearings. Figure 3.4 is a schematic representation of a flywheel system. The electrical energy is stored in the form of kinetic energy. Electrical energy is inputted into the flywheel to accelerate the rotor of a motor and when it is needed, it is tapped off using the same motor as a generator.

The main problem that these systems encounter is the loss of the stored energy by the electrical magnetic bearings.

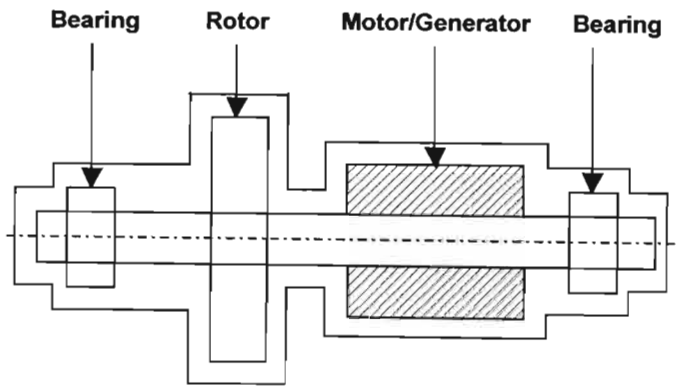

Figure 3.4: Schematic of a typical flywheel storage system.

According to Higasa [44], any mechanical bearing in contact with a stationary or moving part will produce enough energy losses to render the system uneconomical. The magnetic bearings in the flywheel system consume power which is dissipated as heat in the copper electromagnets. Thus, a cooling system needs to be added to the system to cool down the magnets. This addition will also consume a significant amount of power.

HTSC bearings are used in place of the electronically controlled magnetic bearings. These passive superconducting bearings reduce the energy loss in the system since there is no system required to control the superconductor.

Energy is inputted into the flywheel system by rotating the armature of the motor which is levitated by the superconducting bearing. Energy is stored in the form of kinetic energy. When the motor is switched off, the armature of the motor will continue to spin at the generated speed in a vacuum. To use the stored energy, the motor is switched into generation mode and the kinetic energy is converted back into electrical energy.

The levitation force (F) produced by the superconducting bearing is proportional to trapped magnetic field density. But the magnetic field intensity is estimated as the product of J_c and the diameter of the bearing. From this, it can be concluded that since the levitational force is directly proportional to the diameter of the bearing a greater amount of energy can be stored by the flywheel.

At present, the largest single grain superconductor that can be fabricated is a few centimeters in diameter. As one attempts to create larger diameter samples, the quality of the sample decreases rapidly due to the large amount of crystal defects that are formed. To obtain good quality samples of larger diameters, single grains need to be joined to form one large superconducting bearing.

Flywheels can be effective and useful tools in a power utility since they can be used to:

- help counteract disturbances (sags, dips and interruptions) in the primary electrical source
- improve transmission line stability

Advantages of Flywheel storage systems are:

- long life
- low life cycle costs
- compact and self contained
- does not contain hazardous chemicals and does not produce flammable gases

Disadvantages of Flywheel storage systems are:

- safety concerns due to the high speeds of masses
- initial cost is relatively high

Table 3.2: Summary of Energy Storage Technologies [45].

Technology Type	Typical Power Rating	Typical Energy Rating (Operating times)	Applications
Mechanical Pumped Hydro Storage	100-2000 MW	4 – 10 h	• Daily load leveling • Frequency control and reserve
Compressed air energy storage	100 – 300 MW	6 – 20 h	• Peak shaving • Power plant improvement • Reserve
Flywheels	5 kW – 1.5 MW	15 s – 15 mins	• Peak shaving • Frequency Control • UPS/Power quality
Electrical Superconducting magnetic storage	10 kW – 1 MW	5 s – 5 mins	• UPS/Power quality • Transmission/distribution line stability
Capacitors/Ultra Capacitors	1 kW – 100 kW	1 s – 1 min	• UPS/Power quality • Transmission/distribution line stability
Electrochemical Batteries (Lead Acid)	1 kW – 50 MW	1 min – 3 h	• Power quality • Reliability • Frequency Control • Reserve

3.6 Conclusion

This chapter briefly discussed the applications that use superconductors. Advantages and disadvantages of using this type of material were presented. Much research is conducted on utilising superconductors in various applications.

Chapter 4

Processing and Joining of Superconductors

4.1 Overview

This chapter describes the different processing techniques that are used to produce HTSC material. Different joining techniques that have been investigated by various researchers are also discussed.

4.2 Single crystal, thin films and bulk superconductors

Production of HTSC samples takes one of three routes, namely:

- single crystal
- thin film
- bulk

The application where a material is used determines the type of processing route to be taken.

4.2.1 Thin films

Thin films are widely used in the electronics industry. There are two main categories of producing thin film superconductors namely:

- droplet transfer method (arc spraying/plasma spraying)
- atom transfer method (sputtering, evaporation etc)

4.2.1.1 Droplet Transfer Technique

The droplet transfer technique is a relatively easier process and can produce fairly thick films. However, the critical current density of the film is not very high. In applications where a large critical current density is required a highly textured film is required. To achieve this

type of texturing, a single crystal that has crystal lattice dimensions similar to the superconducting medium is used as the substrate of the thin film.

4.2.1.2 Atom Transfer Method

Here, the materials to be evaporated are placed in a vacuum chamber near the substrate. Usually, laser beams or electrical discharge are used to heat the superconducting material. Figure 4.1 shows a schematic view of the evaporation process.

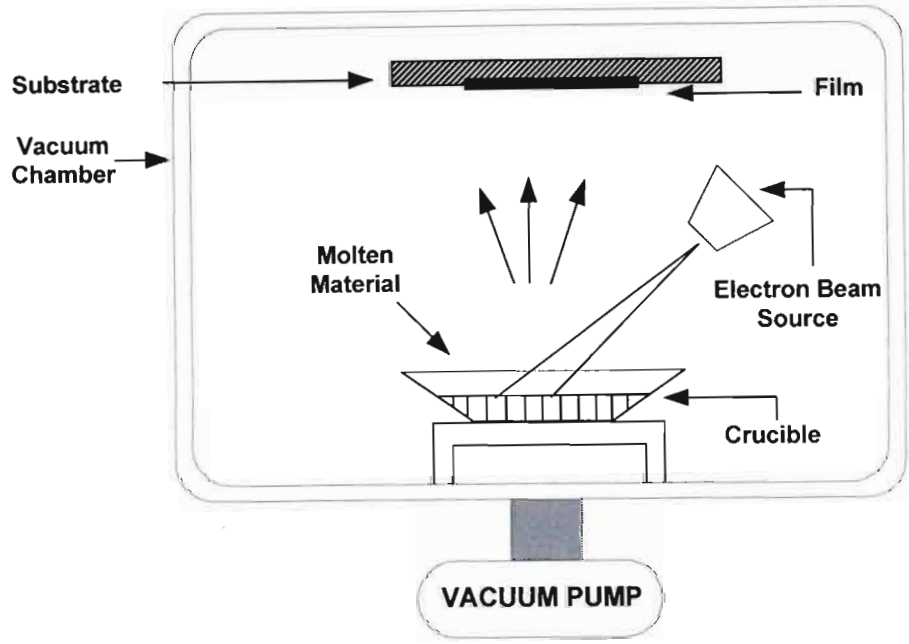

Figure 4.1 Schematic view of the evaporation process [36].

4.2.2 Single crystal

Single crystal HTS are produced by first melting the superconducting powder which is achieved by exposing the material to a temperature greater than its peritectic temperature. The molten material is then held at a temperature slightly below the melting point for a period of time known as the holding time. The size of the crystals depends on the holding time as well as the cooling rate. The resultant sample contains crystals in the form of plates. The processing of the HTS will be discussed in more detail later on in this chapter. The critical current densities obtained from single crystals are much higher than that of thin films and bulk samples. This is expected because there are many defects such as grain boundaries and twins that occur in thin films and bulk samples which reduce the critical current densities.

4.2.3 Bulk samples

Bulk samples are commonly used in levitation applications such as flywheel storage systems, railway tracks (Maglev train), etc. The processing of these types of superconductors is explained in detail in the next section.

4.3 Texturing processes for bulk HTSC

There are two commonly used processes for creating bulk HTSC superconductors namely:

- sintering
- melt texture processing (this method is discussed in detail as this was the technique used to manufacture the parent samples in this research)

The aim of these processing techniques is to produce superconducting samples in various shapes and sizes with relatively good transport characteristics.

4.3.1 Sintering

Initially, this method was very commonly used since it was easy to produce superconductors of various shapes for different applications. However it was found that the transport characteristics of the material were very poor.

The first step of this process is to prepare the powders for the sample. The powder is prepared using the following techniques:

- solid state reaction
- co-precipitation
- sol-gel

The solid-state method involves individual constituents of the superconductor in the form of oxides or carbonates which are thoroughly mixed and ground. This method is much faster than the other two however the resulting sample has a large amount of undesirable phases.

In the co-precipitation technique, the individual constituents of the superconductor are in the form of nitrates which are precipitated out of a solution to obtain the carbonate forms. The sol gel technique involves the transformation of a colloidal liquid (sol) into a solid (gel). Metal oxide precursors are polymerised first by hydrolysis to form the colloidal solution which when cast into a mould forms a gel [46-47]. Sintering this gel at relatively low temperatures, results in the formation of crystalline metal oxides. The co-precipitation and the sol-gel technique are much better than the solid-state method since they produce a finer and more homogenous powder resulting in less production of the unwanted phases.

Once the powder is prepared, it is pressed into the desired shape and heated according to a chosen temperature profile. The heating temperature is around 900 ^{0}C. The aim is to sinter the materials at the highest temperature possible at which melting does not occur. This is followed by an essential oxygenation process i.e. annealing, which is conducted at a temperature between 400 °C and 500 °C.

The samples produced from this method of processing have a very low critical current density of approximately 10^3 A/cm^2 which is attributed to the large amount of weak links boundaries and the anisotropic nature of the superconducting material.

4.3.2 Melt texturing of High Temperature Superconductors

Melt texturing is a much more favoured processing method in the processing of bulk material since the samples produced have much higher critical current densities than the samples produced from sintering. Magnetic texturing uses magnetic fields to try and align the a-b planes. This method does improve the microstructure but there are still a large number of grain boundaries that exist in the sample which do not improve the critical current density. Melt texturing processes have substantially reduced the grain boundary problem by producing a sample that consists of quasi-oriented single crystals aligned along the a-b plane. This results in a J_c of approximately 10^5 A/cm^2 at 77 K compared to sintered material which has a J_c of approximately 10^3 A/cm^2 at 77 K.

4.3.2.1 Growth process

A good understanding of the growth process of HTSC material is essential to this research as the joining technique is directly related to it. The growth of $YBa_2Cu_3O_{7-\delta}$ (Y123) has been

selected to explain and understand the general growth mechanism of HTS. It is important to understand what material transformation occurs and to utilise this information to produce high quality bulk samples and joins.

The melt texturing process begins by heating the bulk above its peritectic i.e. melting temperature which is about 1010 °C for Y123. This results in the following phase reactions:

For **1010 °C < *T* < 1300 °C**

$$YBa_2Cu_3O_{7-x} \rightarrow Y_2BaCuO_5 + \text{Liquid}\left(3BaCuO_2 + 2CuO\right) \tag{4.1}$$

For **1300 °C < *T* < 1500 °C**

$$Y_2BaCuO_5 + \text{Liquid}\left(3BaCuO_2 + 2CuO\right) \rightarrow Y_2O_3 + \text{Liquid}\left(BaO + CuO\right) \tag{4.2}$$

On slow cooling, a Y123 microstructure forms with Y_2BaCuO_5 (Y211) phases trapped within the Y123 phase. This is clearly illustrated in Figure 4.2. Normally, considering classical peritectic reactions, one would expect the Y211 particles to act as nucleation sites for the growth of the Y123 particles. If this were the case, due to the large number of Y211 particles, the resulting microstructure would have very small Y123 grain sizes. However, this does not happen in reality. Salama et al [34] proposed a Y-diffusion controlled model which explains the growth of the Y123 phase. According to this model, when Y123 is heated above 1010 °C, it melts into Y211 solid and a Ba-Cu rich liquid phase. After the Y123 has decomposed completely, the semisolid melt is slowly cooled past the peritectic temperature to minimise the number of Y123 nuclei and maintain a stable growth front. Once a single grain has nucleated, it can grow rapidly in the ab [110] direction but this requires a constant supply of Yttrium (Y). It is believed that this is provided by the dissolution of the Y211 particles in the liquid ahead of the growing interface. This will continue to occur until the Y211 particles are engulfed by the Y123 phase.

To summarise, when a grain of Y123 nucleates, it can grow rapidly in the a-b plane provided it has a continuous supply of Y. This is obtained from the dissolving Y211 particles in the liquid phase.

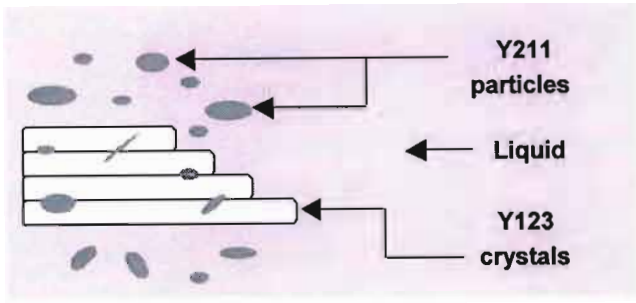

Figure 4.2: Diagram showing the nucleation process of the Y123 microstructure. The Y211 particles become embedded in the Y123 matrix.

New Y123 particles are sympathetically nucleated from this Y123 grain structure. This creates a low angle and low energy grain boundary between the grains. The layered Y123 microstructure is formed once this nucleation growth process stops. Figure 4.2 demonstrates the nucleation-growth process.

4.3.2.2 Explanation of addition of Y_2BaCuO_x (Y211)

For continuous grain growth both the Y211 and the liquid phases need to be supplied. Thus, a microstructure that has an uneven distribution of Y211 will result in poor Y123 growth in areas where there is a low density of Y211 particles [34]. To avoid this from occurring, several mechanisms can be used such as:

- adjusting the duration of holding time
- adding Y211 phase to the starting materials
- addition of Pt/Ce

The holding time is the time that the sample is kept in a semisolid state. Increasing the holding time results in large Y211 particles forming and reducing holding time results in the formation of pores, thus an optimum holding time needs to be applied for the minimisation of pores and Y211 particle size. It has been found that by adding Y211 to the starting powders, the resultant microstructure has [34]:

- finer Y211 particles
- a homogenous distribution of Y211 particles through out the sample

The decrease in the Y211 particle size is attributed to the increase in nucleation sites for Y211 precipitate during the decomposition of the Y123. According to Izumi *et al* [1], addition of Pt causes an acceleration in the growth of the Y211 particles since it alters the interfacial energy of the 211-liquid interface resulting in a much finer 211 particle size.

4.3.2.3 Oxygenation of Y123

Y123 is a quasi-perovskite because is contains a mixture of metal oxides that display the mechanical and physical properties of a ceramic. The CuO planes of Y123 contain copper and oxygen atoms bonded together and these planes determine the behaviour of the material. Y123 can change from a semiconductor $YBa_2Cu_3O_6$ to a superconductor at $YBa_2Cu_3O_7$ without losing its crystalline structure. The sensitivity of the material to oxygen is due to the ease at which oxygen can diffuse into and out of the molecular lattice. A subtle electronic charge balance exists between the one dimensional copper oxygen chains and the two dimensional copper-oxygen pyramidal planes, where superconductivity exists. Thus any change in this balance results in a change in the behaviour of the material. The dependence of the superconductive strength of the material on the oxygen content is shown graphically in Figure 4.3.

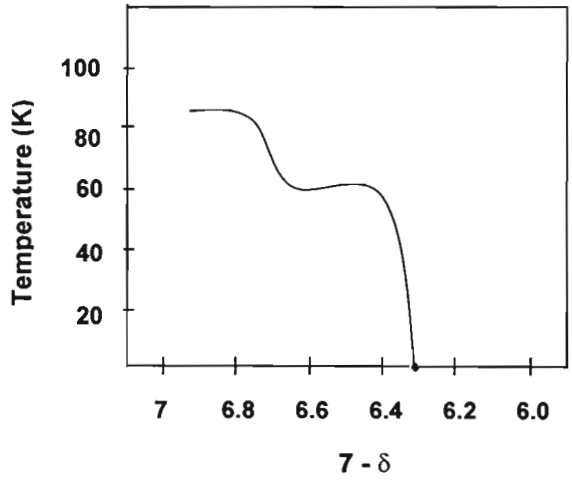

Figure 4.3: Relationship between *Tc* and oxygen content of Y123 [48].

In oxygen deficient $YBa_2Cu_3O_{7-\delta}$ oxygen is removed from the CuO chains affecting the charge equilibrium existing between the chains and the planes which results in a behavioral change in the material. From the graph in Figure 4.3 it can be seen that as the oxygen content decreases, the T_c of Y123 decreases. Over oxygenation of polycrystalline Y123 samples also

reduces the superconductivity of the material. A fully oxygenated version of the orthorhombic Y123 cell does not superconduct. Removal of a few oxygen atoms results in a change of state of the copper atoms which affects the density of the electron states on the Fermi surface making it more amenable to the Cooper pairing process. Thus, it is important to find the optimum oxygen content of the superconducting material to optimise its superconducting properties.

4.3.3 Top Seed Melt Texturing (TSMT)

Top seed melt texturing is another method of melt texturing which results in a highly structured sample. This method uses a single crystal (seed) as a nucleation site for the growth of Y123 crystals. The seed material has a much higher peritectic temperature but similar crystalline structure thus, when the Y123 is melted, the seed remains in its solid form. The crystal orientation of the Y123 microstructure will match that of the seed as demonstrated in Figure 4.4.

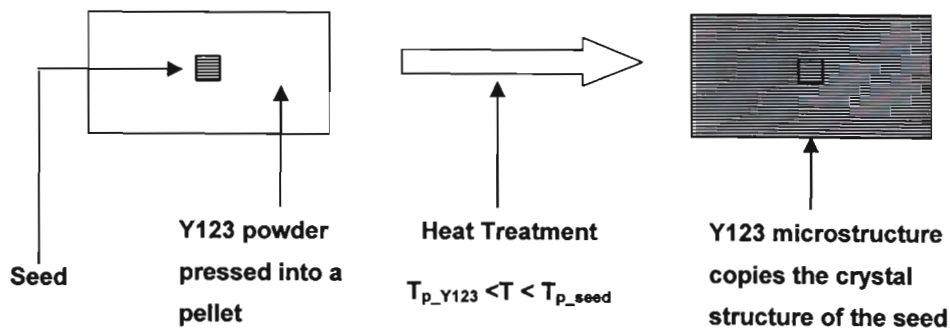

Figure 4.4: Representation of TSMT growth process. The sample material mimics the texturing of the seed material.

4.4 Joining of HTSC

Melt texturing helps reduce the number of grain boundaries and thus increases the J_c of the superconducting sample. Due to this, superconductors have found their way into applications such as fault current limiters and flywheel storage systems. As discussed in Chapter 3, the flywheel storage system stores electrical energy and the amount of energy stored is directly proportional to diameter of the superconducting bearing, thus to increase the amount of stored energy, one method is to increase the diameter of the superconducting bearing. Melt texturing methods can only produce samples that are a few centimetres in diameter. Increasing the diameter using melt texturing processes was found to be too difficult and time consuming, thus other techniques such a joining single domain samples were investigated.

The aim of joining is to produce a seam between two superconducting domains that have similar microstructural and transport qualities to that of the parent. Microstructurally, a good join should have:

- few voids and pores - these defects reduce the effective contact area between the two parent samples thus hindering the transport capabilities of the joined sample
- few trapped secondary phases – these defects are non-superconducting phases that are trapped within the join and also hamper the critical current density of the combined sample

There are a few joining techniques that have been developed to join single domain and bulk HTS namely:

- natural joining using multiseeded melt growth
- joining in the absence of a soldering agent
- joining using a superconducting solder

Each of these methods will be briefly discussed in the sections below.

4.4.1 Multiseeded joining

In this technique, rectangular bars consisting of 2 or 3 single domain crystals of HTS were produced. Joining of these single domains occur during the crystallisation process. Superconducting powder was first pressed into a rectangular bar of a chosen dimension. The top seeded melt texturing process was used to melt texture these bars using seeds of a chosen crystal orientation. The samples were subjected to a heat treatment which resulted in the crystallisation of each of these bars as well as the crystallisation of a bond between these superconducting bars. Results obtained from this technique show that the angle between the a-b planes of each parent was less than 7 ° however a large amount of structural defects were present at the join boundaries. These defects impede the current flow through the combined superconducting unit [26].

4.4.2 Joining without the presence of a soldering agent

There are three techniques of this type of joining that were investigated namely:

- joining using the Ba-cuprate liquid
- solid state diffusion bonding
- melt texture bonding

The first method mentioned above achieves coherent joins between single HTSC grains by using a barium-cuprate liquid phase as a means of forming a bond. This liquid is released from the platelet boundaries which are parallel to the a-b planes, when the material is heated to a temperature just below the peritectic temperature of the Y123. Vanderbemden et al [25] and Bradley et al [22],[23] used this method to form joined samples. Vanderbemden heated the samples to a temperature between 920 °C and 980 °C. A pressure of 0.5 MPa was applied to the samples as well. Transport and magnetic measurements were performed on the joined samples. Bradley similarly heated his samples to a temperature between 920 °C and 1000 °C with an applied pressure of 0.5 MPa. Transport measurements revealed that the joined samples could support a J_c of 2000 A/cm^2 in a magnetic field of 4 T applied parallel to the c axis.

Solid state diffusion joining was also investigated as a means of joining two HTS [49]. Each parent surface that forms the join was first polished to a surface roughness of approximately 3 μm. The a-b planes of the parent materials were aligned to within 5 ° and the samples are heated to a temperature of 930 °C with an applied pressure of 2-6 MPa. The theory depicted in this paper suggests that bonding occurs through a solid state diffusion of atoms rather than through the formation of a liquid phase. Transport measurements were conducted on the samples. A T_c of 91.6 K was obtained for the joined sample with a transition width of 1.3 K which is comparable to bulk Y123 material. Using the 1 μV criterion, a critical current density of 6300 A/cm^2 at 77 K and 0 T was measured. The 1 μV criterion is commonly used to calculate J_c. The current flowing through the join that result in a 1 μV volt drop across the join is defined as the critical current. Using this, J_c is calculated as this critical current value divided by the cross sectional area of the join.

A direct contact method whereby two Y123 monoliths are joined by heating them to maximum temperature of 1025 °C was developed by Lihua Chen et al [24]. This technique is very different from all the others discussed in this section because the maximum heating temperature that the sample was raised to is greater than the melting temperature of the parent (Y123) which is approximately 1010 °C. The heat treatment was conducted in flowing oxygen to prevent nitrogen molecules from getting trapped in the join. The samples were subjected to an oxygenation treatment for 7-10 days at 450 °C Transport measurements revealed a J_c of 1.04 x 10^4 A/cm^2 for the joined sample. The samples were also field cooled at 77 K in the presence of a 0.5 T magnetic field. Field maps plotted show that no depression of the trapped field exists in the join area implying the high quality of the join.

4.4.3 Joining with a soldering agent

This technique uses a mixture of superconducting powders with a few other ingredients to create a solder that forms a bond between the parent materials. Various mixtures of different powders have been investigated and interesting results have been achieved. Donglu Shi [20] investigated the joining of two Y123 domains using a combination of Y123, Y211 and PtO powders as the solder. PtO reduces the size of the Y211 particles formed in the microstructure [1]. Once the solder was applied to the parent surfaces to be joined, the sample was heated to a temperature between 1010 °C and 1060 °C. It was then quickly cooled to 1000 °C to avoid severe melting of the parent domains. It was found that the original shapes of the parent domains were retained and only the parent faces that were to be

joined were melted as was desired. SEM analysis was conducted on the join and it was found that no interfaces between the parent and the join could be identified indicating the good microstructural quality of the join. The transport quality of the join was tested using magnetic hysteresis measurements and it was found that hysteresis widths of pre-joined sample and the joined samples were the same indicating that the join formed a strong coupling between the parent domains.

A solder composed of silver doped Y123 and cerium (Ce) to join two textured Y123 domains was also researched [17]. The addition of silver to the solder reduces the peritectic temperature of the solder by approximately 50 °C. Thus, the joined sample need not be heated to temperatures greater than the peritectic temperature of Y123, thus there is no risk of melting the parent domains. The samples were heated to a temperature of 990 °C. Interestingly, the solder was first pressed into a pellet of 1 mm thickness and then sintered at 940 °C prior to joining. Microstructural investigations using a SEM revealed joins with few non-superconducting phases and cracks. The superconducting properties of the join were investigated using field maps. It was found that no reduction in the field was observed in the vicinity of the join.

Manton et al [13] and Walter et al [21] investigated the joining between melt textured bulk Y123 domains. The solders that were investigated were made using $ErBa_2Cu_3O_{7-\delta}$ (ErBCO) powder. The a-b planes of the two parent domains were aligned and the solder was applied. A pressure of 0.5 MPa was exerted on the sample during the heat treatment to aid the joining. Once again, microstructural analysis revealed a microstructure with no visible grain boundaries or grain misalignment.

Zheng et al [50], Prikhna et al [16-18] used a combination of $TmBa_2Cu_3O_{7-\delta}$ and Y211 powders as a soldering agent. The joined sample was heated to a maximum temperature of 1005 °C. Zheng oxygenated the joined samples at a temperature between 440 °C – 480 °C for 16 days and used microstructural and force levitation analyses to verify the quality of the join while Prikhna used microstructural tests, magnetisation loops and field mapping analyses to investigate the quality of the join. A J_c of 34000 A/cm^2 at 77 K and 0 T was obtained for the joined samples [16].

Melt texture joining of HTSC bulks using $YbBa_2Cu_3O_{7-\delta}$ as a soldering agent was investigated by Noudem et al [15], Mukhopadhyay et al [14] and Schmitz et al [19]. In [19], a 60:40 ratio of Yb123 and Yb211 powder was used. PtO_2 was also used to reduce the size of the 211 particles formed in the join. The solder was combined with glycerine and then applied to the surfaces to be joined. The maximum temperature the samples were raised to was 980 °C. A pressure of 20kPa was applied to some of the samples. They were oxygenated at 450 °C for 100 hrs. Microstructural investigations using a SEM and transport measurements were conducted. It was found that the application of pressure to the join of samples and addition of PtO_2 improves the microstructural aspects of the join. Fewer voids and liquid phases were noted as compared to the samples without an applied pressure and PtO_2. The transport measurements revealed a J_c of greater than 12000 A/cm^2. Mukhopadhyay et al [14] on the other hand, only used Yb123 powder to make the solder. Ethanol was used to moisten the solder which was painted onto the parent surfaces to be joined. The joined samples were subjected to a temperature profile with a peak temperature of 960 °C. Oxygen annealing was conducted at a temperature between 450 °C and 700 °C for a period of 8-10 days. Levitation measurements, microstructural analysis and Energy Dispersive X-rays (EDX) were conducted on the joined samples. The levitation results showed that the joined sample was able to provide a levitation force that was approximately 92% the levitation force achieved by the parent material. The SEM images reveal cracks that are parallel to the a-b planes and run from the parent material through the interface without disruption. This indicates strongly linked regions. SEM analysis revealed regions in the join with relatively good microstructure.

4.5 Conclusion

This chapter discussed the processing techniques that were developed to produce various forms of HTS. The melt texturing process was explained in detail as this was the technique that was used to process the parent material in this research. Different joining techniques and the different mechanisms of joining were presented. The results obtained by the various researchers were discussed.

Chapter 5

Experimental Procedure

5.1 Overview

This chapter discusses the experimental procedure used in this research. The sample preparation is first presented followed by the experimental setup used to carry out the transport and magnetic investigations.

5.2 Sample Preparation

This section discusses the techniques used to prepare the joined samples that are investigated.

5.2.1 Processing of the Superconducting Levitators™

The bulk superconducting samples were purchased from **Superconductive Components Incorporated (SCI – USA, Ohio)**. These superconducting Levitators™ as shown in Figure 5.1 were processed using the top seeded melt texturing process. Phase pure, low pressure calcined $YBa_2Cu_3O_x$ and Y_2BaCuO_5 powders were used as the bulk material and a $Nd_{1+x}Ba_{2-x}Cu_3O_y$ crystal was used as the seed. As explained in chapter 4, the Neodydium (Nd) seed will act as a nucleation site for the growth of the Y123 crystals. Growth directly below the seed is mainly along the c axis. After slow cooling, the Y123 crystals begin nucleating in the form of a small square with well developed (001), (010) and (100) planes.

(a) (b)

Figure 5.1: **(a) Nd Crystal used as a seed in the TSMT process of the Levitators™ [42] and (b) A bulk superconducting Levitator purchased from SCI [42].**

(a) (b)

Figure 5.2: **(a) Y211 phase inclusions in c axis growth region of the Levitators™ [42].**
(b) Y211 phase inclusions a-b axis growth (more Y211 inclusions) [42].

The microstructure directly below the seed (along the c axis) has much less Y211 inclusions as compared to growth along the a-b axis which occurs towards the centre of the bulk. This is clearly shown in Figure 5.2. The a-b axis growth region has a stripped sub-domain structure which is made up of small domains which are less than 0.1 mm in size [51]. The picture in Figure 5.3 demonstrates this stripped region. Appendix 1 contains field and force plots of a Levitator™.

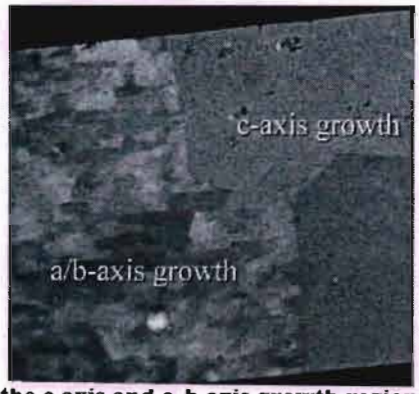

Figure 5.3: **Structure of the c axis and a-b axis growth regions in the Levitators™ [42].**

5.2.2 Cutting

The bulk sample is cut up into smaller pieces using a diamond saw. The process of cutting is demonstrated in Figure 5.4.

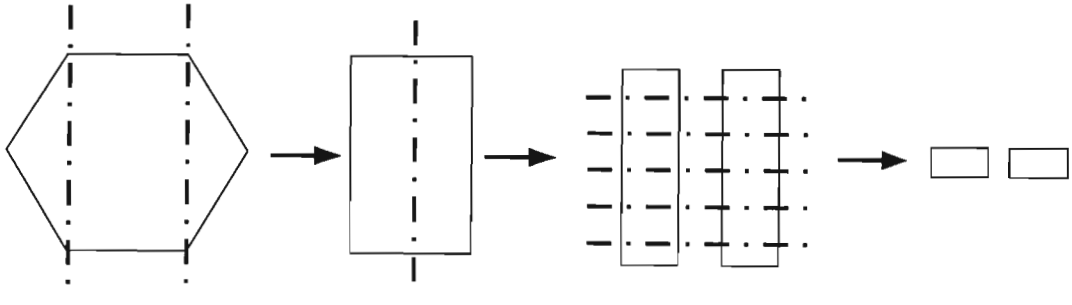

(a) (b) (c) (d)

Figure 5.4: **Demonstration of the cutting procedure used to cut samples.**

The bulk sample is first cut into a rectangular piece as shown in Figure 5.4(a). This rectangular piece is cut into half and each half is cut into smaller pieces shown in Figure 5.4(c). The final bulk pieces that are used for joining are shown in Figure 5.4(d). The c axes of each sample are aligned prior to joining as shown in Figure 5.5

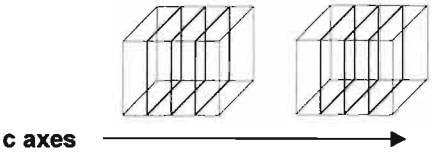

Figure 5.5: Alignment of c axes prior to joining.

5.2.3 Solder Ratios

The core solder material chosen for this research was $YbBa_2Cu_3O_{7-\delta}$. The reasons for choosing this powder are:

- it is a superconducting material
- has a lower peritectic temperature than Y123 (approximately 925 ^{0}C)
- has a similar structure to $YBa_2Cu_3O_{7-\delta}$

The solder mixtures were developed using the following materials

- $YBa_2Cu_3O_{7-x}$ (Y123) – superconducting material
- $YbBa_2Cu_3O_{7-x}$ (Yb123) - superconducting material
- $Yb_2Ba_1Cu_1O$ (Yb211) – non-superconducting
- Silver (Ag) - acts as a flux for scavenging impurities [52]

Using the above materials, solder mixtures as shown in Table 5.1 were made.

Table 5.1: **List of solders used in experiments.**

Sample No	Solder Mixture	Group Allocation
1-A	Yb123 = x	**Group 1**
1-B	0.6 Yb123 + 0.4 Yb211 = y	
1-C	0.75 Yb123 + 0.25 Yb211 = z	
2-A	0.95 (x) + 0.05 Ag_2O	**Group 2**
2-B	0.95 (y) + 0.05 Ag_2O	
2-C	0.95 (z) + 0.05 Ag_2O	
3-A	0.95 Y123 + 0.05 Ag_2O	**Group 3**
3-B	0.9 Y123 + 0.1 Ag_2O	

The exact quantity of Yb211 particles to be added to the Yb123 particles is not known. Some researchers have used a 60% Yb123 : 40% Yb211 (60:40) ratio [19], while others have experimented with a 75:25 ratio [50]. Different ratios of the Yb211 were mixed to investigate which ratio produces a better microstructure at a chosen temperature profile. The addition of silver was also investigated. Silver is known to have the following effects on the microstructure of Y123:

- reduces the melting point of the solder [41]
- cleans out grain boundaries [52]
- improves mechanical strength

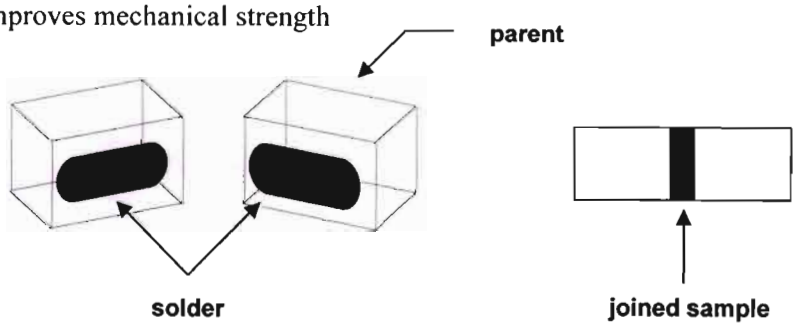

Figure 5.6: **Application of solder to the parent surfaces and joined sample.**

Glycerine was used as a wetting agent to allow for easy application of the solder onto the parent material. Once the solder is applied, and the parent material is assembled in the desired orientation as indicated in Figure 5.6, it is then placed in a sample holder which adds 5 KPa of pressure to the join. The orientation of the joined sample in the sample holder is displayed in Figure 5.7.

The sample which is now secured by the sample holder is placed in the furnace as shown in Figure 5.8. Figure 5.9 illustrates the temperature profile which was used to program the furnace. The details of the cooling controller designed for this furnace is provided in Appendix 2.

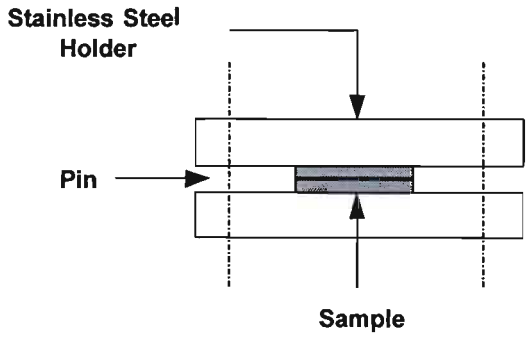

Figure 5.7: **Diagram of the stainless steel holder that exerts a pressure of 5 KPa onto the sample.**

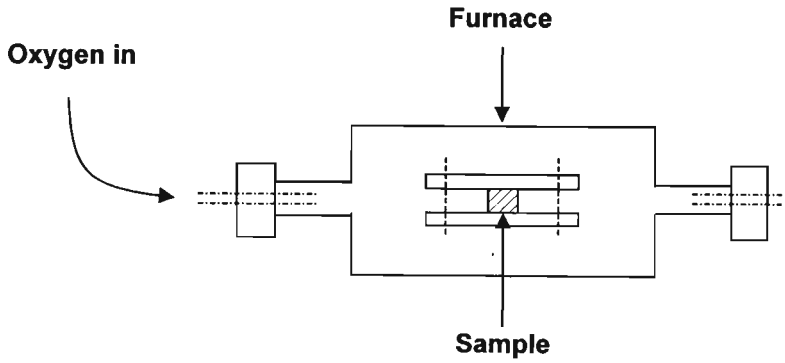

Figure 5.8: **Diagram of the furnace setup.**

All heating and cooling in the furnace is carried out in a flowing oxygen (O_2) atmosphere. When superconductors are heated above a certain temperature, the oxygen escapes from the microstructure. As discussed in Chapter 4, the oxygen content significantly impacts on the superconductivity of the materials and thus becomes a critical issue in the processing stage.

In order to reduce the magnitude of current required to bring samples to its critical point, the cross sectional area of the joined sample is reducing by sanding.

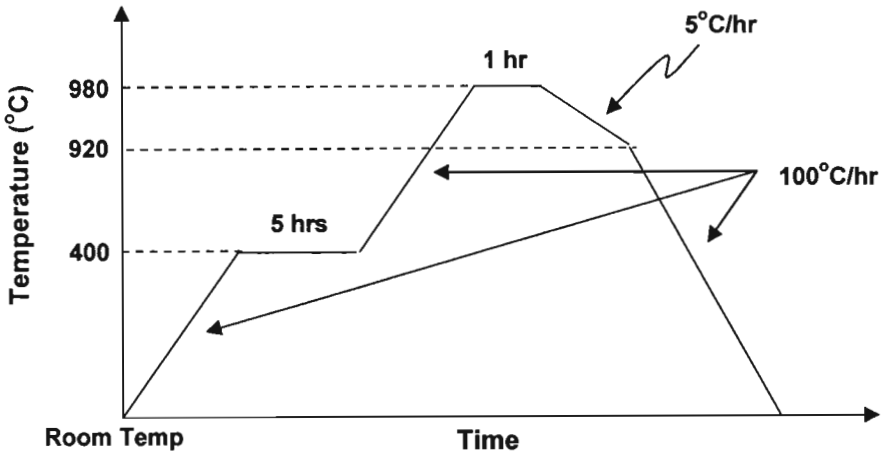

Figure 5.9: Temperature schedule used to join all the samples.

5.2.4 Sanding Process

Once the samples were joined, they were sanded down from an initial size of 5 mm x 4 mm x 2 mm to a final dimension of approximately 3 mm x 4 mm x 0.6 mm using a sanding wheel.

The joined sample was first glued down onto a glass slide using super glue. It was then sanded down to the chosen dimension. Care must be taken in this step to prevent over sanding of the sample. Once the sanding was completed, the sample was then removed from the slide. This was achieved by placing the slide in some liquid nitrogen. When the super glue gets very cold, it begins to contract and thus loses its bond with the glass slide. Little pressure is required to lift the sample off the slide.

5.2.5 Sample Contact Resistance

Contact resistance plays a major role in the transport measurements and it is essential to produce contacts with the lowest resistance. Research has been conducted in this field and the factors to achieve good quality contacts are discussed below.

Attaching good contacts onto superconductors has been a problem that many researchers are faced with. High contact resistance causes localized heating of the contact during critical current measurements which affects the characteristics of the sample. Thus, it is of the

utmost importance to produce low contact resistances to the superconducting samples to enable proper testing of the properties of the sample. The following aspects must be considered for optimum contacts:

- contact material (Gold, Silver, Indium etc)
- method of material deposition on sample (sputtering, pressing etc)
- curing temperature
- annealing temperature

Several studies have been done on the type of material to be used for the contact pads [53-58]. It was found that Indium produces high resistance and semiconducting contacts [53]. The semiconducting effect is produced because Indium has a high oxygen affinity which results in the production of an In_2O_3 layer at the interface with the parent. Gold (Au) and silver (Ag) produce some of the best contacts for superconductors because they are noble metals. They have a low oxygen affinity and they can also withstand high temperatures.

A silver paste was painted onto the superconducting samples to form the electrical contact pad. It was cured at 900^0C for 30 minutes. The oxygen content of a superconductor is very important. It can cause the material to act as a superconductor or semiconductor depending on the level of oxygen in the sample thus after curing, the material beneath the contact must be re-oxygenated.

5.3 Experimental Setup

This section explains the design and operation of the apparatus used to conduct experiments on the samples.

5.3.1 Cryomech Refrigeration System

The Cryomech GB-15 **(Gifford – McMahon)** cryo-refrigerator was used to cool down the samples below their critical temperature. The Cryomech can cool down samples to approximately 10 K. Figure 5.10 contains a block diagram of the experimental setup used to cool down the superconducting samples.

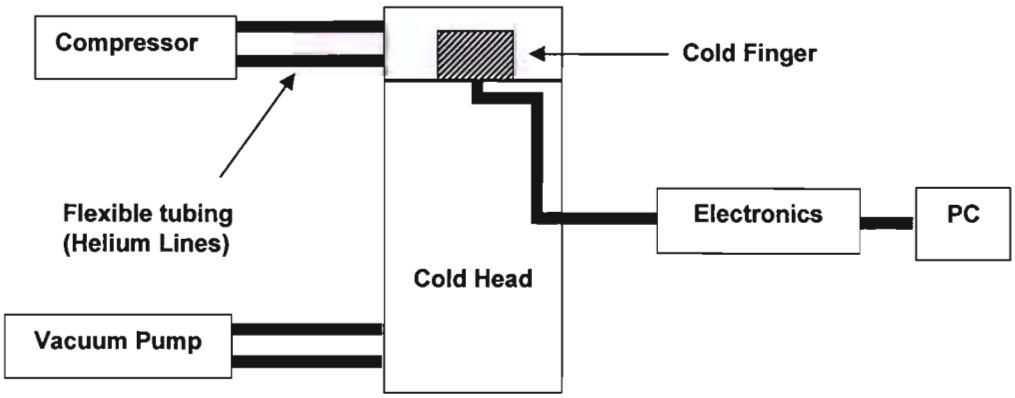

Figure 5.10: Block diagram representation of the Cryomech refrigeration system.

5.3.2 Cold Finger

The cold finger shown in Figure 5.11 is attached to the top of the cold head. A PT111 Lakeshore temperature sensor is mounted in the cold finger to provide accurate temperature readings. A heater coil which is used to raise the temperature of the sample is wound around the finger.

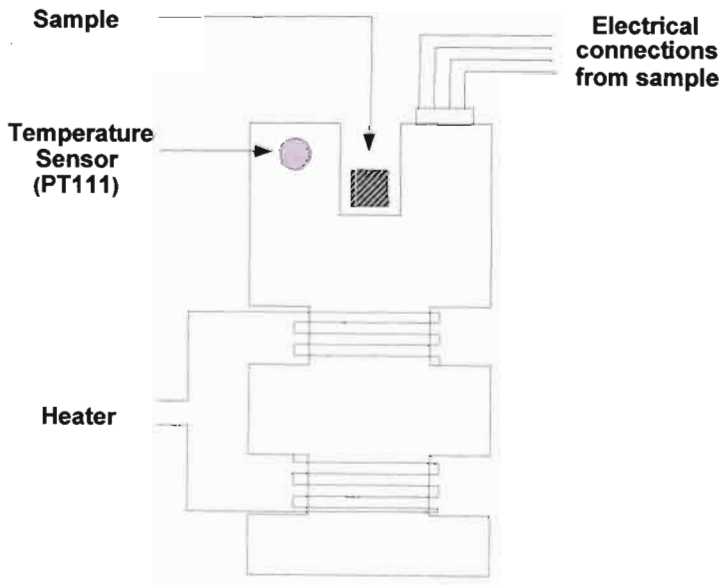

Figure 5.11: Diagram of the cold finger.

5.3.3 Design of Cryomech Electronics

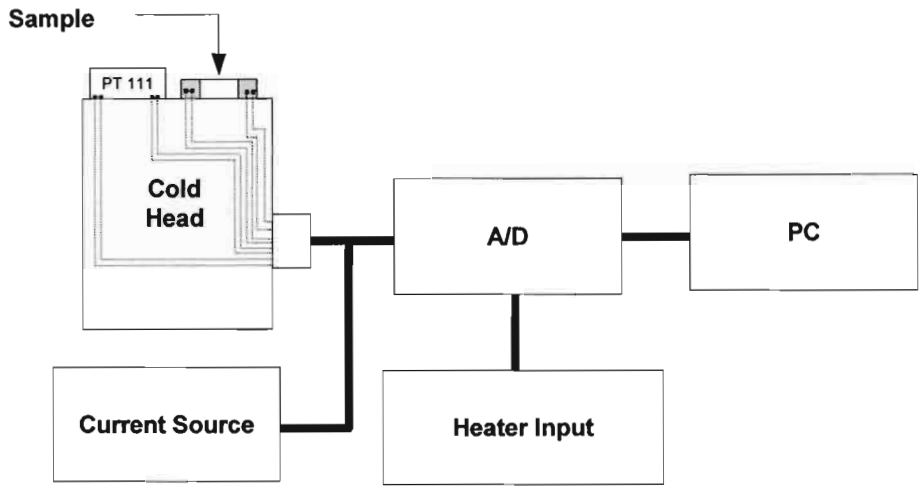

Figure 5.12: Block diagram of the electronic circuitry attached to the cold head.

Figure 5.12 is a block diagram of the electronic circuitry connected to the cold head. Electronic Workbench (EWB), a program manufactured by Strawberry Tree (now IOTECH), was used to design a temperature controller to control the temperature of the sample on the cold finger. It was also used to capture temperature and voltage readings across the sample. Pictures of the experimental setup are shown in Appendix 3.

5.3.4 Magnetic Measurements

In this experiment, a Levitator^{TM} displayed in Figure 5.13(a), was sliced in half by cutting it parallel to the c-axis as shown in Figure 5.13(b). These halves were rejoined using Yb123 and 5 % Ag_2O as a solder.

(a) (b)

Figure 5.13: Pictures of (a) parent sample and (b) cut sample.

Oxygenation time for these samples was increased to 100 hrs. A rare earth magnet with a magnetic field of approximately 200 mT was used to trap a magnetic field in the joined

sample. The parent is first cooled to 77 K using liquid nitrogen. The magnet was placed approximately 13 mm from the sample and held there for a few seconds to trap the field in the parent sample. A field plot is then captured using a transverse field probe which is connected to a gauss teslameter and an x-y plotter with a resolution of 0.01 mm. The field plot of the joined sample and the cut sample was also captured in the method explained above. The cut sample is obtained by placing the two parent halves as close together as possible.

5.4 Conclusion

This chapter presented the procedures used to manufacture and assess the quality of the samples.

Chapter 6

Results

6.1 Overview

This chapter presents and discusses the results obtained from transport, microstructural and magnetic scan measurements. A total of 8 samples were prepared for the current study as follows:

Group 1: Ytterbium solders with no silver oxide added
(Sample 1-A (Yb123), Sample 1-B (75:25), Sample 1-C (60:40))

Group 2: Ytterbium solders with 5% silver oxide added
(Sample 2-A (Yb123 + 5% Ag_2O), Sample 2-B (75:25 + 5% Ag_2O), Sample 2-C (60:40 + 5% Ag_2O))

Group 3: Yttrium solders with 5% and 10% silver oxide added
(Sample 3-A (Y + 5% Ag_2O), Sample 3-B (Y + 10% Ag_2O))

Each set of measurements will be explained separately. A discussion of the results is included at the end of each section. Appendix 2 contains all the data captured for each experiment.

6.2 Microstructural Measurements

SEM and optical imaging techniques were used to examine the microstructure of the joins. These images allow one to determine the structural quality of the joins. It is important to note that a structurally good join can actually have poor transport capabilities. As mentioned earlier, a structurally good join has:

- few voids and pores
- few trapped 'liquid' phases
- small degree of misalignment between the a-b planes

Figure 6.1 to Figure 6.3 show the SEM images of Group 1 samples taken at a magnification of X53. It can seen that Sample 1-A in Figure 6.1 has the most homogenous join in Group 1 as indicated by both SEM and optical images. The quality of the join is verified in the optical image displayed in Figure 6.1(b) with evidence such as minimal voids, pores and liquid phases. Due to the homogeneity of the join, there is a much higher effective contact area between the two parent materials in the Sample 1-A as compared to Sample 1-B and Sample 1-C.

Figure 6.4 to Figure 6.6 display SEM images of the interface i.e. solder and parent material, taken at a higher magnification. These images reveal microstructural features present in each sample in Group 1. The higher magnification and Electron Back Scattering (EBS) mode allows one to easily distinguish the Y123, Yb123 and Yb211 crystals. The EBS mode brightens particles according to their atomic mass, thus Yb211 will be the brightest while Y123 will appear the darkest in the image since it is has the highest atomic mass in the structure. In the optical images, many cracks/striations are visible in both parent materials. These striations form due to the stresses caused by a-b planes having a faster growing rate and are parallel to the a-b planes [3]. Thus they provide an easy and visible indication of the direction of the a-b planes. They also enable one to determine the angle of alignment between the two parent samples as presented in Figure 6.4(b). The degree of misalignment between the a-b planes of the two parent samples is one of the factors that impacts on the transport quality of the sample [59]. Table 6.1 lists the angle of misalignment for Group 1 samples.

Table 6.1: Angle of misalignment between two parent pieces for Group 1.

Sample	Angle of Misalignment
Sample 1-A	$\sim 78^0$
Sample 1-B	$\sim 88^0$
Sample 1-C	$\sim 38^0$

The effect of the addition of Yb211 particles is clearly visible when comparing the SEM images shown in Figures 6.4-6.6. The SEM image of Sample 1-C illustrated in Figure 6.6 demonstrates a much better distribution of Yb211 particles in the join as compared to Sample 1-A and Sample 1-B. This verifies the initial assumption that by adding Yb211 particles to the solder join to obtain a smaller Yb211 particle size was correct. This is also supported by [49] where Y123 and Y211 were used.

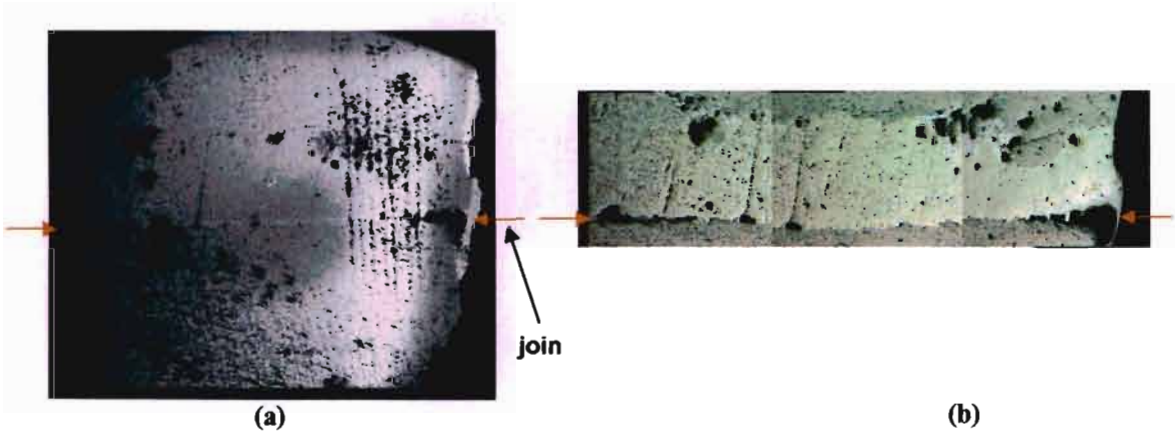

Figure 6.1: **(a) SEM image taken at X53 magnification of Sample 1-A.**
(b) Optical image of the join area of Sample 1-A.

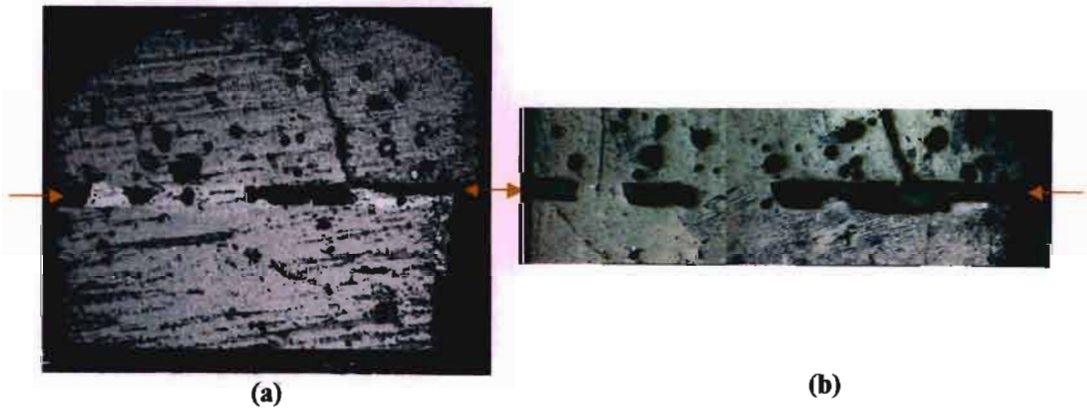

Figure 6.2: **(a) SEM image taken at X53 magnification of Sample 1-B.**
(b) Optical image of the join area of Sample 1-B.

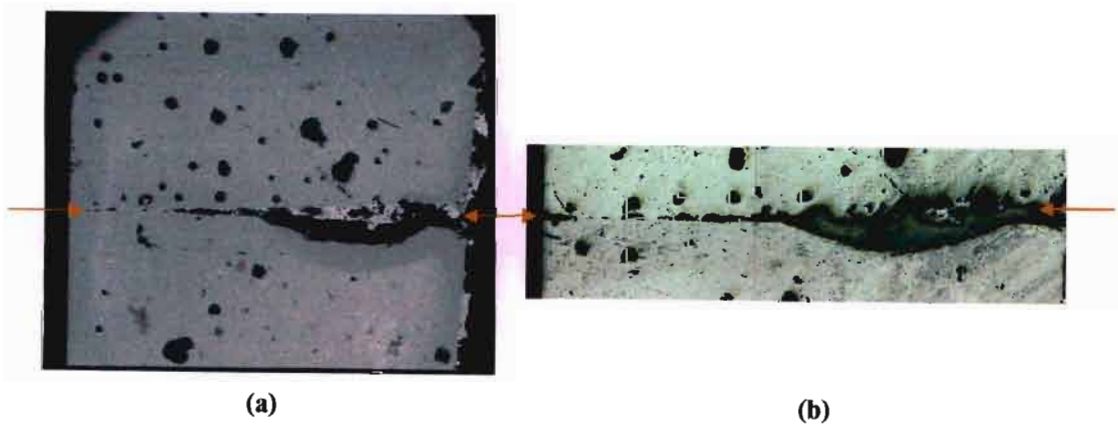

Figure 6.3: **(a) SEM image taken at X53 magnification of Sample 1-C.**
(b) Optical image of the join area of Sample 1-C.

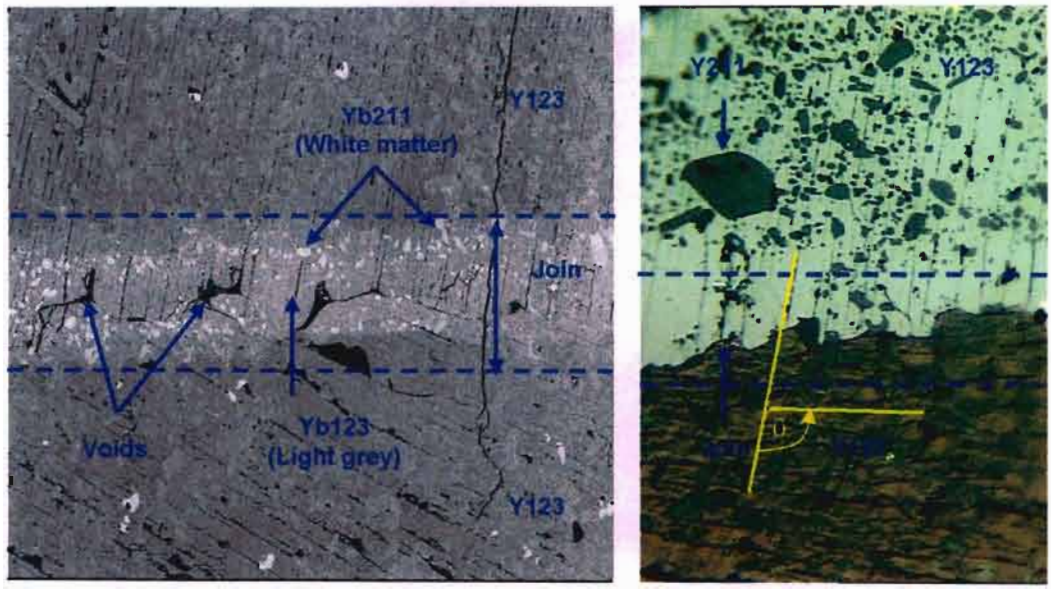

(a) (b)

Figure 6.4: **(a) SEM image taken at X650 magnification of Sample 1-A.**
(b) Optical image of the join area of Sample 1-A.

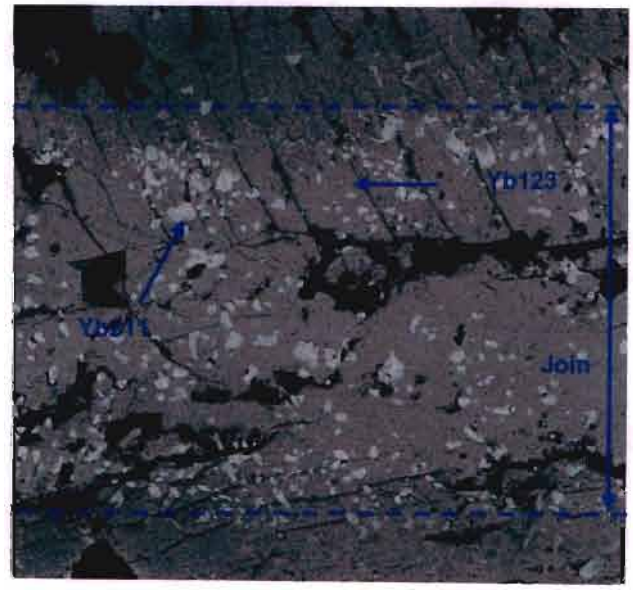

Figure 6.5: **SEM image taken at X650 magnification of Sample 1-B.**

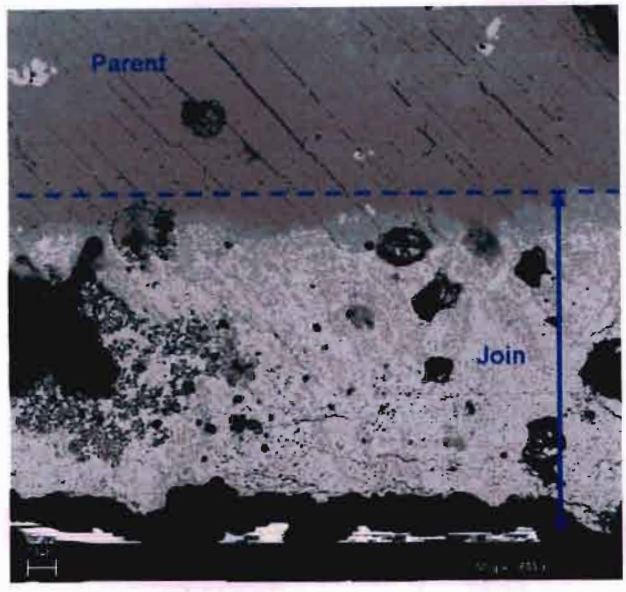

Figure 6.6: **SEM image taken at X650 magnification of Sample 1-C.**

Figure 6.7 to Figure 6.9 present SEM images taken at a magnification of X3500. In these images, the striations are much more visible. Zheng et al [50] noticed that cracks/striations present in the parent microstructure are continuous through the seam indicating that the crystallographic orientation of the parent is continuous in the join. This is clearly present in Figure 6.9. In reference [50], it was also noticed that voids present in the seam prevented the propagation of these cracks. Figure 6.7 and Figure 6.9 clearly demonstrates this observation.

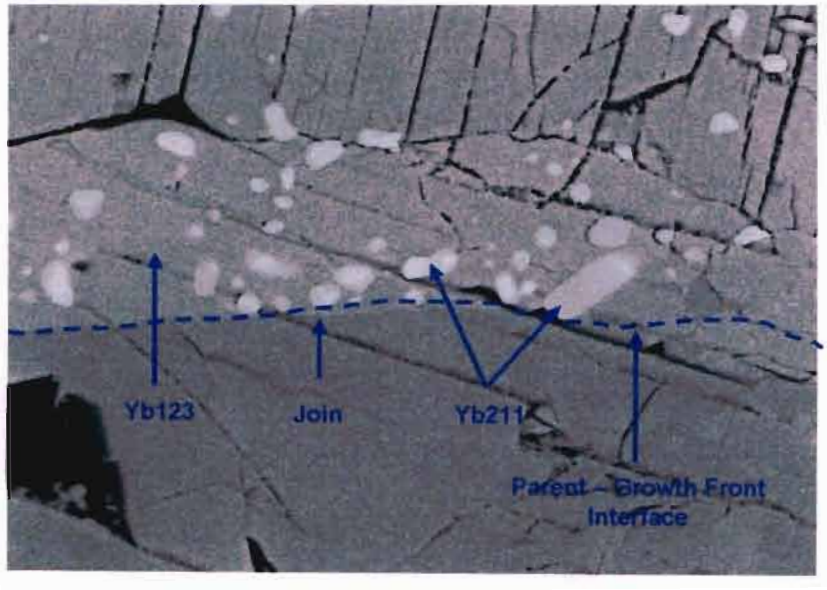

Figure 6.7: **SEM image taken at X3500 magnification of Sample 1-A.**

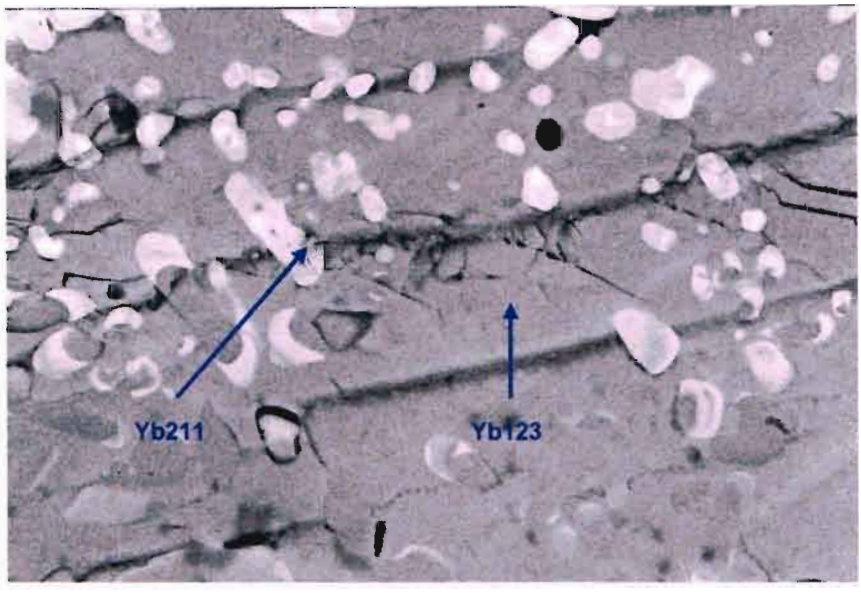

Figure 6.8: **SEM image taken at X3500 magnification of Sample 1-B.**

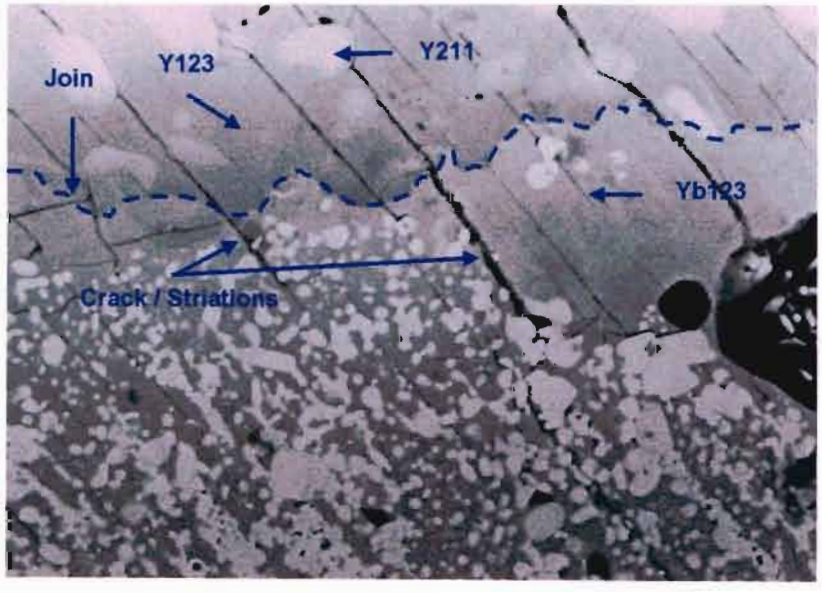

Figure 6.9: **SEM image taken at X3500 magnification of Sample 1-C.**

Figure 6.10 to Figure 6.12 presents the SEM images of Group 2 samples taken at a magnification of X53. In this group of solder, silver was added to:

- reduce the peritectic temperature of the solder
- clean out the join since it is already proven that silver cleans out grain boundaries

As can be noticed in the images, the resulting samples from this group are very porous. This could be attributed to a decrease in the viscosity of the solder caused by a reduction in the peritectic temperature. The effects of the addition of Yb211 particles can also be observed in Figure 6.13 to Figure 6.15 where SEM images of Group 2 samples were taken at a magnification of X650. Table 6.2 lists the angle of misalignment for Group 2 samples.

Table 6.2: Angle of misalignment between two parent pieces for Group 2 samples.

Sample	Angle of Misalignment
Sample 2-A	$\sim 85^0$
Sample 2-B	$\sim 72^0$
Sample 2-C	$\sim 20^0$

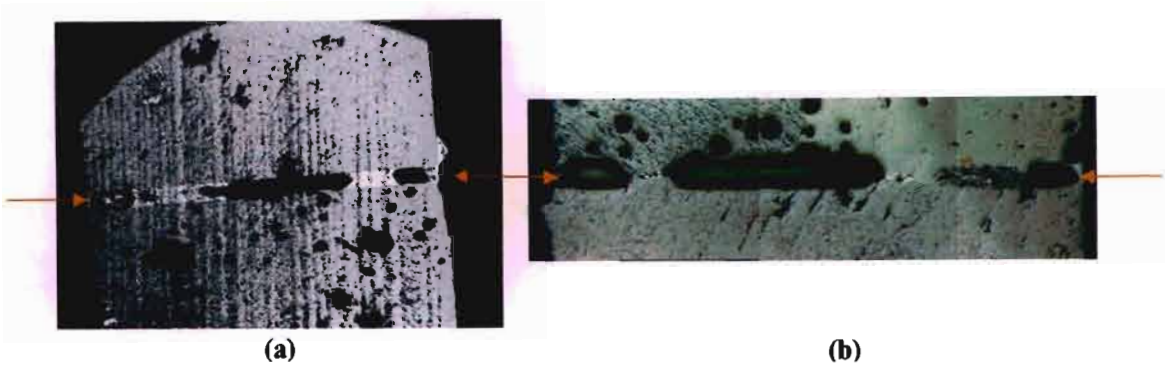

(a) (b)

Figure 6.10: **(a) SEM image taken at X53 magnification of Sample 2-A.**
(b) Optical image of the join area of Sample 2-A.

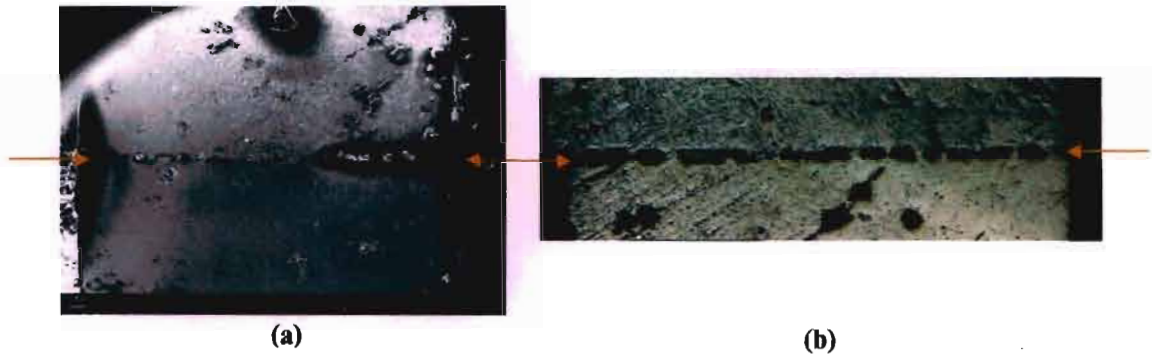

(a) (b)

Figure 6.11: **(a) SEM image taken at X53 magnification of Sample 2-B.**
(b) Optical image of the join area of Sample 2-B.

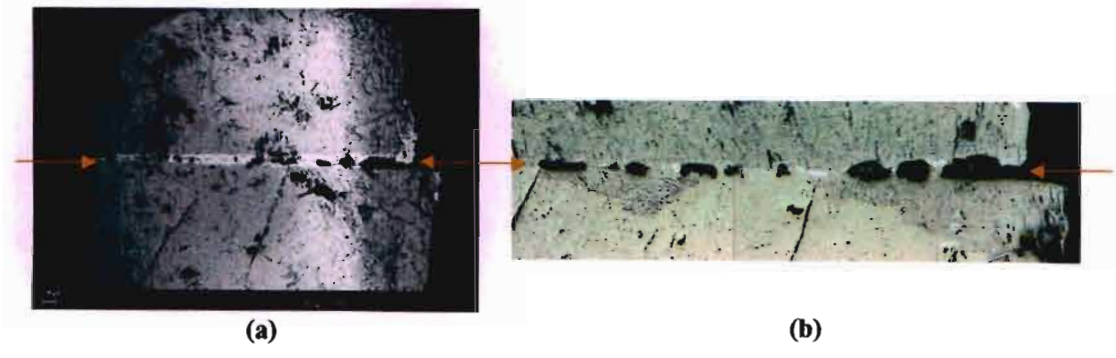

(a) (b)

Figure 6.12: **(a) SEM image taken at X53 magnification of Sample 2-C.**
(b) Optical image of the join area of Sample 2-C.

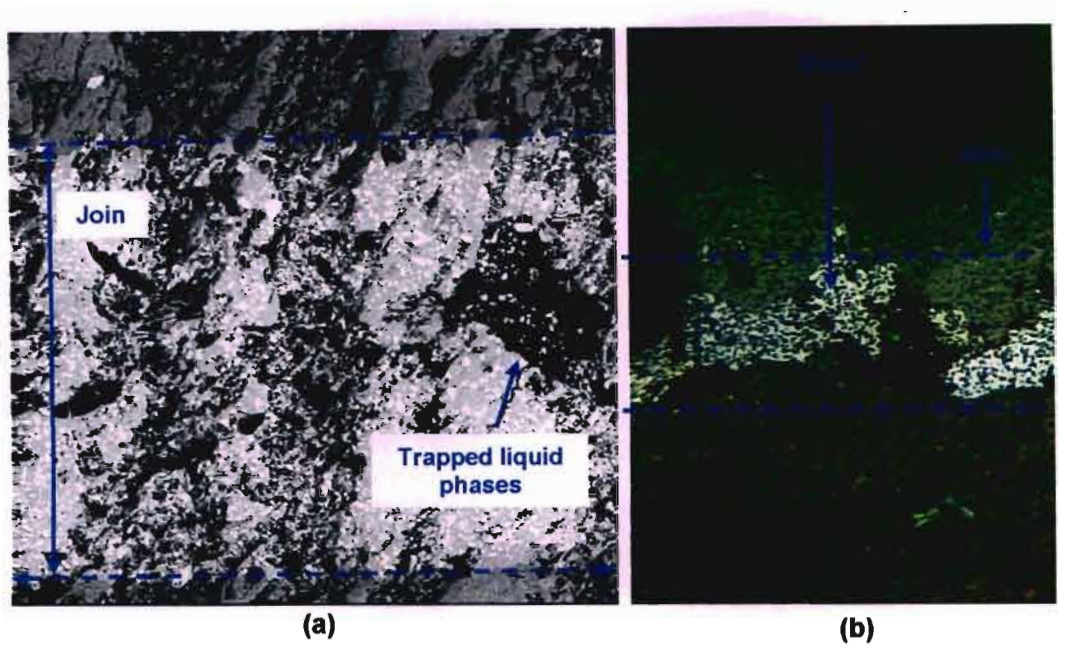

Figure 6.13: **(a) SEM image taken at X650 magnification of Sample 2-A.**
(b) Optical image of the join area of Sample 2-A.

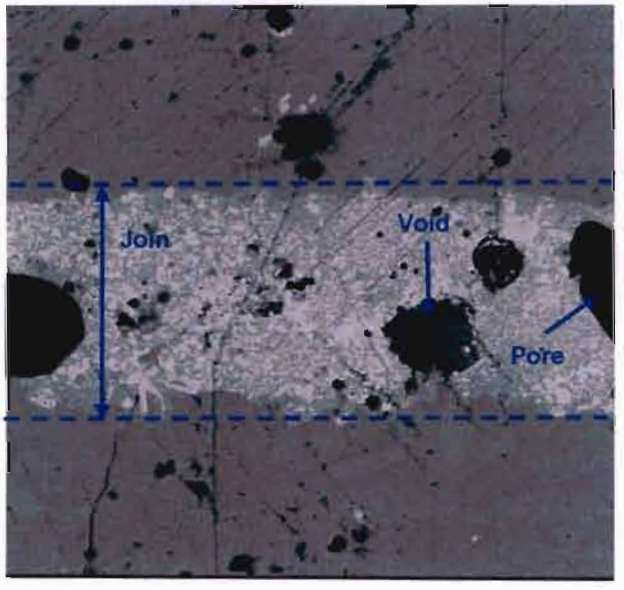

Figure 6.14: **SEM image taken at X650 magnification of Sample 2-B.**

The striations are again evident in the parent materials of this Group of samples. Figure 6.16 to Figure 6.18 are SEM images of Samples 2A, 2B and 2C captured at a magnification of X6500. Figure 6.16 clearly shows the propagation of the striations from the parent into the join. The void near the centre of the join stops the progression of the crack.

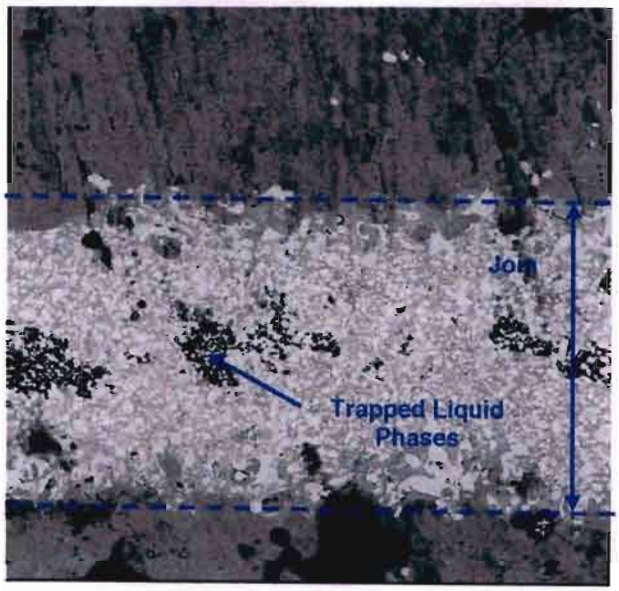

Figure 6.15: **SEM image taken at X650 magnification of Sample 2-C.**

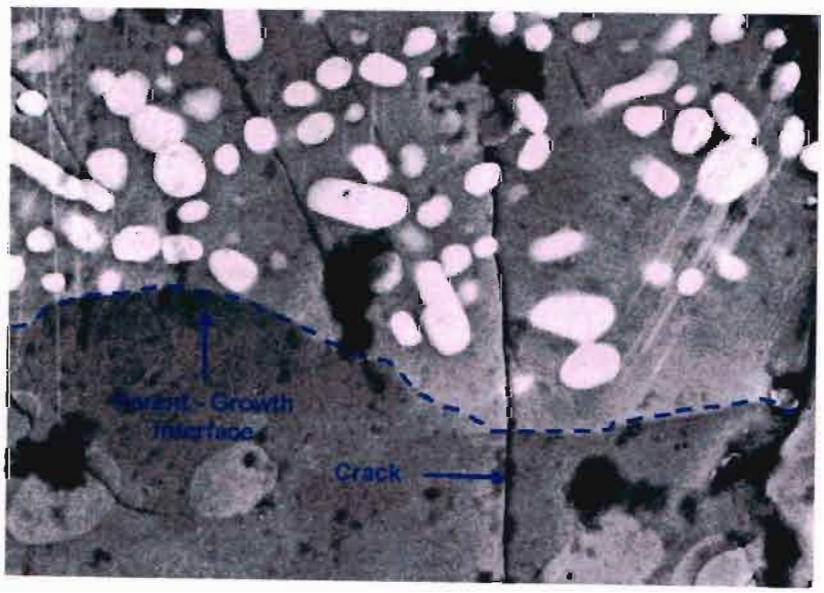

Figure 6.16: **SEM image taken at X6500 magnification of Sample 2-A.**

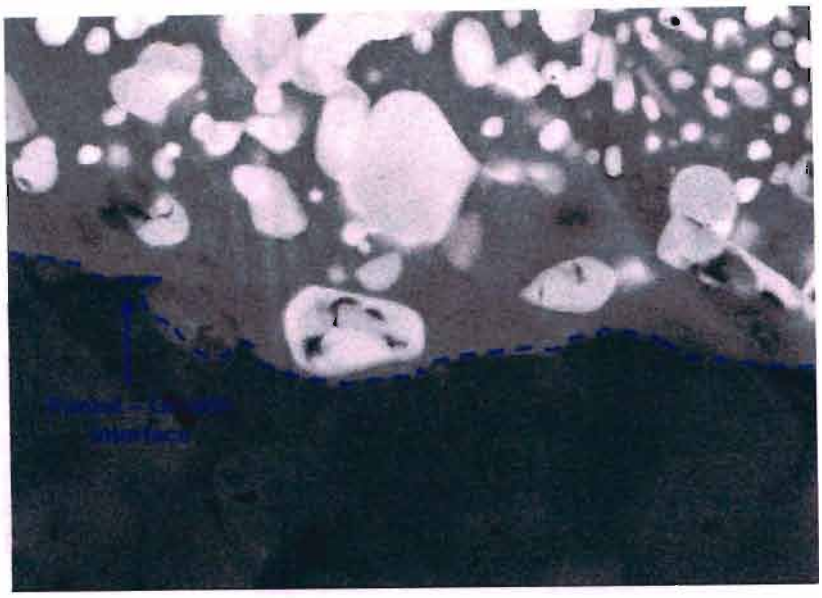

Figure 6.17: SEM image taken at X6500 magnification of Sample 2-B.

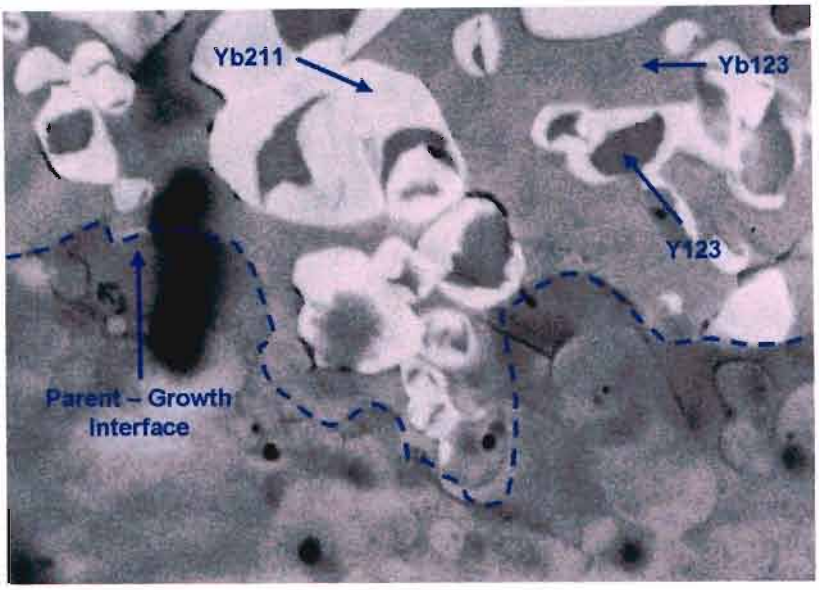

Figure 6.18: SEM image taken at X6500 magnification of Sample 2-C.

Energy dispersive X-ray analysis was conducted on the parent and joined sample. This analysis shows the chemical composition of the samples examined. From Figures 6.19 and 6.20, one can clearly see the composition of the parent and join respectively. In the composition of the join, we see that Ytterbium (Yb) replaces the Yttrium (Y) component in the parent material. Also, the presence of silver is also detected in the join.

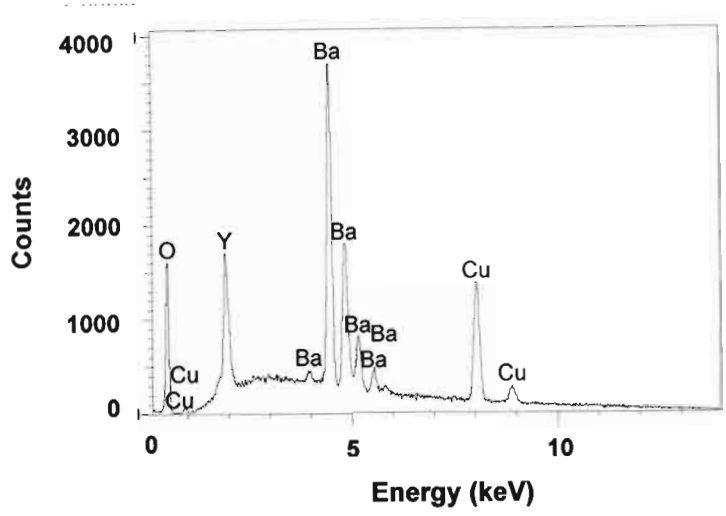

Figure 6.19: EDX scan of the parent sample showing the elemental composition.

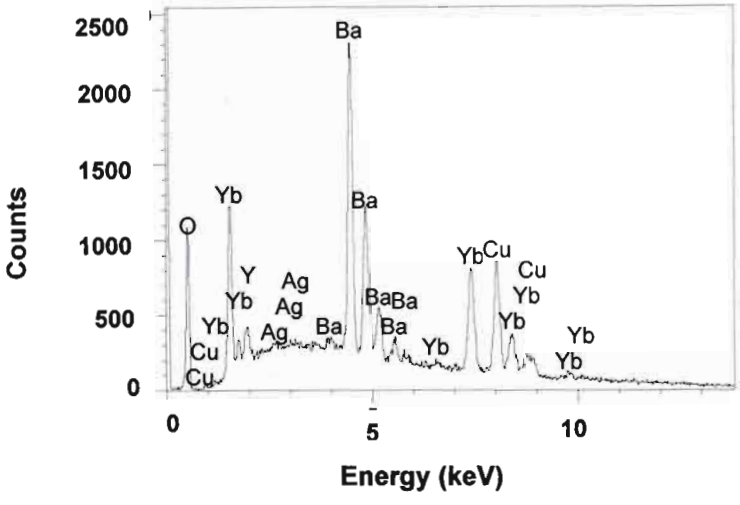

Figure 6.20: EDX scan displaying the elemental composition of the join.

The samples produced in Group 3 have the worst microstructure (Figure 6.21 – 6.22). Both samples are extremely porous. This could be attributed to two factors namely:

- insufficient holding duration which could have resulted in the solder not melting totally
- an inadequate amount of solder being applied to the join

It can be deduced that the temperature profile must be optimised based on the constituents of the solder.

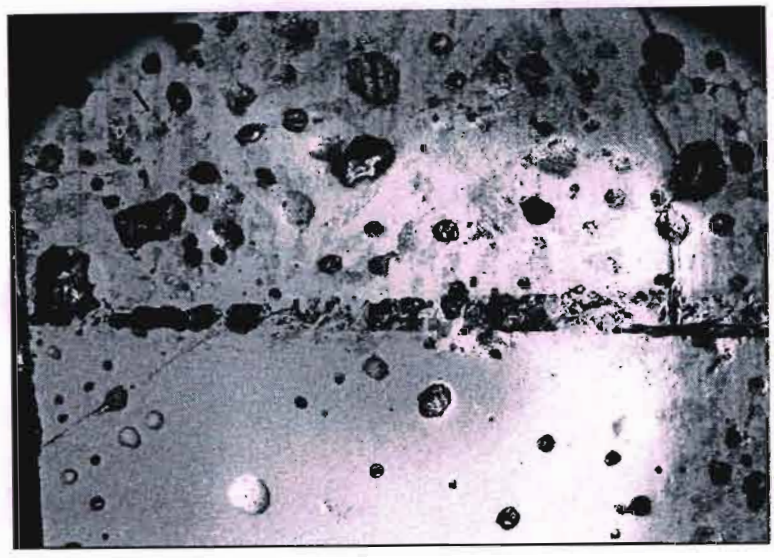

Figure 6.21: SEM image taken at X53 magnification of Sample 3-A.

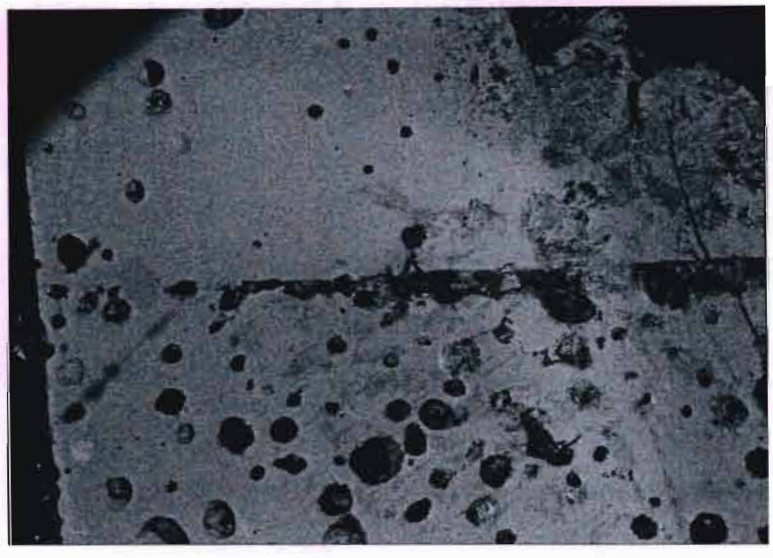

Figure 6.22: SEM image taken at X53 magnification of Sample 3-B.

6.2.1 Discussion of Microstructural Results

The microstructural investigation revealed some important results. A microstructural analysis generally can give a good indication of the transport quality of the sample. The features that help predict the quality are:

- voids and pores i.e. effective contact area
- degrees of misalignment between the a-b planes of parent samples
- distribution of Yb211 particles

- amount of non-superconducting material in the join

The texturing of the join is very different from the top seed melt texturing process used to manufacture the parent samples. In the TSMT process, a single seed/crystal forms a controlled nucleation point from which the parent textures while in the texturing of the join, the whole surface of the parent samples serve as multiple nucleation points. During this growth process, three interfaces are created as shown in Figure 6.23.

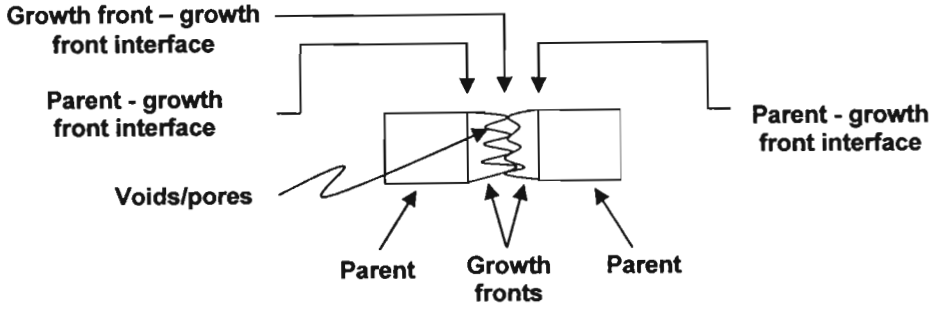

Figure 6.23: Formation of the interfaces during the process of joining.

The growth fronts formed are very irregular due to the actual texturing mechanism as well as the presence of Yb211 particles which change the local geometry of the growth front [49],[19]. Surface roughness of the parent will also contribute to the profile of the growth front. The growth front – growth front interface is also referred to as the impingement boundary [19]. Voids and pores are created in the impingement boundary when the irregular growth fronts meet as indicated by Figure 6.23.

From all the SEM figures, it can be seen that the parent – growth front interfaces are completely intimate with almost no presence of voids or pores. Ideally, this is how the impingement boundary should be. It is actually quite surprising that such a good bond is created since no melting of the parent surfaces occur. Many researchers believe that when the 'solder' melts into a liquid and solid phase, the liquid material dissolves the parent material and thus creates such a high quality bond [23],[25].

Figure 6.18 reveals the formation of small Y123 microstructures in the join area. The formation of these structures has also been noticed by Manton et al [13]. This phenomenon could be attributed to:

- solid state diffusion of Y atoms from the parent into the join during the processing of the joined sample or,
- when the sample is heated to 980 °C, the liquid that is trapped in the platelet boundaries is released and moves to the surface of the parent through capillary action. Thus, Y123 microstructures are created

These theories could also explain why such a good contact is created between the parent and the growth front without the melting of the parent material.

During the texturing process, Salama *et al* [49] found that the Yb211 particles and impurities generally move to the front of the growth front. This results in a large collection of non superconducting particles at the impingement boundary which affects J_c since it reduces the effective cross-sectional area. This is illustrated in Figure 6.24.

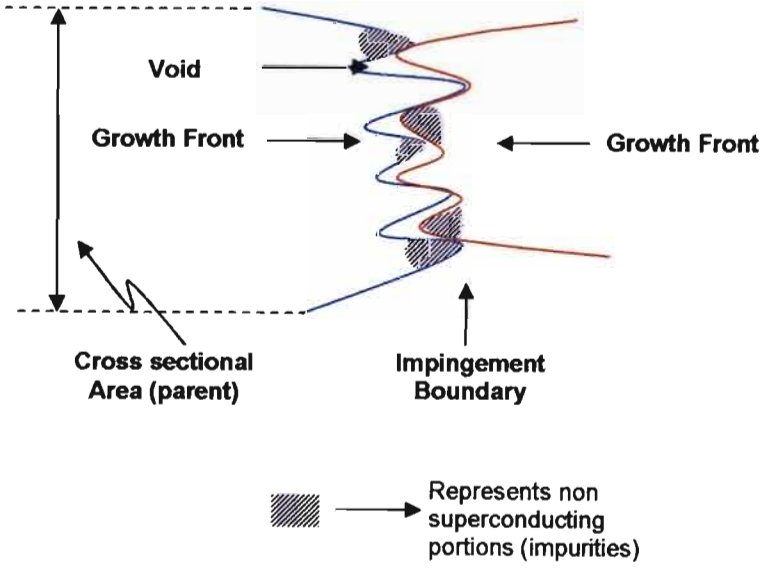

Figure 6.24: Representation of how voids and large collections of non-superconducting particles reduce the cross sectional area of the sample.

This explains why the J_c of the joined sample is generally lower than that of the parent. Thus, the addition of the non-superconducting particles (silver and Yb211) needs to be optimised.

The angle of misalignment between the parent a-b planes were estimated for Group 1 and Group 2 samples. It was found that a large degree of misalignment was present in all samples.

6.3 Transport Measurements

Transport measurements were conducted on each of the samples. The following tests were conducted:

- Resistivity vs. Temperature
- Voltage vs. Current
- Critical Current Density vs. Temperature

Each of these results are presented and discussed in this section.

6.31 Resistivity Vs. Temperature

A current of 200mA was passed through each of the samples and their resistivity values at different temperatures were recorded and plotted as shown in Figure 6.25 to Figure 6.31. These graphs prove that all the joined samples are superconducting and thus confirm that the joining technique is successful in providing a superconducting link between two bulk pieces.

As can be seen from Figure 6.26, there are two slopes that are present during the transition from the normal state to the superconducting state. This is because ytterbium superconducting solders have a lower critical temperature (approximately 89K) than yttrium (approximately 92 K). This second slope is not evident in Group 3 samples since yttrium was used as the solder material.

The second transition begins at a temperature which is greater than the T_c of Yb123. This could be due to the proximity effect where the superconductivity state of the solder is influenced by that of the parent. The critical temperatures (T_c) where

$$T_c = (T_{co} + T_{cf})/2 \tag{6.1}$$

and the transition widths (ΔT) were

$$\Delta T = T_{co} - T_{cf} \tag{6.2}$$

are shown in Table 6.1.

Transition widths are an indication of the quality of the sample. Narrow widths indicate that the oxygen in the samples is homogenously distributed. Although a sample can have a high T_c, the J_c can still be poor since it is also dependant on the cross sectional area of the sample.

Table 6.3: Values for T_{co}, ΔT and T_c for each sample.

Solder Group	T_{co} (K)	T_c (K)	ΔT (K)
Group 1 – Ytterbium solder – no silver			
Sample A	90.2	89.55	0.8
Sample B	90.42	90.21	0.42
Sample C	91.1	90.97	0.639
Group 2 – Ytterbium solder - silver			
Sample A	89.3	88.3	0.34
Sample B	90.7	90.3	0.65
Sample C	87.6	87.3	0.63
Group 3 – Yttrium solder - silver			
Sample A	91.33	90.7	1.22
Sample B	90.4	88.87	2.8

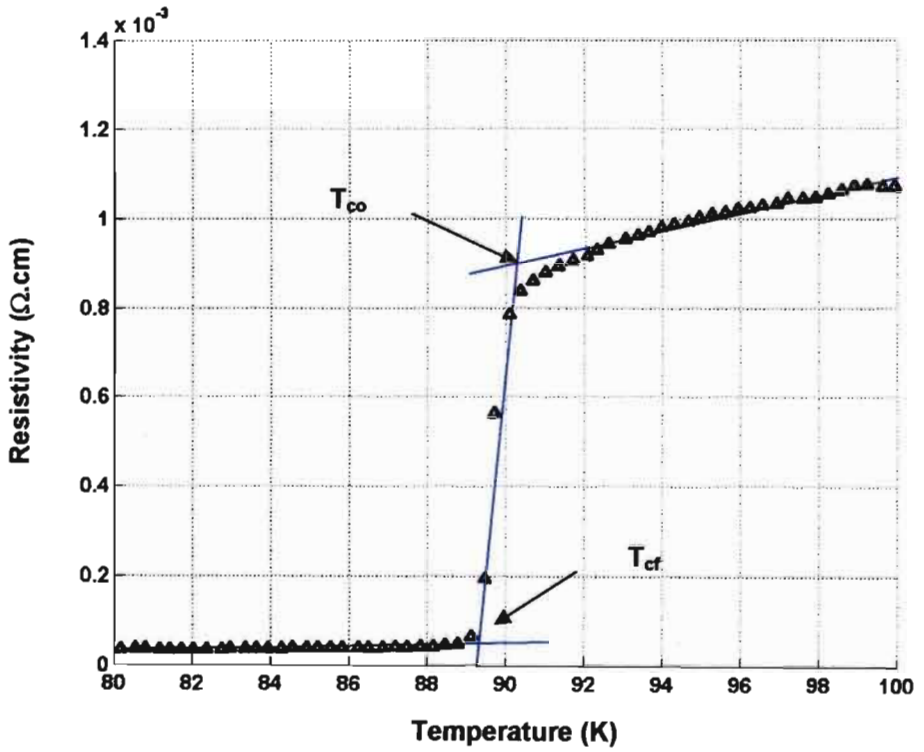

Figure 6.25: **Diagram showing how T_c and ΔT_c is calculated for a Sample 1-A.**

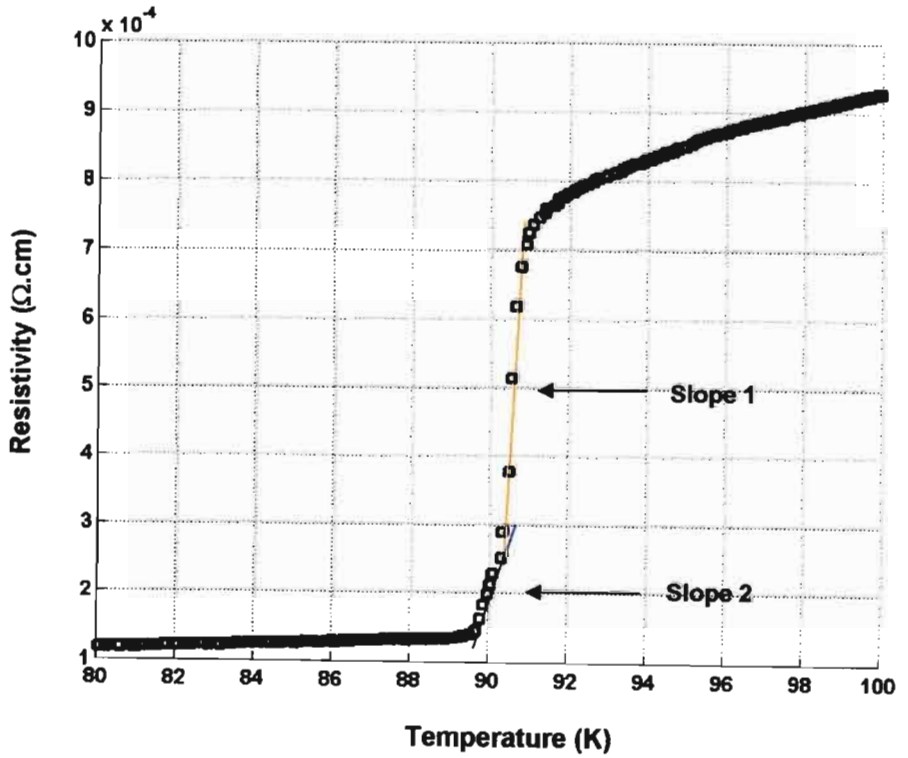

Figure 6.26: **Resistivity vs Temperature for Sample 1-B.**

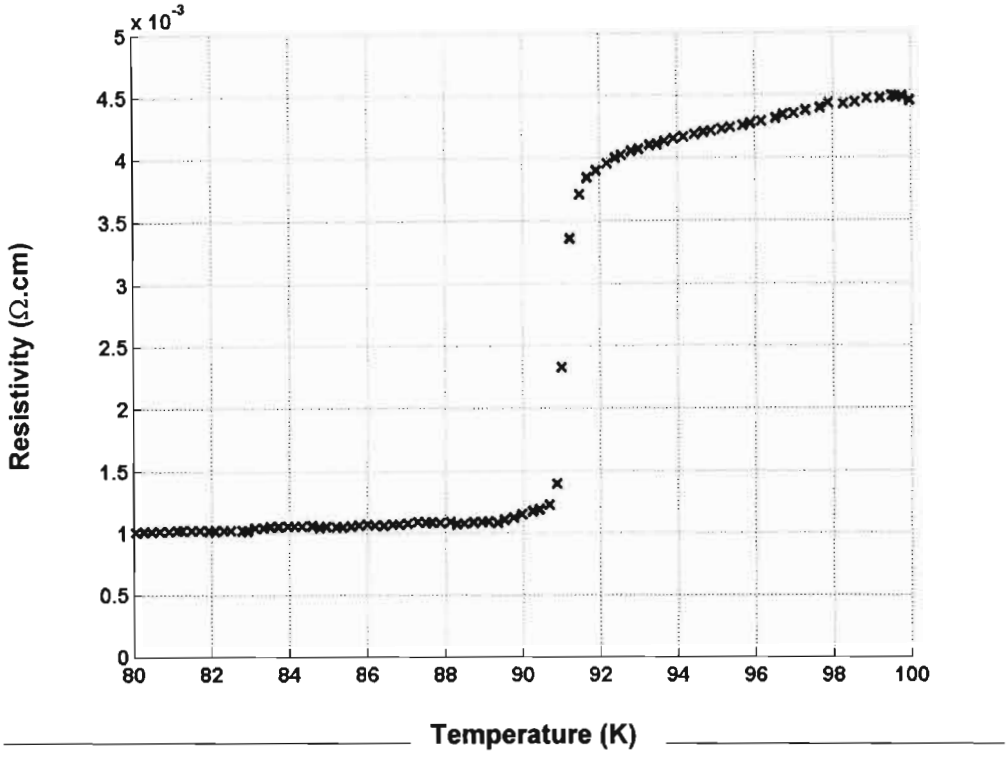

Figure 6.27: **Resistivity vs Temperature Graph for Sample 1-C.**

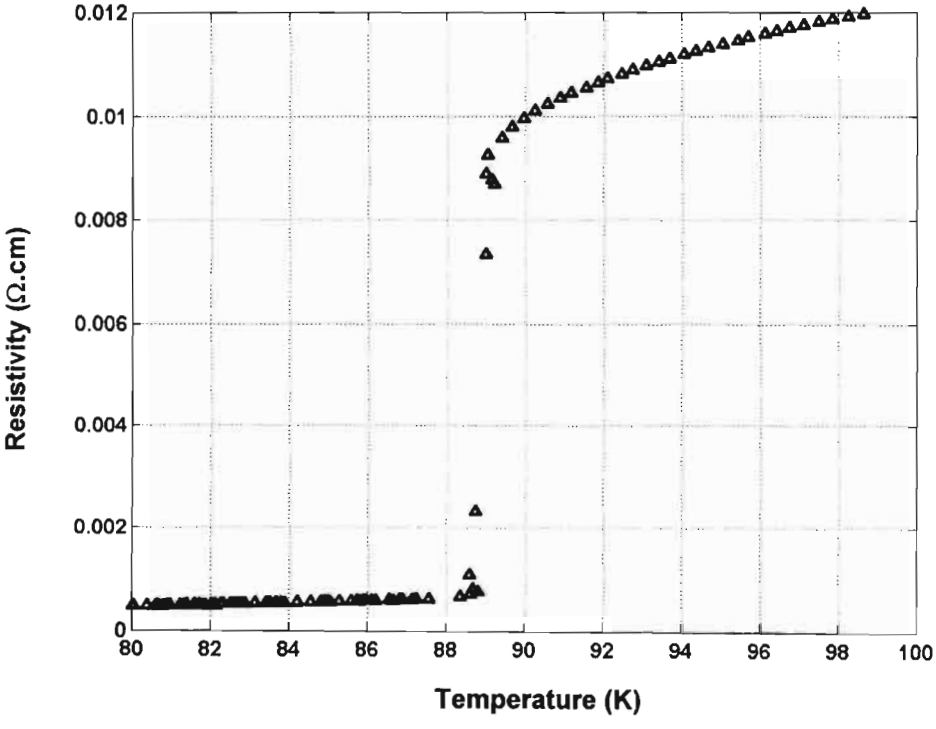

Figure 6.28: **Resistivity vs Temperature graph for Sample 2-A.**

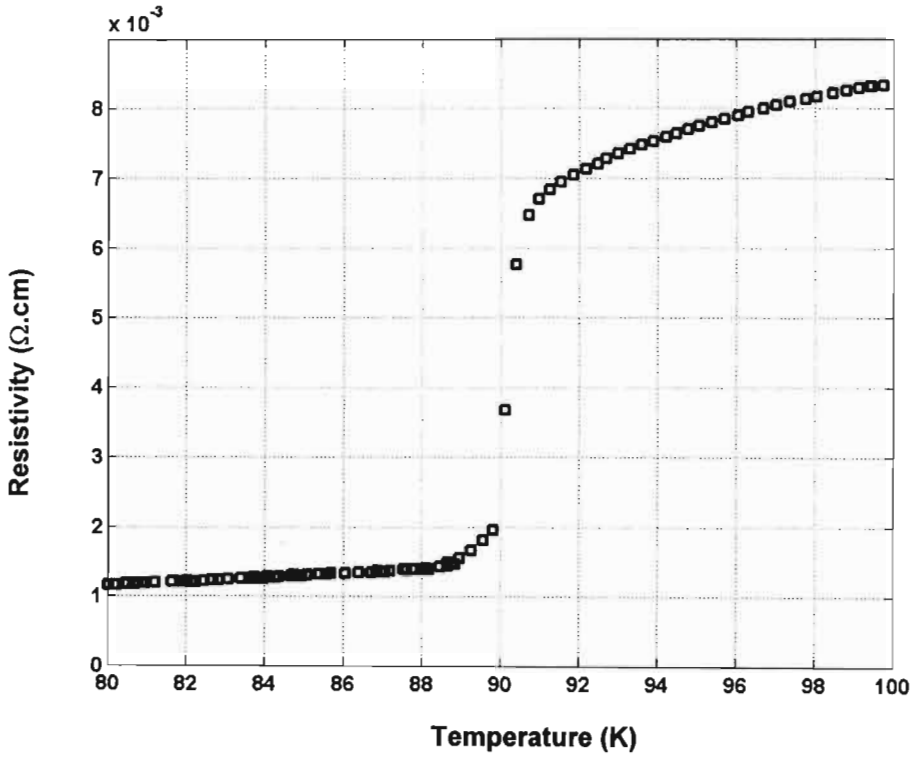

Figure 6.29: **Resistivity vs Temperature graph for Sample 2-B.**

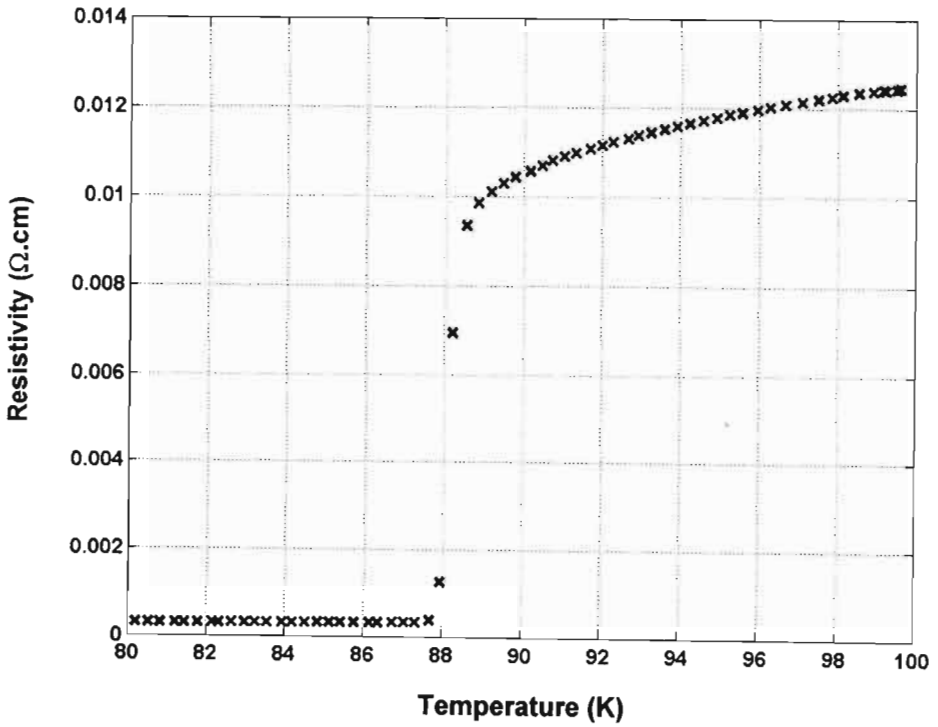

Figure 6.30: **Resistivity vs Temperature graph for Sample 2-C.**

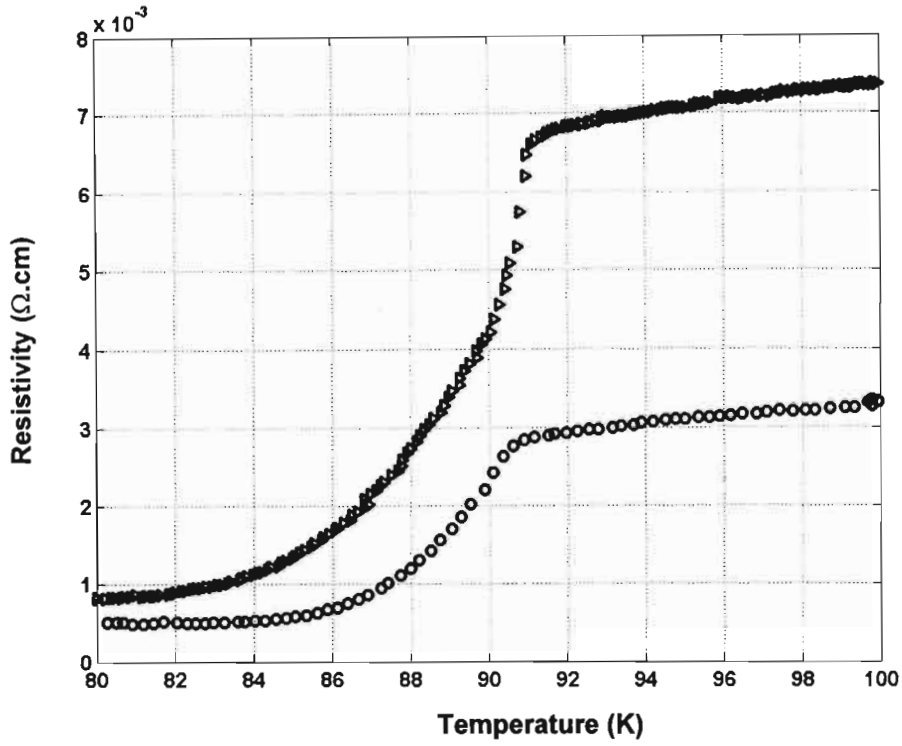

Figure 6.31: Resistivity vs Temperature graph for Samples 3-A and 3-B.

6.3.2 Voltage vs Current and Critical Current Density Vs Temperature

The first step in calculating the critical current density is to first plot the voltage-current characteristic of the samples. This was obtained by cooling the sample down to the chosen temperature and passing different currents through the sample and noting the voltage generated across the sample. From these voltage vs current graphs displayed in Figure 6.32 to Figure 6.34, Figure 6.36 to Figure 6.38 and Figure 6.40 to Figure 6.41, one can easily note the point at which the material transcends from a superconducting to a non-superconducting state. This point is known as the critical point and the critical current density (J_c) is calculated by dividing the current at this point by the cross sectional area of the sample Figure 6.35 contains the J_c graph of Group 1, Figure 6.39 displays the J_c graph of Group 2 and Figure 6.42 shows the J_c graph of Group 3 samples.

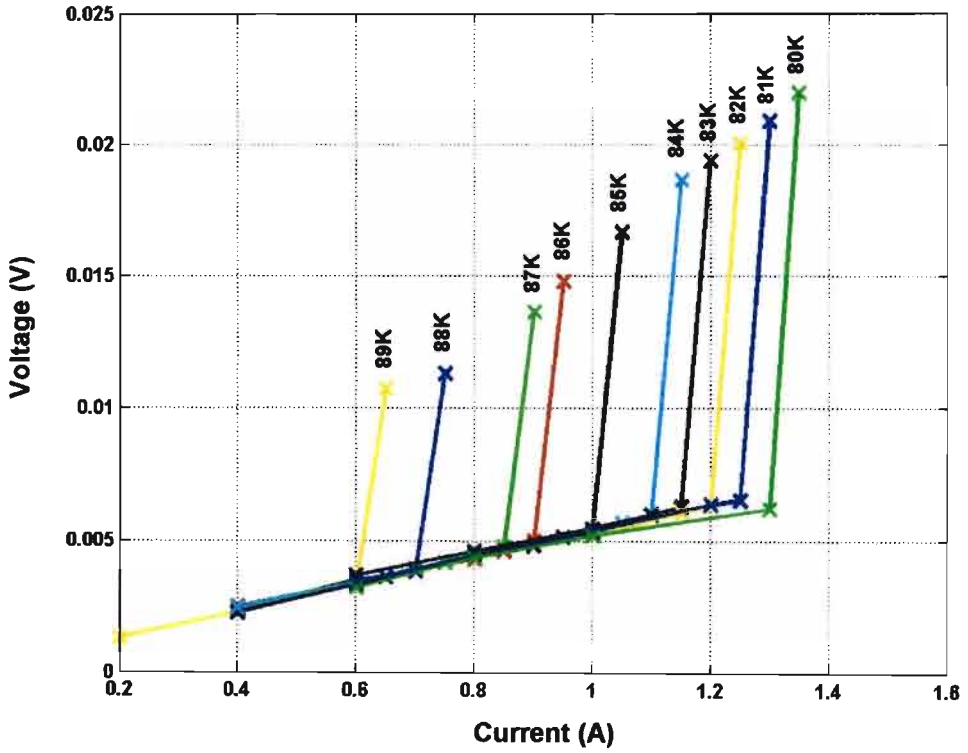

Figure 6.32: **Voltage vs Current for Sample 1-A.**

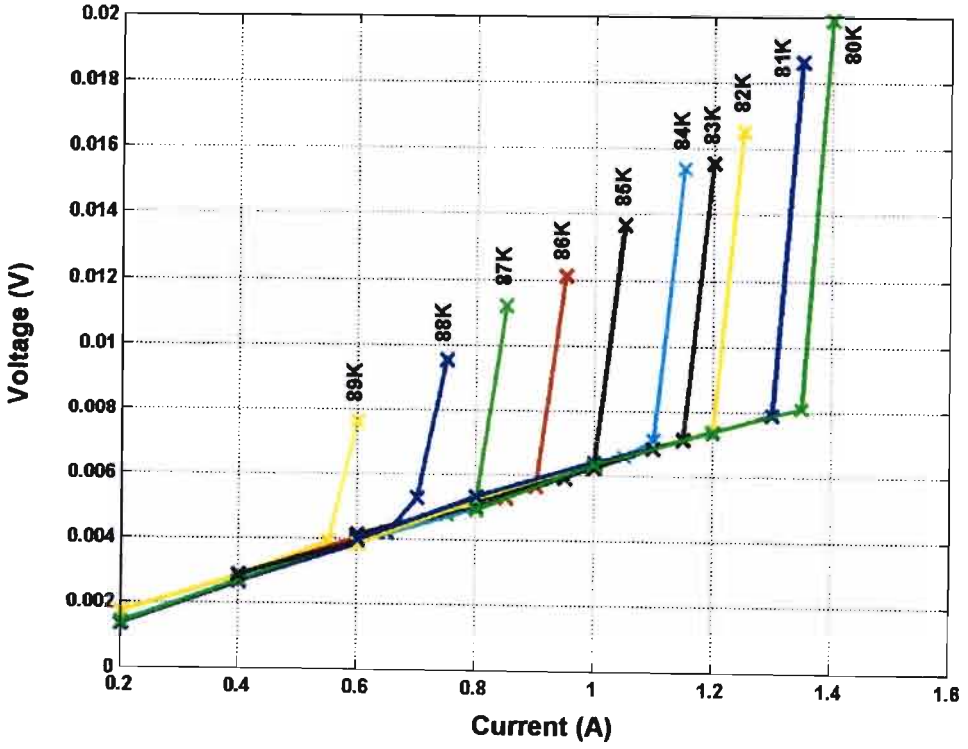

Figure 6.33: **Voltage vs Current for Sample 1-B.**

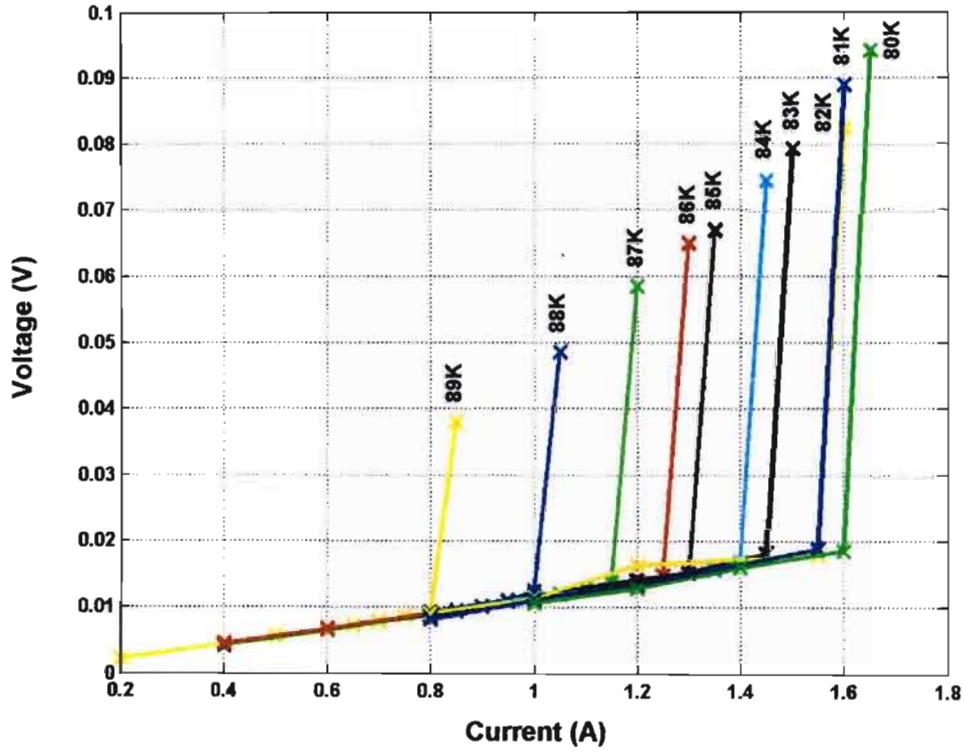

Figure 6.34: **Voltage vs Current for Sample 1-C.**

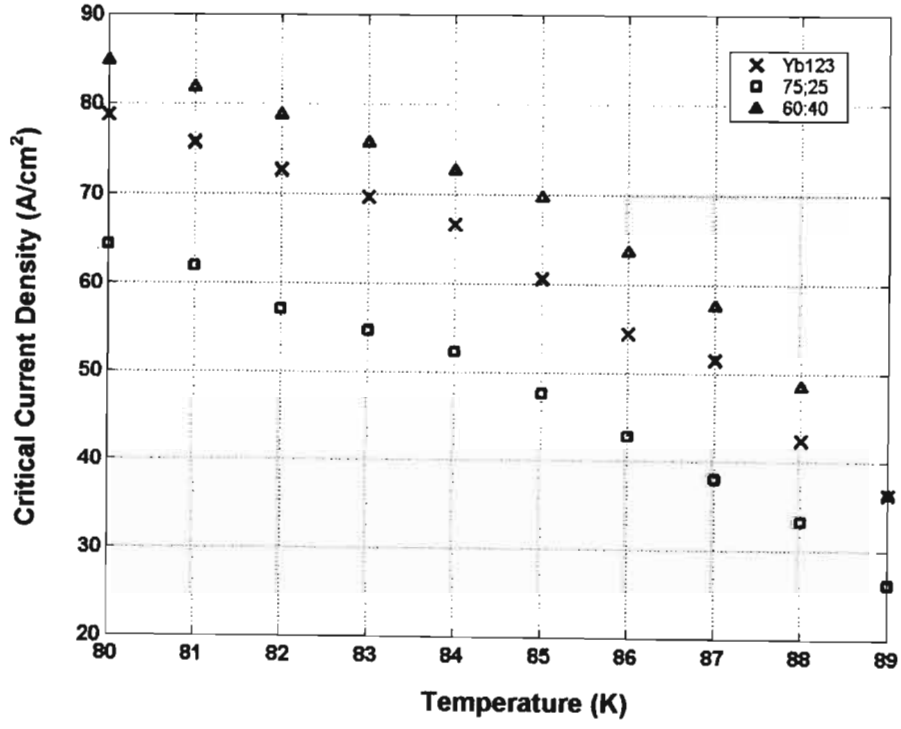

Figure 6.35: **Critical current density graph for Group 1.**

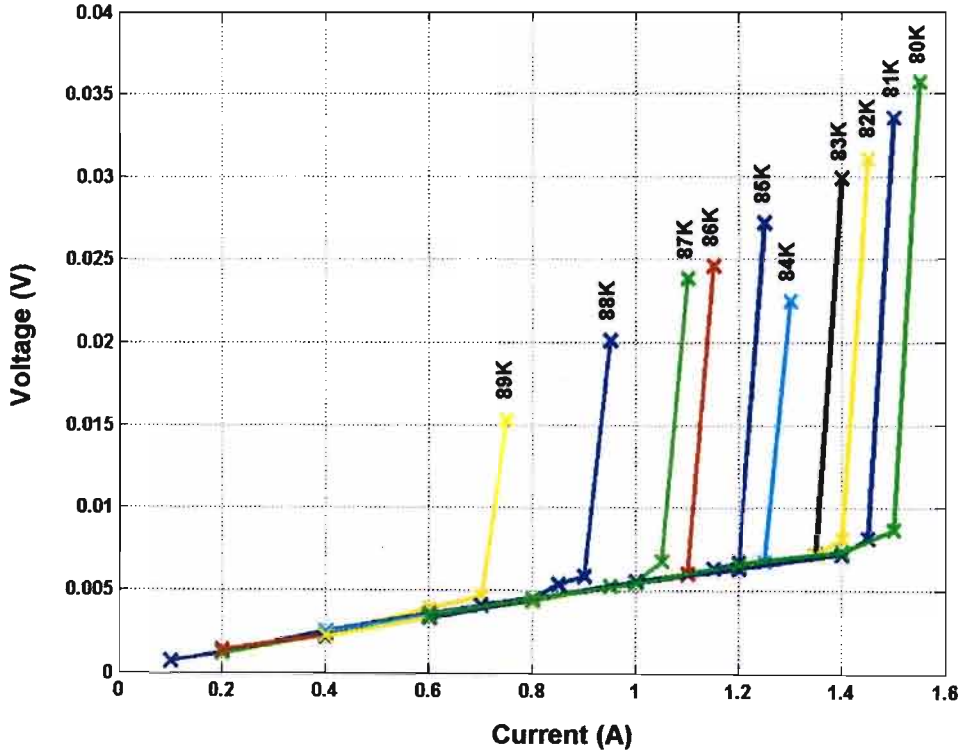

Figure 6.36: **Voltage vs Current for Sample 2-A.**

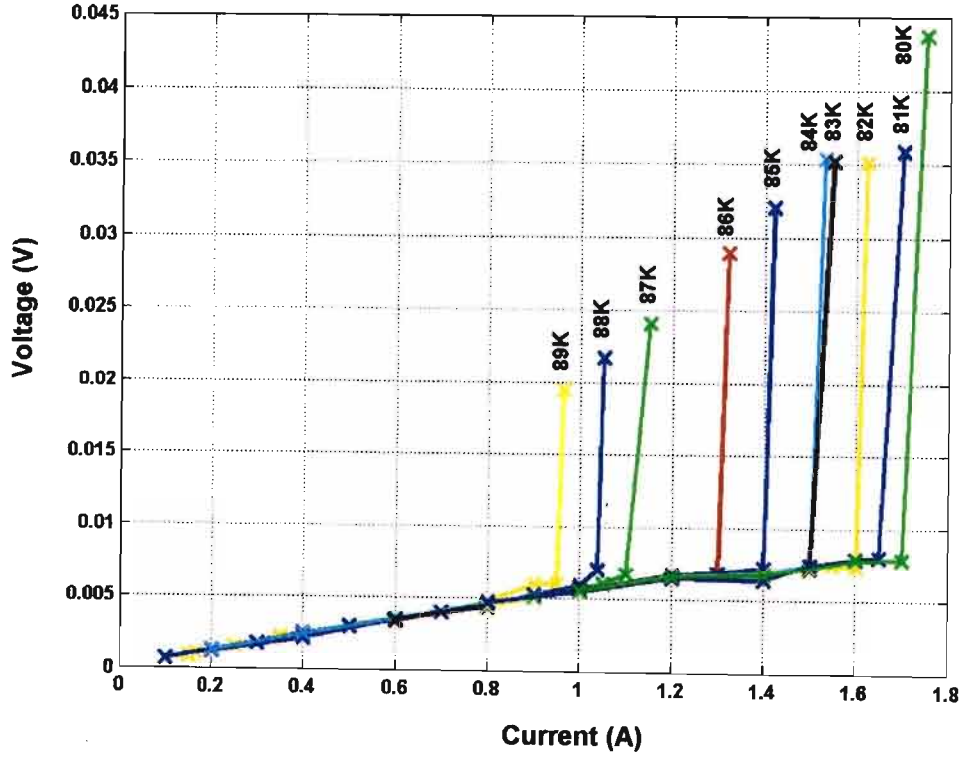

Figure 6.37: **Voltage vs Current for Sample 2-B.**

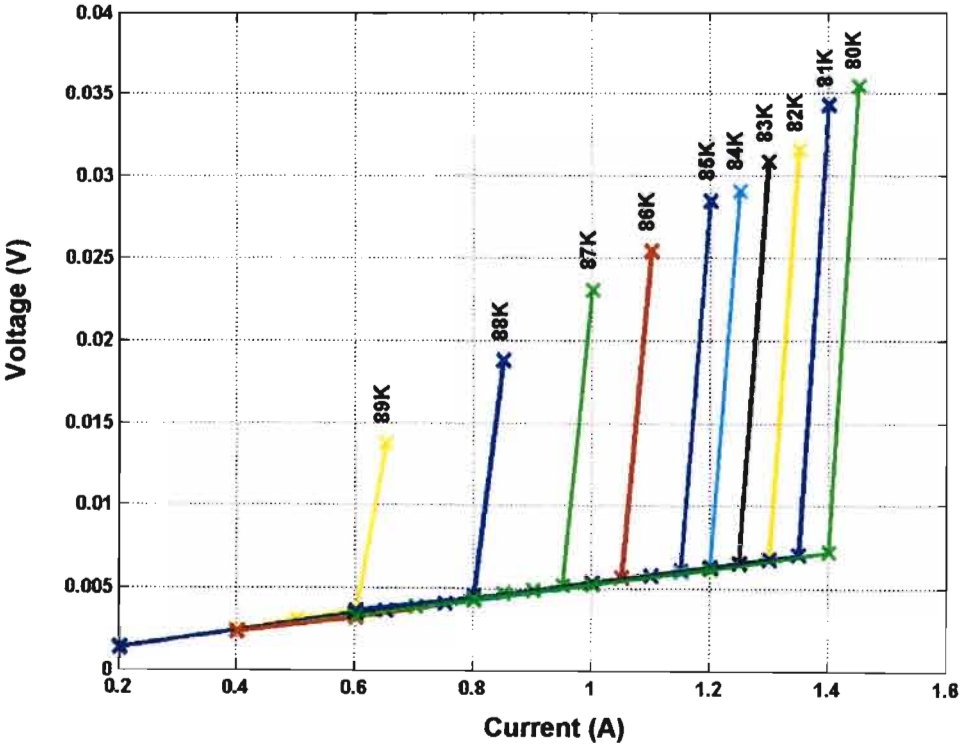

Figure 6.38: **Voltage vs Current for Sample 2-C.**

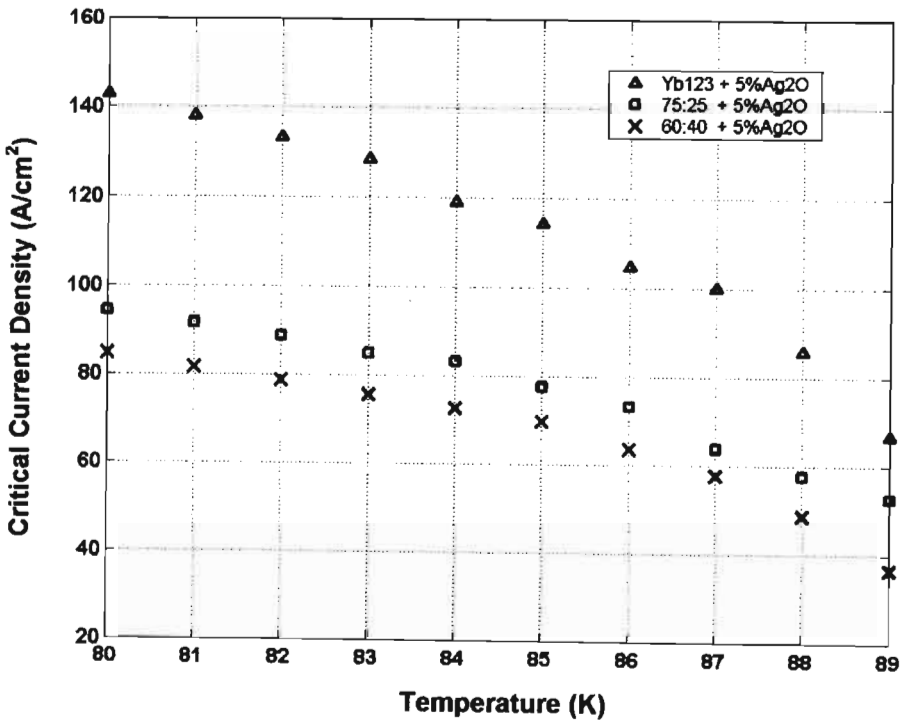

Figure 6.39: **Critical current density graph for Group 2.**

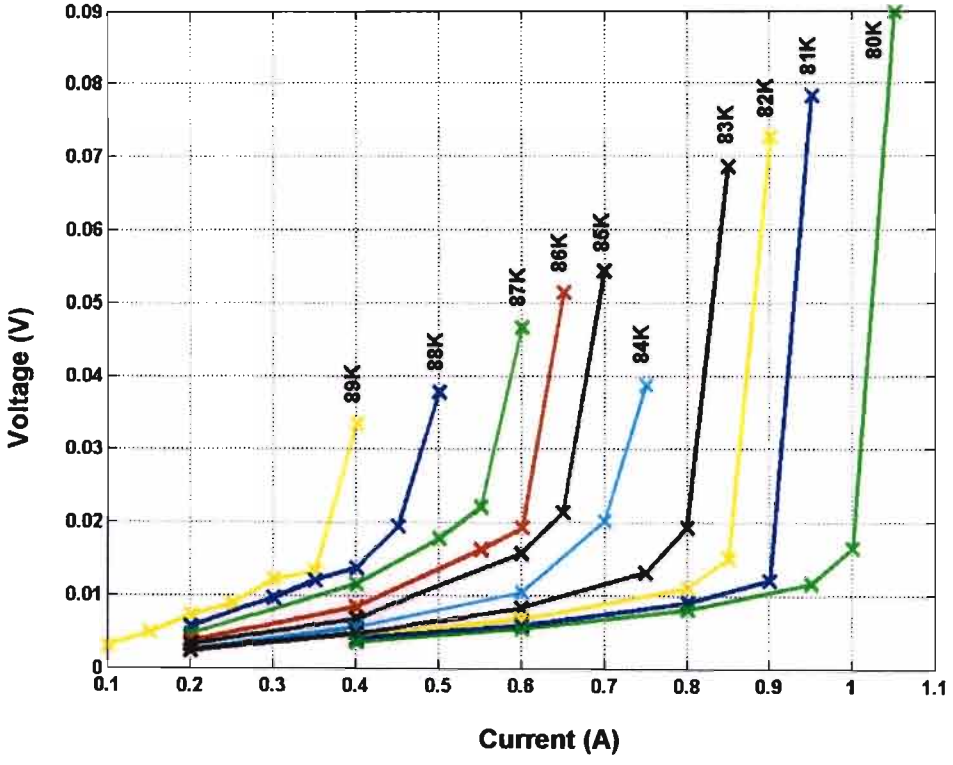

Figure 6.40: **Voltage vs Current for Sample 3-A.**

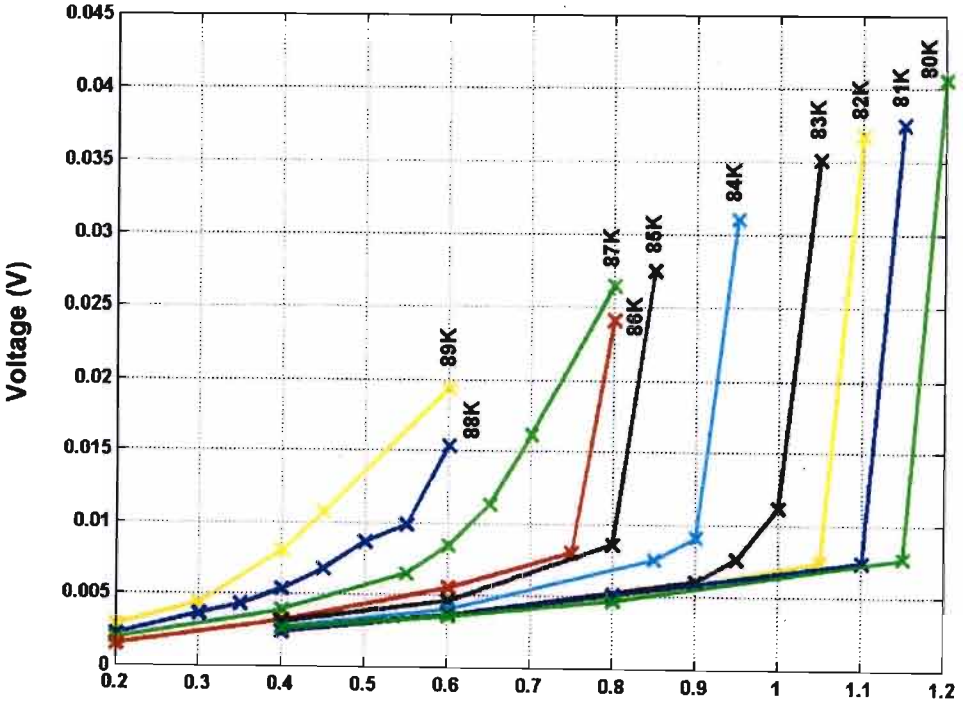

Figure 6.41: **Voltage vs Current for Sample 3-B.**

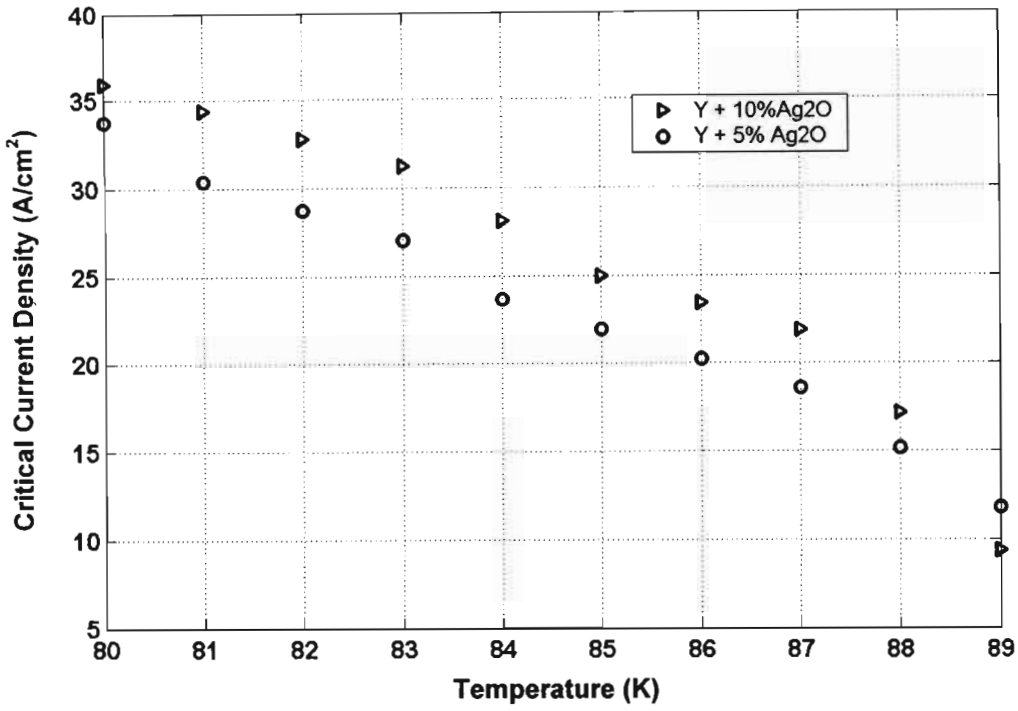

Figure 6.42: Critical current density graph for Group 3.

6.3.3 Discussion of the Transport Analysis

The resistivity vs temperature graphs, Figure 6.25 to Figure 6.31, show that all the samples were superconducting after joining. This proves that the joining technique used was successful in producing a superconducting seam between two high temperature superconductors. The J_c curves for each group of samples were plotted. From these results, it can be seen that Sample 2-A (Yb123 + 5%Ag_2O) has the highest J_c of about 142 A/cm^2 at 80 K while Sample 3-A (Y + 5%Ag_2O) had the lowest J_c of approximately 37 A/cm^2. These values are approximately two decades off when compared to the values obtained by other researchers [19], [20] and [25]. Shi et al [20] obtained a J_c of approximately 2000 A/cm^2 using the solid state diffusion method of joining. Noudem et al [15] acquired a J_c of approximately 12 kA at 77 K. Reasons as to why such a discrepancy in J_c was obtained in this research are:

- Reduced cross sectional area – As explained in Section 6.2.1, the voids and collection of non-superconducting particles at the impingement boundary severely reduces the cross sectional area of the joined sample and hence J_c.

- Damage of the join structure during sanding – The only current source that was available for this research could supply a maximum of 4 A. This current is very low

relative to the current carrying capability of the superconducting samples thus, the joined samples had to be sanded down considerably to reduce the cross sectional area of the sample. This sanding process could have damaged the microstructure of the seam which will therefore reduce the J_c.

- Large degree of misalignment between the parent samples – Dimos et al [59] found that J_c reduces by a factor of 1/(degree of misalignment) for angles less than 20°. For angles greater than 20°, the factor saturates at 1/50. Thus, due to the high degree of misalignment between the parent samples, J_c was severely reduced. If the J_c value obtained for Sample 2-A and Sample 3-A are multiplied by 50, their J_c values increase to 7100 A/cm^2 and 1850 A/cm^2 respectively. These adjusted values of J_c are in the range of results achieved by others [20].

- Poor oxygenation of the samples – According to [52], when heat processing of superconductors is carried out in air, which has 20% oxygen and 80% nitrogen, a large amount of nitrogen atoms can become trapped in the material, thus it was decided to carry out the heat treatment in a flowing oxygen environment. An assumption was made that since the heat processing of the joined sample was carried out in the flowing oxygen, the oxygenation period can be reduced. Thus an oxygenation period of 40 hours was selected. Other researchers have oxygenated for periods between 100 – 400 hrs [50]. It can be deduced that the samples may not be sufficiently oxygenated.

The effect of silver doping was also investigated. Jin et al [60] discovered that 10 % wt silver doping increased the zero field intergranular current by a factor of 3 at 77 K for polycrystalline Y123. The improvement that silver has on melt textured joins is seen clearly in Figure 6.35 and Figure 6.39. It is interesting to note that when 5% wt Ag_2O is added to Yb123, it produces the highest J_c of all the samples and yet plain Yb123 solder was only second best in Group 1 samples. This can be explained by the fact that Sample 2-A had the optimum number of non-superconducting material relative to the other samples and thus performed the best. As expected in Group 3, Sample 3-B, which has a higher quantity of silver, performed the best. The reason as to why the J_c values are so low in Group 3 as compared to the other two groups could be attributed to:

- poor melting of the solder

- too little solder being used

6.4 Field Mapping

6.4.1 Results

The parent sample was exposed to the same heat treatment that was used to texture the joined sample. This was conducted to investigate the effect of the heating on the parent material. It was found that the parent sample could only trap about 68 % of the field that it could trap prior to the heating process (Figure 6.43 and Figure 6.44). This could be attributed to poor oxygenation. The field plot captured for the joined sample is presented in Figure 6.45 and Figure 6.46

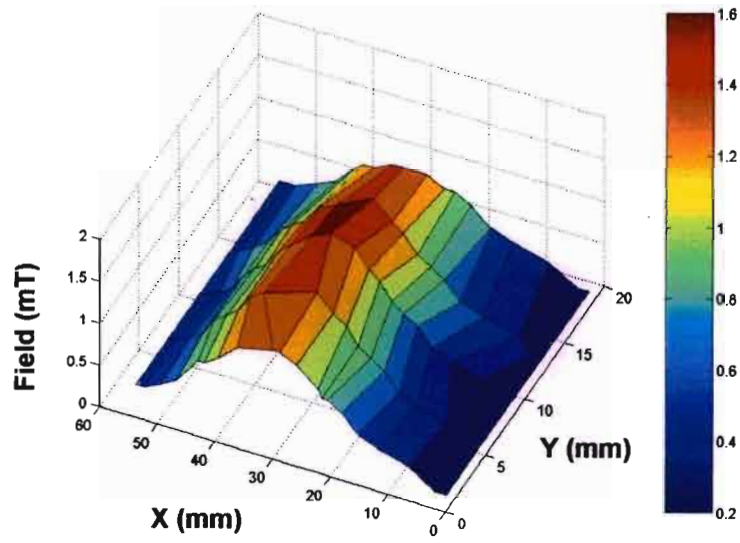

Figure 6.43: Field plot of the parent sample before heating.

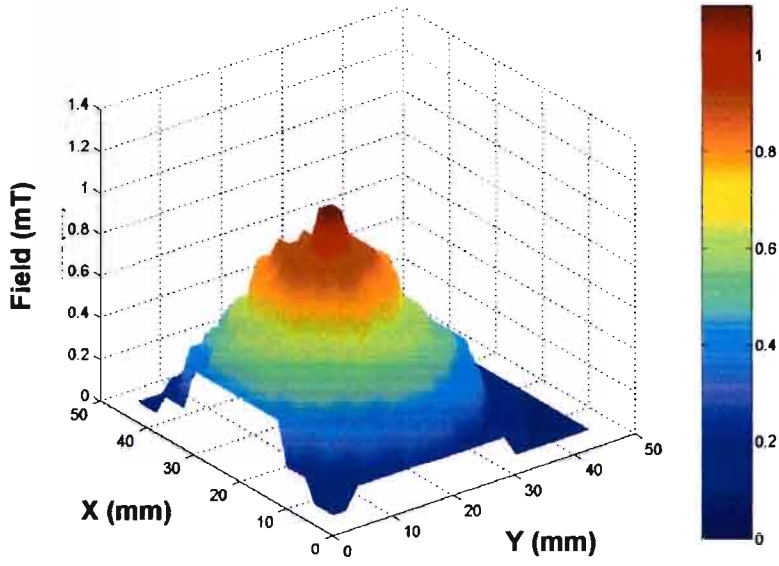

Figure 6.44: **Field plot of the parent sample after heating.**

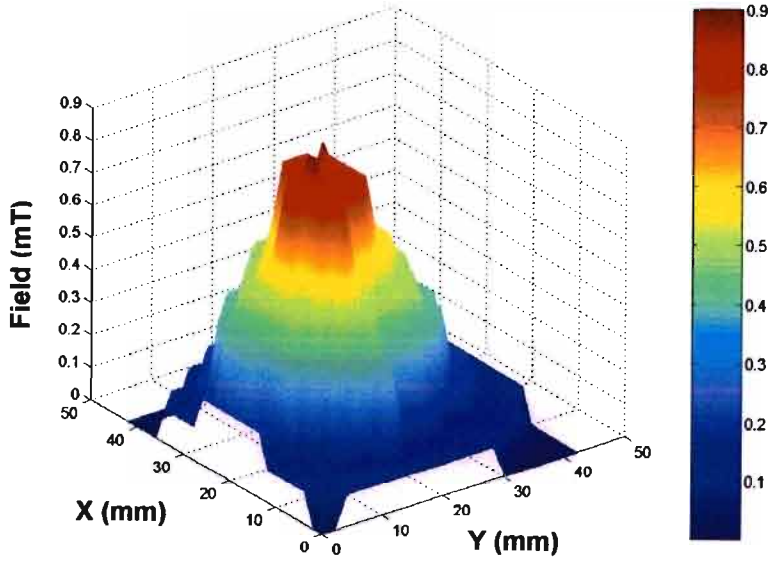

Figure 6.45: **Field plot of the joined sample.**

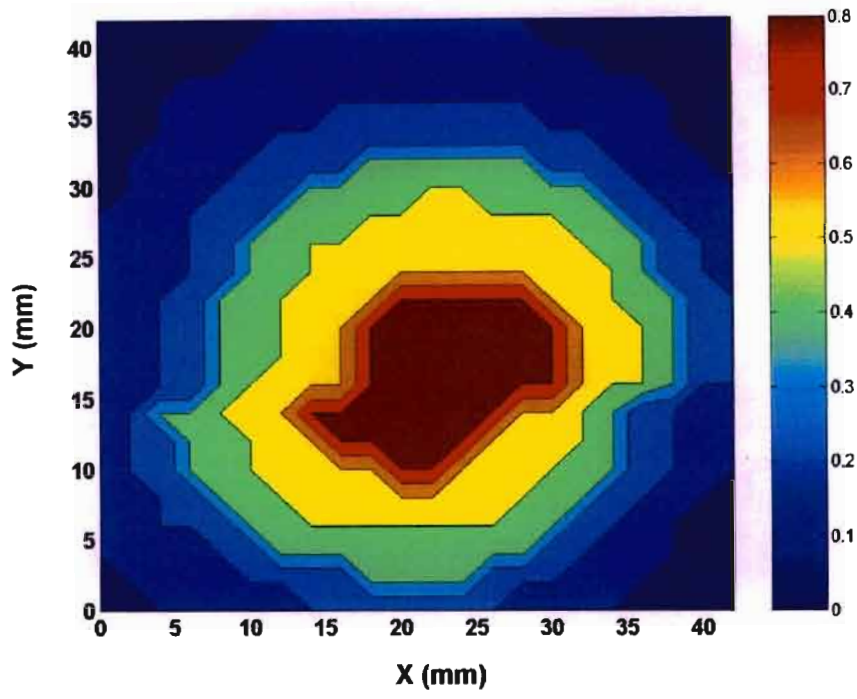

Figure 6.46: **Field contours of the joined sample.**

From the results obtained, one can assume they are correct based on the fact that if both pieces of the superconductor did not join properly, then each individual piece would set up its own screening currents resulting in a depression at the centre of the field plot (Figure 6.47). This assumption however could be incorrect based on the alignment of the c axis and the applied magnetic field. This is discussed further in section 6.4.2.

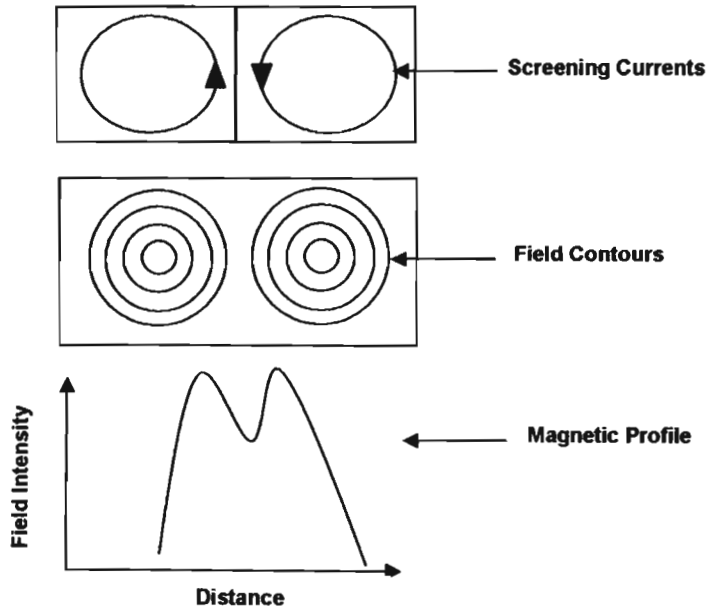

Figure 6.47: **Representation of how screening currents affect the magnetic profile of joined samples.**

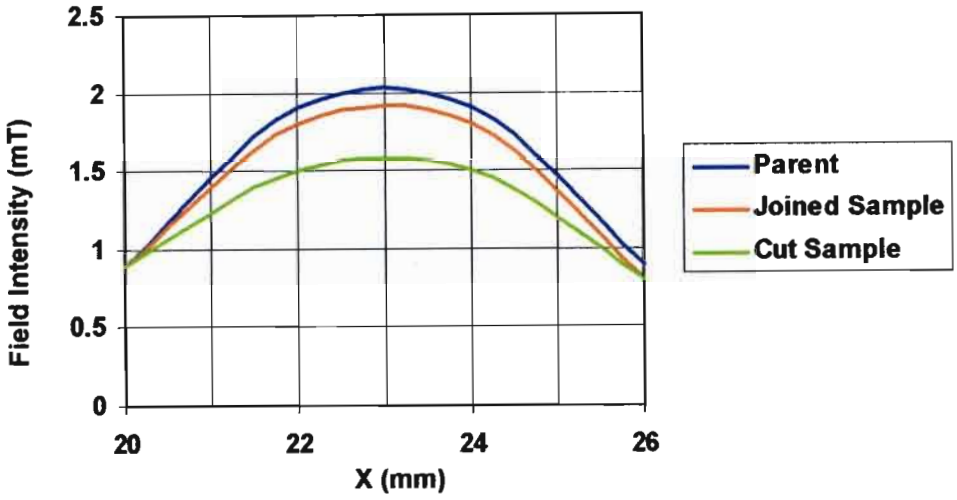

Figure 6.48: Magnetic Profile of Parent, Cut and Joined Samples.

The magnetic profile shown in Figure 6.48 was obtained by scanning across each sample. The parent sample is cut and placed together to obtain measurements for the cut sample. The hall probe was ~ 10mm closer to the sample in this measurement. It can be seen that the joining procedure was able to restore the trapped field to approximately 95% of the original trapped field of the parent. A similar result was obtained by Mukhopadhyay et al [14]

6.4.2 Discussion of Magnetic Measurements

It is important to be able to correctly interpret the results obtained from field measurements. As shown by Vanderbemden et al [25], the results obtained can be very misleading. Vanderbemden [25] joined two single domain superconducting samples together using GE varnish (General Electric Varnish) which implies that there was no superconducting link between the two samples. Various configurations of the c axis (parallel to join and perpendicular to the join) were tested with the magnetic field always kept parallel to the join. The configurations with their field profile are presented in Figure 6.49.

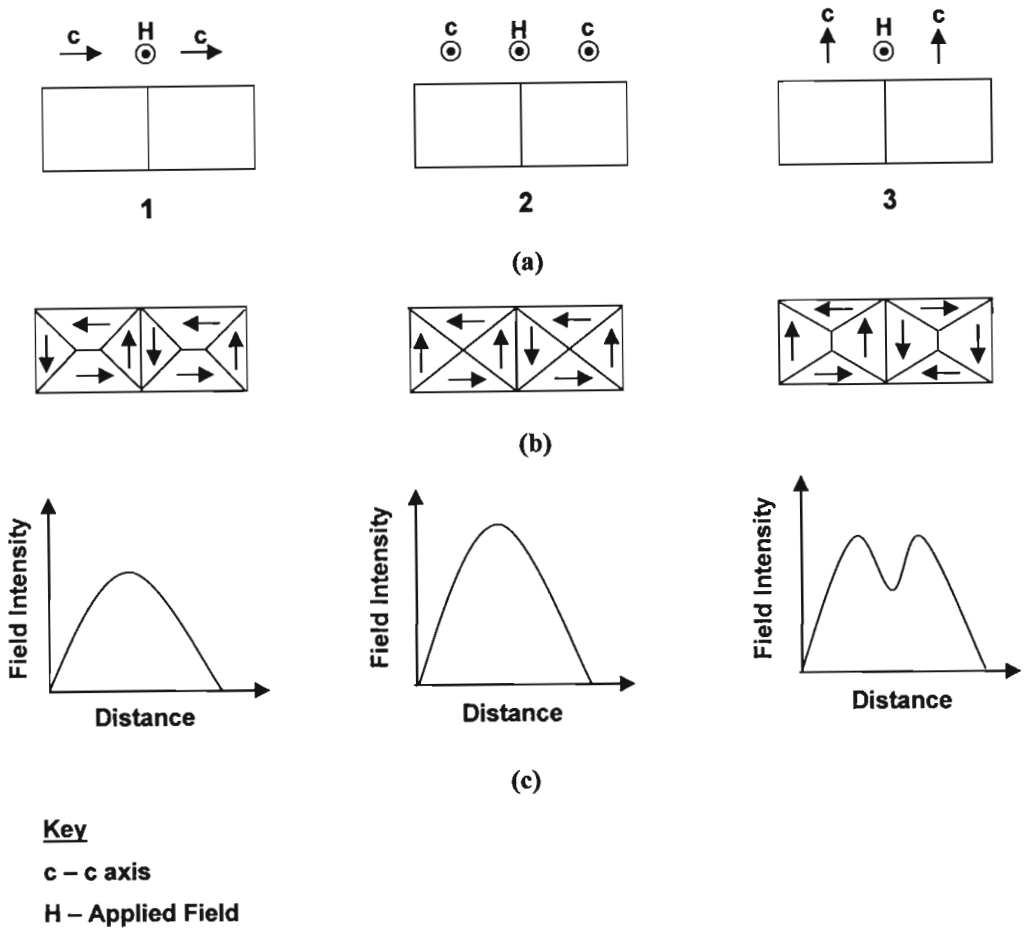

Figure 6.49: **(a) Configuration showing the direction of the c axis and magnetic field used for the experiment [25].**

(b) Current loops from each configuration [25].

(c) Field Profiles of each configuration [25].

The profiles obtained for configuration 1 and 2 indicate that the join between the samples is superconducting which is false. The field profile obtained from configuration 3 is correct indicating a depression of the field across the join. This is explained using the current flow in each configuration which is indicated in Figure 6.49 (b).

It was shown that a lack of good resolution of the hall probe used for the magnetic experiments could provide misleading results [25]. Vanderbemden et al [25] explains that the correct result was obtained using configuration 3 due to the relatively larger current sheets in the area of the join. The configuration used in this thesis was configuration 2. The graph in Figure 6.48 clearly illustrates that the joined sample is much better than the cut sample proving that there must have been a superconducting link for this to be possible.

6.5 Conclusion

In this chapter, the results obtained from the microstructural, magnetic and transport investigations were presented and discussed.

Chapter 7

Conclusion

Currently, large single domain HTS cannot be easily manufactured due to the difficulties experienced during texturing. This problem prevents more widespread use of HTS in magnetic levitation applications such as flywheel storage systems and magnetic trains. In these applications, the diameter of the levitational force is directly proportional to the bearing hence the importance of creating large superconducting bearings.

Research has been conducted to investigate various joining techniques. There are basically two methods of joining, namely:

- joining without using an external soldering agent
- joining using an external soldering agent

This research investigates the joining of melt textured Y123 bulk samples (parent) using the latter technique. The external soldering agent was created using a superconducting powder with a lower peritectic temperature than the parent material. Yb123, Yb211, Y123 and Ag_2O powders were utilised to develop eight solders to investigate this joining technique.

Microstructural, magnetic and transport analyses were conducted on each of the samples to assess the quality of the join. These results are presented and discussed in Chapter 6.

The microstructural analysis was conducted using a SEM and an optical microscope. It was found that there are three interfaces created during the texturing of the join:

- the interfaces between the parent samples and the growth front that develops from each parent face
- the interface called the impingement boundary created by the joining of the two growth fronts

The interface between the parent and the growth front was of excellent quality without the presence of any microstructural defects. This is actually quite surprising since no melting of the parent sample occurs during the heat treatment of the join. Some researchers believe that such intimate contact between the parent and the growth join is achieved due to dissolution of the parent face by the liquid phase created during the texturing of the solder.

In a few samples, small Y123 structures are found a small distance away from the actual parent interface. This research attributes the cause of this occurrence to solid state diffusion of the parent atoms or dissolution of trapped liquid at the platelet boundaries. It also provides reason for the formation of a relatively good seam between the parent and the growth front.

The effect of the addition of Yb211 particles to the join was investigated. It was found that addition of Yb211 particles to the solder helps in creating a more even distribution as well as a smaller Yb211 particle size. It was also noticed by [19] that Yb211 particles increase the viscosity of the solder. It was observed that silver has the ability to lower peritectic temperature as well as clean out the grain boundaries of impurities which improves the J_c of the sample [52].

Transport measurements posed a challenge due to the high J_c values. The cross-sectional area of the joined sample was first reduced in order to measure J_c. It was found that Sample 2-A (Yb123 + 5% Ag_2O) had the highest current carrying capability of approximately 142A/cm^2 while Sample 3-A (Y + 5% Ag_2O) had the lowest J_c of approximately 37 A/cm^2. The reasons for the low J_c could be attributed to:

- large misalignment between the a-b planes of the parent sample
- reduced cross-sectional area of the joined sample due to the large amount of microstructural defects
- poor oxygenation of the joined samples

Resistivity vs. Temperature graphs were plotted and these proved that the joined samples were superconductive. Thus, it was proven that a superconducting link could be established using joining techniques.

A field map of both the parent and a sample joined with Yb123 + 5% Ag_2O were captured using a rare earth magnet to trap the magnetic field and a hall probe to measure the trapped

flux across the sample. This experiment was conducted at 77 K. It is important to note that these were oxygenated for about 100 hours as opposed to all the previous samples which were oxygenated for only 40 hours. The parent sample underwent the same heat treatment as the joined sample to investigate the effects the heating had on the quality of the sample. It was found that the parent sample could only trap about 68% of the field that could be trapped by the parent prior to heating. This could imply that the oxygenation period of 100hrs was not sufficient (under oxygenation) or it could be too long (over oxygenation). The reduction in the performance of the parent could also be attributed to other mechanisms that occur when the sample is heated.

From the magnetic measurements, it was found that no depression of J_c could be measured across the join. One cannot use this result to conclusively prove that the join is superconductive as the results obtained are dependent on the orientation of the c axis relative to the join and to the applied magnetic field. A single scan of the hall probe across the joined, parent and cut samples reveals that joining of the samples was successful in restoring approximately 95% of the trapped field. This result thus confirms that the samples are joined and that the join is superconducting.

From these results, one can conclude that joining HTSC bulk pieces is possible using an external 'soldering' agent.

The following recommendations are provided for future work in this area of research.

- Conduct transport measurements using a higher current source. This removes the sanding process prior to measurements since sanding could negatively impact the results.

- Adjust temperature profile to reduce maximum heating temperature when using solders that contain silver as silver reduces the peritectic temperature of the solder. This will prevent the solder from becoming too fluid in nature and thus flowing out from the join during the melt texturing phase.

- The 1μV criterion should be used to measure J_c. This is the standard that is used by most researchers. It becomes necessary to use the same standard to allow a comparison of results with previous work.

References

1. Izumi t, Nakamura Y, Sung T H, and Shiohara Y, J. Mater. Res, 1992. 7: p. 801.
2. Onnes H K, Commun Phys Lab, 1911. 12: p. 120.
3. Meissner W and Oschenfeld R, Naturwiss, 1933. 21: p. 787.
4. London F and London H. *The electromagnetic equations of a supraconductor.* in *Proc. R. Soc A.* 1935.
5. Ginzburg V L and Landau L D, Zh. Eksp. Toer. Fiz (In Russian), 1950. 20: p. 1064.
6. Bardeen J, Cooper L N, and Schreiffer J R, *Theory of Superconductivity.* Physics Review, 1957. 108: p. 1175-1204.
7. Bednorz J G and Muller K A, *Possible High Tc Superconductivity in Ba-La-Cu-O systems.* Zeitschrift Fur Physik B - Condensed Matter, 1986. B64: p. 189-193.
8. Wu M K, Ashburn J R, Torng C J, Hor P H, Meng R L, Gao L, Huang Z J, Wang Y Q, and Chu C W, *Superconductivity at 93K in a new mixed phase Y-Ba-Cu-O compound system at ambient pressure.* Phys Rev Letters, 1987. 58: p. 908-910.
9. Murakami M, *Processing of bulk YBaCuO.* Superconducting Science and Technology, 1992. 5: p. 185-203.
10. Sengupta S, Corpus J, Agarwal M, and Gaines J R, Material Science Engineering B-Solid State Materials for Advanced Technology, 1998. 53: p. 62.
11. Harnois C, D.G., Chaud X, *A new way of welding YBCO bulk textured domains.* Superconducting Science and Technology, 2001. 14: p. 708 - 711.
12. Iida K, Kono T, Kaneko T, Sakai N, Murakami M, and Koshizuka N, *Joining of Y-Ba-Cu-O/Ag bulk superconductors using Er-Ba-Cu-O/Ag solder.* Superconducting Science and Technology, 2004. 2: p. S46 - S50.
13. Manton S J, Beduz C, and Yang Y. *Rejoining of Single Grain Melt Textured Bulk* $YBa_2Cu_3O_{7-x}$. in *Applied Superconductivity Conference.* 1998.

14. Mukhopadhyay S M, Mahadev N, and Sengupta S, *Microstrutural and spectrosopic analyses of a strongly linked joint formed in a superconductor.* Physica C, 2000. 329: p. 95-101.
15. Noudem J G, Reddy E S, Tarka M, Noe M, and Schmitz G J, *Melt-texture joining of $YBa_2Cu_3O_y$ bulks.* Superconducting Science and Technology, 2001. 14(2001): p. 363-370.
16. Prikhna T, Gawalek W, Novikov N, Moschchil V, Sverdun V, Sergienko N, Surzhenko A, Wendt M, Habisreuther T, Litzkendorf D, Dub S, Muller R, Kordyuk A, Kracunovska S, and Alexandrova L, *Soldering of MT-YBCO: Method to produce superconductive junctions.*
17. Prikhna T, Gawalek W, Surzhenko A, Moshchil V, Sergienko N, Sverdun V B, Litzkendorf D, Muller R, Dub S N, Koval A, Alexandrova A L, Kordyuk A, and Melnikov V, *Superconducting joining of melt textured YBCO.* Physica C, 2000: p. 1528-1530.
18. Prikhna T, Gawalek W, Moshchil V, Surzhenko A, Kordyuk A, Litzkendorf D, Dub S, Melnikov V, Plyushchay A, Sergienko N, Koval A, Bokoch S, and H. T, *Superconducting joining of melt textured Y-Ba-Cu-O bulk material.* Physica C, 2001. 354: p. 333-337.
19. Schmitz G J, Tigges A, and Schmidt J C, *Microstructural aspects of joining superconductive components using (RE)Ba2Cu3O7-x solder.* Superconducting Science and Technology, 1998. 11: p. 73 - 75.
20. Shi D, *Formation of strongly coupled YBa2Cu3Ox domain by melt-joinig method.* Applied Physics Letters, 1995. 66: p. 2573-2575.
21. Walter H, Jooss CH, Sandiumenge F, Bringmann B, Delamare M P, Leenders A, and Freyhardt C, *Large intergranular critical currents in joined YBCO monoliths.* Europhysics Letters, 2001. 55: p. 100-104.
22. Bradley A D, Doyle R A, Lo W, Cardwell D A, and Campbell A M, *Large transport*

critical currents across boundaries in artificially joined large grained YBCO. Superconducting Science and Technology, 1999. 12: p. 1054 - 1058.

23. Bradley A D, Lo W, Mironova M, Babu N H, Cardwell D A, Campbell A M, and Salama K, *Microstructure and growth of joins in melt textured* $YBa_2Cu_3O_{7-\delta}$ Journal of Materials Research, 2001. 16: p. 2298-2305.
24. Chen L, Claus H, Paulikas A P, Zheng H, and Veal B W, *Joining of melt textured YBCO: a direct contact method.* Superconducting Science and Technology, 2002. 15: p. 672-674.
25. Vanderbemden Ph, Bradley A D, Doyle R A, Lo W, Astill D M, Cardwell D A, and Campbell A M, *Superconducting properties of natural and artificial grain boundaries in melt-textured YBCO.* Physica C, 1998. 302: p. 257-270.
26. Schatzle P, Krabbes G, Stover G, Fuchs G, and Schlafer D, *Mulit-seeded melt crystalisation of YBCO bulk material for cryogenic applications.* Superconducting Science and Technology, 1999. 12: p. 69-76.
27. http://www.chemsoc.org/exemplarchem/entries/igrant/theory_noflash.html#phonon
28. Cryot M and Pavuna D, *Introduction to superconductivity and High* T_c *Materials.* 1992: World Scientific Publishing. P. 249.
29. http://www.hyperphysics.phy-astr.gsu.edu/hbase/solids/meis.html
30. http://www.azom.com/details/asp?ArticleID=941&head=superconductors%2B%96%2BAn%2BIntroduction
31. Bean C P, *Magnetisation of hard superconductors.* Physical Review Letters, 1962. 8: p. 250-253.
32. Hein R A, Francavilla T L, and Lienbenburg D H, *Magnetic Susceptibility of Superconductors and other Spin Systems*: Plenum Publishing Corporation.
33. Jospehson B D, *Possible new effects in superconductive tunneling.* Physical Review Letters, 1962. 1: p. 251-253.

34. Salama K and Lee D F, *Progress in melt texturing of YBa2Cu3Ox superconductor.* Superconducting Science and Technology, 1994. 7: p. 177-193.

35. Pillay M, Jarvis A L L, and Graham F. *Joining of single domain HTSC.* in *AFRICON.* 2002. George.

36. Doss J D, *Engineer's Guide to High-Temperature Superconductivity.* 1989: John Wiley and Sons Inc.

37. http://pavel.physics.sunysb.edu/RSFQ/Research/WhatIs/rsfqwtel.html

38. http://www.irl.cri.nz/mat-tech-group/research/wire.html

39. http://english.people.com.cn/200112/03/eng20011203_85852.shtml

40. http://www.wtec.org/loyola/scpa/04_03.htm

41. Nakamura Y, Tachibana K, Kato S, Ban T, Yoo S I, and Fujimoto H, Physica C, 1998. 294: p. 302.

42. http://www.ornl.gov/info/ornlreview/rev29_3/text/hotwire.htm

43. http://www.superconductors.org/uses.htm

44. Higasa H, ISTEC Journal, 1994. 7: p. 43.

45. http://www.electricitystorage.org/technologies_papers.htm

46. http://darwing.uoregon.edu/~chem/page.html

47. http://www.chemat.com/html/solgel.html

48. http://www.physnet.uni-hamburg.de/home/vms/reimer/htc/pt3.html

49. Salama K and Selvamanickam V, *Joining of high current bulk Y-Ba-Cu-O superconductors.* Appl. Phys. Lett, 1992. 60: p. 898-900.

50. Zheng H, Jiang M, Nikolova R, Welp U, Paulikas A P, Huang Y, Crabtree G W, Veal B W, and Claus H, *High critical current "weld" joints in textured YBCO.* Physica C, 1999. 322: p. 1-8.

51. http://www.igc.com/superpower/products/htsprods.htm

52. Jarvis A L L and Doyle T B, Inst Physics Conference Ser, 1997. 158: p. 1149.

53. Ekin J W, Larson T M, Bergen N F, Nelson A J, Swartzlander A B, Kazmerski L L,

Panson A J, and Blankenship B A, *High Tc superconuctor/noble-metal contacts with surface resistivities in the10-^{10} ohm cm^{2} range.* Applied Physics Letters, 1988. 52: p. 1819-1821.

54. Harashima E, K.N.A., Sekita Y, Ishida K, Ihara H, *Low-resistivity contacts to the surface of superconductive thin films.* Superconducting Science and Technology, 2002. 15: p. 29-31.
55. Kirkup L, Kalceff W, and McCredie, *System for the study of localised heating at the curent contacts on ceramic superconductors.* Measurement Science and Technology, 1992. 3: p. 1141-1145.
56. Liu T, Zhao G, Li T B, Zhu M H, Zhang L W, Huang H S, Liu M L, Zhou Y L, He M, Lu H B, and Cao B S, *Correlation between the morphology of Ag and the contact resistivity of the Ag/$YBa_2Cu_3O_{7-d}$ thin film contact.* Journal of Superconductivity: Incorporating Novel Magnetism, 2001. 14: p. 455-459.
57. Saha S, Tripathi R B, and Das B K, *Properties of co-sintered silver contacts to pure and silver doped bulk YBCO superconductors.* Superconducting Science and Technology, 1992. 5: p. 703-706.
58. Van de Maas J, Gasparov V A, and Pavuna D, *Improved low contact resistance in high-Tc Y-Ba-Cu-O ceramic superconductors.* Letters to Nature, 1987. 328: p. 603-604.
59. Dimos D, Chaudhari P, Mannhart J, and LeGoues F K, *Orientation Dependence of Grain-Boundary Critical Currents in $YBa_2Cu_3O_{7-d}$ Bicrystals.* Physical Review Letters, 1988. 61: p. 219-222.
60. Jin S, Tiefel T H, Sherwood R C, van Dover R B, Davis M E, Kammlot G W, and Fastnauht R A, *Melt Texturing Growth of Polycrystalline YBa2Cu3O7-x with high transport Jc at 77 K.* Phys Rev B, 1988. 37: p. 7850-7853.
61. Yoshioka J, Iida K, Negichi T, Sakai N, Noto K, and M. M, *Joining Y123 bulk*

superconductors using Yb-Ba-Cu-O and Er-Ba-Cu-O sodlers. Superconducting Science and Technology, 2002. 15: p. 712-716.

Appendix *1*

Field and Force plots of the Levitator

A field plot and levitation graph plotted by the manufacturer of the levitator is shown below

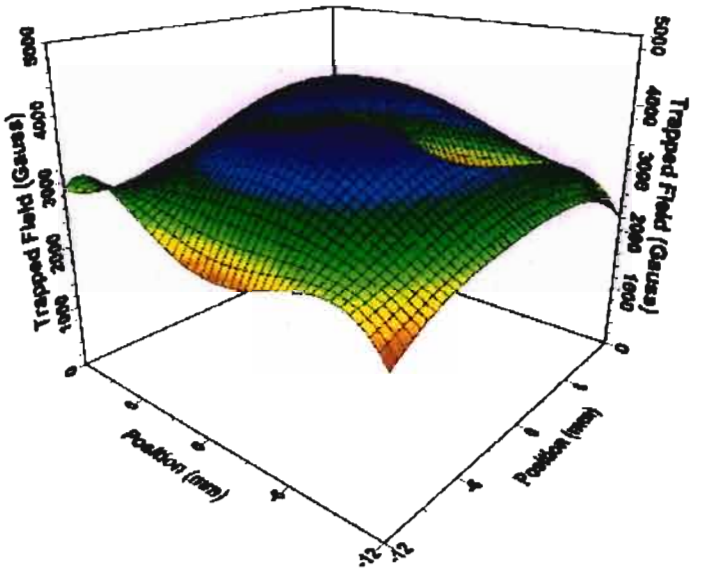

Figure A1: **Field plot of levitator captured by the manufacturer**

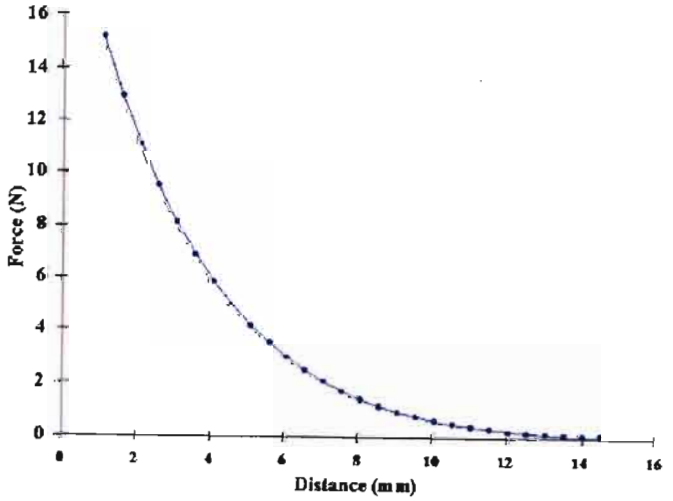

Figure A2: **Force vs Distance graph of levitator**

Appendix 2

Design of furnace controller

The superconducting samples need to be cooled at a relatively slow rate of 5 ^{0}C/hr from a temperature of 980 ^{0}C to 920 ^{0}C to allow for the growth of large crystals. A cooling controller was design using an **Atmel** microcontroller to control the cooling of the sample. This controller worked in conjunction with the temperature controller of the furnace. The temperature controller of the furnace contains three separate modules

- Calibration Module
- Amplification Module
- Output Module

Voltage Temperature Relationship of the Calibration Board

Temperature (^{o}C)	Voltage (V)
200	7.42
250	7.67
300	7.91
350	8.18
400	8.44
450	8.71
500	8.98
550	9.25
600	9.51
650	9.78
700	10.05
750	10.31
800	10.57
850	10.81
900	11.06
950	11.3
1000	11.54
1100	11.99

The calibration module converts the temperature setting which is set by the user via a dial into a voltage called the Set Point Voltage (*SP*). The temperature voltage conversion table is shown in Table A-1

This *SP* voltage is first attenuated (via a resistive divider) and then compared to voltage output of the thermocouple (*PV*). The error between the *SP* and the *PV* is then fed into an error amplifier in the Amplification Module.

COOLING CONTROLLER

The cooling controller reduces the set point (SP) voltage without changing the dial over a specified amount of time. The microcontroller is programmed to provide a cooling rate of 5^0C/ hr. The D/A converter converts the output of the microcontroller into an analogue signal and feeds it into an error amplifier after it is attenuated. The error amplifier subtracts this voltage from the initial (SP) voltage (voltage at point 1 in the diagram) and outputs this to pt 2 shown in the diagram above.

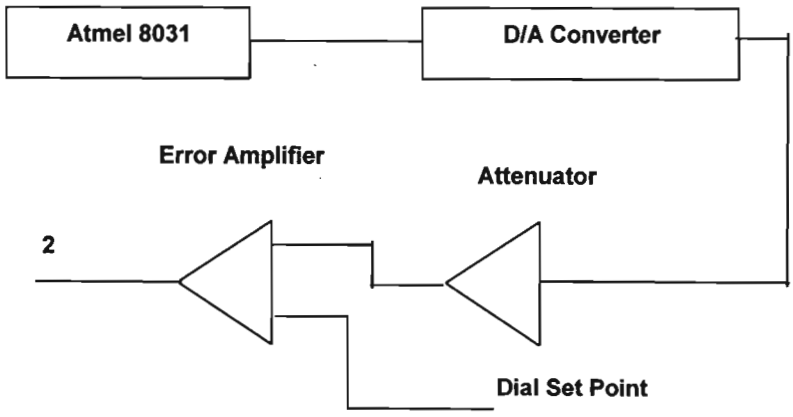

Figure A3: Cooling controller

This voltage is then fed into the resistive divider and compared to the thermocouple voltage (PV). The temperature controller of the furnace operates as normal from this point i.e. the error amplifier of the amplification board calculates the error between PV and SP and the temperature of the furnace will be adjusted accordingly to reduce the error between the PV and the SP.

Figure A2 illustrates the layout of the furnace controller with the input from the cooling controller.

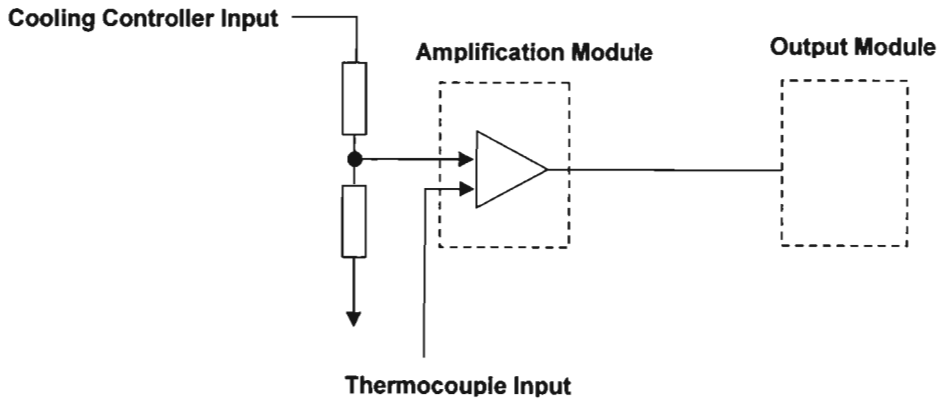

Figure A4: Modified furnace controller

Appendix 3

Experimental Set-up

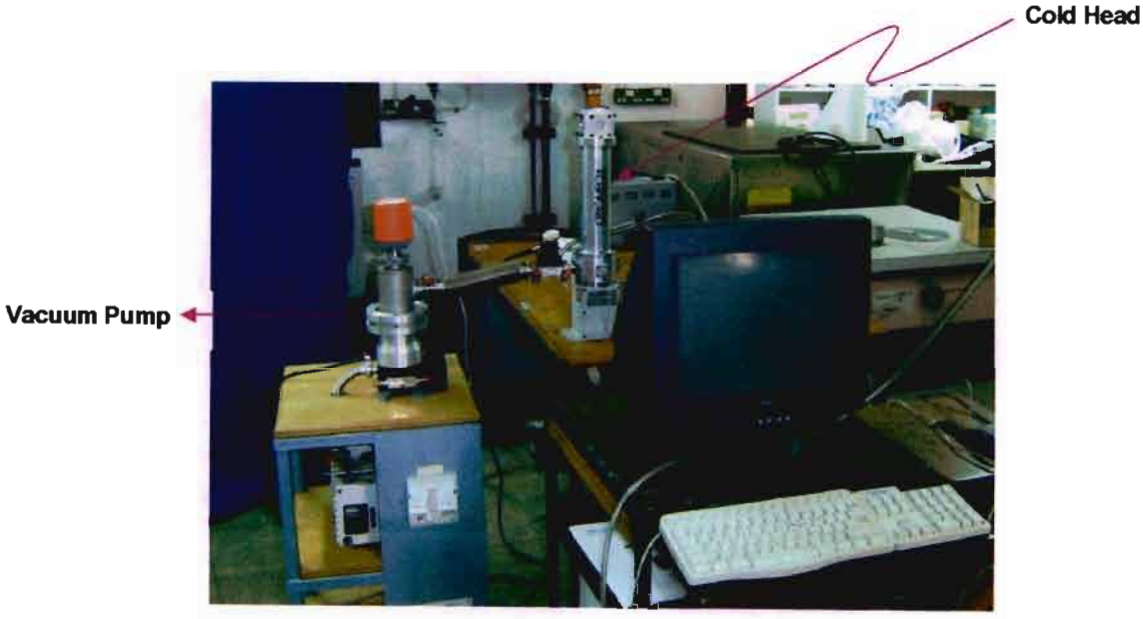

Figure A5: **Photograph of experimental set-up (Cryomech)**

Figure A6: **Picture of Cryomech Compressor unit**

Appendix 4

Data

The tables shown below contain the data obtained for the Voltage vs Current graphs (shown in Chapter 6) conducted on all samples in this research. A current source is placed in series with the sample and the voltage across the joined sample is measured.

Voltage vs Current graphs (Group 1)

Sample 1-A

89K		88K		87K	
Voltage_Res	**Voltage_Sam**	**Voltage_Res**	**Voltage_Res**	**Voltage_Sam**	**Voltage_Res**
1	0.001273	2	0.002333	2	0.002373
2	0.002300	3	0.003484	3	0.003384
3	0.003532	3.25	0.003618	3.5	0.003935
3.25	0.010754	3.5	0.003822	3.75	0.004169
X	X	3.75	0.011320	4	0.004497
X	X	X	X	4.25	0.004772
X	X	X	X	4.5	0.013611

86K		85K		84K	
Voltage_Res	**Voltage_Sam**	**Voltage_Res**	**Voltage_Res**	**Voltage_Sam**	**Voltage_Res**
2	0.002452	2	0.002229	2	0.002142
3	0.003377	3	0.003315	3	0.003425
4	0.004306	4	0.004393	4	0.004442
4.25	0.004636	4.5	0.004842	5	0.005388
4.5	0.005003	4.75	0.005158	5.25	0.005686
4.75	0.014779	5	0.005315	5.5	0.006038
X	X	5.25	0.016673	5.75	0.018623

83K		82K		81K	
Voltage_Res	**Voltage_Sam**	**Voltage_Res**	**Voltage_Res**	**Voltage_Sam**	**Voltage_Res**
3	0.003687	3	0.003379	3	0.003401
4	0.004610	4	0.004422	4	0.004427
5	0.005476	5	0.005218	5	0.005365
5.5	0.006018	5.75	0.006095	6	0.006391

5.75	0.006309	6	0.006323	6.25	0.006542
6	0.019378	6.25	0.020026	6.5	0.020860

80K	
Voltage_Res	**Voltage_Sam**
3	0.003223
4	0.004380
5	0.005208
6.5	0.006224
6.75	0.021973

Sample 1-B

89K		88K		87K	
Voltage_Res	**Voltage_Sam**	**Voltage_Res**	**Voltage_Res**	**Voltage_Sam**	**Voltage_Res**
1	0.001713	1	0.001330	1	0.001373
2	0.002852	2	0.002647	2	0.002702
2.75	0.003920	3	0.003837	3	0.003950
3	0.007654	3.25	0.004178	3.75	0.004754
X	X	3.5	0.005243	4	0.005291
X	X	3.75	0.009546	4.25	0.011191

86K		85K		84K	
Voltage_Res	**Voltage_Sam**	**Voltage_Res**	**Voltage_Res**	**Voltage_Sam**	**Voltage_Res**
2	0.002852	2	0.002869	3	0.003860
3	0.004036	3	0.003893	4	0.004938
4	0.004956	4	0.004980	5	0.006316
4.25	0.005287	4.75	0.005898	5.25	0.006586
4.5	0.005626	5	0.006298	5.5	0.007111
4.75	0.012109	5.25	0.013679	5.75	0.015366

83K		82K		81K	
Voltage_Res	**Voltage_Sam**	**Voltage_Res**	**Voltage_Res**	**Voltage_Sam**	**Voltage_Res**
3	0.004109	3	0.003847	3	0.003973
4	0.005144	4	0.005192	4	0.005300
5	0.006209	5	0.006384	5	0.006394
5.5	0.006861	6	0.007390	6	0.007368
5.75	0.007139	6.25	0.016506	6.5	0.007902
6	0.015543	X	X	6.75	0.018598

80K	
Voltage_Res	**Voltage_Sam**
4	0.004903
5	0.006320
6	0.007371
6.75	0.008108
7	0.019856

Sample 1-C

89K		88K		87K	
Voltage_Res	**Voltage_Sam**	**Voltage_Res**	**Voltage_Res**	**Voltage_Sam**	**Voltage_Res**
1	0.002355	2	0.004318	2	0.004403
2	0.004591	3	0.006643	3	0.006607
2.5	0.005688	4	0.008873	4	0.008937
3	0.006793	4.25	0.009480	5	0.011265
3.25	0.007275	4.5	0.010130	5.25	0.011955
3.5	0.007888	4.75	0.011010	5.5	0.012806
3.75	0.008652	5	0.012428	5.75	0.013730
4	0.009280	5.25	0.048600	6	0.058413
4.25	0.038023	X	X	X	X

86K		85K		84K	
Voltage_Res	**Voltage_Sam**	**Voltage_Res**	**Voltage_Res**	**Voltage_Sam**	**Voltage_Res**
2	0.004634	4	0.009244	4	0.009091
3	0.006811	5	0.011739	5	0.011555
4	0.009204	6	0.014170	6	0.013260
5	0.011238	6.5	0.015160	6.75	0.015655
6	0.013945	6.75	0.066849	7	0.016825
6.25	0.014800	X	X	7.25	0.074571
6.5	0.064941	X	X	X	X

83K		82K		81K	
Voltage_Res	**Voltage_Sam**	**Voltage_Res**	**Voltage_Res**	**Voltage_Sam**	**Voltage_Res**
4	0.008785	4	0.009081	4	0.008190
5	0.011211	5	0.011294	5	0.011009
6	0.013366	6	0.016280	6	0.013187
7.25	0.018191	7.75	0.017927	7.75	0.018810
7.5	0.079186	8	0.082539	8	0.088985

80K	
Voltage_Res	**Voltage_Sam**
5	0.010611
6	0.012853
7	0.015984
8	0.018492
8.25	0.094171

Voltage vs Current Graphs (Group 2)

Sample 2-A

89K		88K		87K	
Voltage_Res	**Voltage_Sam**	**Voltage_Res**	**Voltage_Sam**	**Voltage_Res**	**Voltage_Sam**
0.5	0.000737	0.5	0.000736	1	0.001206
1	0.001256	1	0.001264	2	0.002323
2	0.002409	2	0.002538	3	0.003433
3	0.003913	3	0.003596	4	0.004355
3.5	0.004678	3.5	0.004114	4.75	0.005277
3.75	0.015318	4	0.004539	5	0.005556
4	0.016237	4.25	0.005389	5.25	0.006782
X	X	4.5	0.005891	5.5	0.023831
X	X	4.75	0.020124	X	X

86K		85K		84K	
Voltage_Res	**Voltage_Sam**	**Voltage_Res**	**Voltage_Sam**	**Voltage_Res**	**Voltage_Sam**
1	0.001433	2	0.002463	2	0.002501
2	0.002340	3	0.003463	3	0.003535
3	0.003582	4	0.004511	4	0.004516
4	0.004551	5	0.005571	5	0.005512
5	0.005561	5.75	0.006336	6	0.006599
5.5	0.006035	6	0.006697	6.25	0.006720
5.75	0.024604	6.25	0.027210	6.5	0.022468

83K		82K		81K	
Voltage_Res	**Voltage_Sam**	**Voltage_Res**	**Voltage_Sam**	**Voltage_Res**	**Voltage_Sam**
2	0.002218	2	0.002238	3	0.003348
3	0.003370	3	0.003373	4	0.004487
4	0.004495	4	0.004422	5	0.005567
5	0.005474	5	0.005575	6	0.006307
6	0.006437	6	0.006562	7	0.007180
6.75	0.007225	6.75	0.0071982	7.25	0.008143
7	0.029879	7	0.008114	7.5	0.033535
X	X	7.25	0.031060	X	X

80K	
Voltage_Res	**Voltage_Sam**
3	0.003437
4	0.004546
5	0.005474
6	0.006611
7	0.007330
7.5	0.008678
7.75	0.035728

Sample 2-B

89K		88K		87K	
Voltage_Res	**Voltage_Sam**	**Voltage_Res**	**Voltage_Sam**	**Voltage_Res**	**Voltage_Sam**
1.75	0.002187	2	0.002331	2	0.002423
2	0.002392	3	0.003435	3	0.003483
3	0.003444	4	0.004362	4	0.004491
4	0.004739	5	0.005873	5.5	0.006692
4.8	0.019479	5.19	0.007	5.75	0.024062
5	0.020648	5.25	0.021722	6	0.025772

86K		85K		84K	
Voltage_Res	**Voltage_Sam**	**Voltage_Res**	**Voltage_Sam**	**Voltage_Res**	**Voltage_Sam**
2	0.002440	2	0.002288	4	0.004625
3	0.003355	3	0.003379	5	0.005488
4	0.004465	4	0.004542	6	0.006623
5	0.005606	5	0.005555	7	0.006850
6	0.006681	6	0.006673	7.5	0.007420
6.5	0.006834	7	0.007195	7.65	0.0353098
6.6	0.028927	7.1	0.032035	7.75	0.036019

83K		82K		81K	
Voltage_Res	**Voltage_Sam**	**Voltage_Res**	**Voltage_Sam**	**Voltage_Res**	**Voltage_Sam**
4	0.004456	4	0.004405	4	0.004655
5	0.005601	5	0.005522	5	0.005480
6	0.006613	6	0.006600	6	0.006421
7	0.006803	7.75	0.007401	7	0.006634
7.5	0.007161	8	0.007281	8.25	0.00800
7.75	0.035188	8.1	0.035092	8.5	0.035855

80K	
Voltage_Res	**Voltage_Sam**
5	0.005517
6	0.006562
7	0.006706
8	0.007817
8.5	0.007838
8.75	0.043664

Sample 2-C

89K		88K		87K	
Voltage_Res	**Voltage_Sam**	**Voltage_Res**	**Voltage_Sam**	**Voltage_Res**	**Voltage_Sam**
1	0.001435	1	0.001353	2	0.002325
2	0.002477	2	0.002378	3	0.003300
2.5	0.003096	3	0.003507	3.5	0.003858
3	0.003650	3.25	0.003605	4	0.004340
3.25	0.003650	3.5	0.003862	4.25	0.004715
X	0.013728	3.75	0.004406	4.5	0.004892
X	X	4	0.004606	4.75	0.005202
X	X	4.25	0.018826	5	0.023047

86K		85K		84K	
Voltage_Res	**Voltage_Sam**	**Voltage_Res**	**Voltage_Res**	**Voltage_Sam**	**Voltage_Res**
2	0.002337	3	0.003397	3	0.003309
3	0.003201	4	0.004354	4	0.004265
4	0.004279	5	0.005263	5	0.005259
5	0.005370	5.5	0.005797	5.75	0.006011
5.25	0.005694	5.75	0.006121	6	0.006344
5.5	0.025410	6	0.0284323	6.25	0.029005

83K		82K		81K	
Voltage_Res	**Voltage_Sam**	**Voltage_Res**	**Voltage_Res**	**Voltage_Sam**	**Voltage_Res**
3	0.003436	3	0.003298	3	0.003604
4	0.004385	4	0.004411	4	0.004376
5	0.005387	5	0.005427	5	0.005378
6	0.006262	6	0.006359	6	0.006322
6.25	0.006578	6.5	0.006824	6.5	0.006779
6.5	0.030851	6.75	0.031504	6.75	0.007045
X	X	X	X	7	0.034260

80K	
Voltage_Res	**Voltage_Sam**
3	0.003300
4	0.004349
5	0.005268
6	0.006184
7	0.007227
7.25	0.035377

Voltage vs Current graphs (Group 3)

Sample 3-A

89K		88K		87K	
Voltage_Res	**Voltage_Sam**	**Voltage_Res**	**Voltage_Res**	**Voltage_Sam**	**Voltage_Res**
0.5	0.003115	1	0.005758	1	0.004676
0.75	0.004935	1.5	0.009741	2	0.011605
1	0.007342	1.75	0.012067	2.5	0.017795
1.5	0.008930	2	0.013807	2.75	0.022083
1.5	0.012284	2.25	0.019435	3	0.046659
1.75	0.013422	2.5	0.037803	X	X
2	0.033524	X	X	X	X

86K		85K		84K	
Voltage_Res	**Voltage_Sam**	**Voltage_Res**	**Voltage_Res**	**Voltage_Sam**	**Voltage_Res**
1	0.003799	1	0.003359	1	0.002523
2	00.008543	2	0.006892	2	0.005653
2.75	0.016281	3	0.015671	3	0.010464
3	0.019301	3.25	0.021290	3.5	0.020151
3.25	0.051465	3.5	0.054389	3.75	0.038715

83K		82K		81K	
Voltage_Res	**Voltage_Sam**	**Voltage_Res**	**Voltage_Res**	**Voltage_Sam**	**Voltage_Res**
1	0.002500	2	0.004260	2	0.004095
2	0.004843	3	0.006883	3	0.005947
3	0.008282	4	0.011085	4	0.009054
3.75	0.013083	4.25	0.015103	4.5	0.012098
4	0.019191	4.5	0.072647	4.75	0.078259
4.25	0.068547	X	X	X	X

80K	
Voltage_Res	**Voltage_Sam**
2	0.003640
3	0.005465
4	0.008097
4.75	0.011614
5	0.016469
5.25	0.089840

Sample 3-B

89K		88K		87K	
Voltage_Res	Voltage_Sam	Voltage_Res	Voltage_Res	Voltage_Sam	Voltage_Res
1	0.002859	1	0.002176	1	0.001906
1.5	0.004375	1.5	0.00361	2	0.003894
2	0.008070	1.75	0.004272	2.75	0.006456
2.25	0.010776	2	0.005360	3	0.008442
3	0.019370	2.25	0.006779	3.25	0.011325
X	X	2.5	0.008682	3.5	0.016128
X	X	2.75	0.009875	4	0.026409
X	X	3	0.015371	X	X

86K		85K		84K	
Voltage_Res	Voltage_Sam	Voltage_Res	Voltage_Res	Voltage_Sam	Voltage_Res
1	0.001511	2	0.003075	2	0.002682
2	0.003177	3	0.004601	3	0.003987
3	0.005505	4	0.008554	4.25	0.007540
3.75	0.008012	4.25	0.027498	4.5	0.009089
4	0.024094	X	X	4.75	0.030984

83K		82K		81K	
Voltage_Res	Voltage_Sam	Voltage_Res	Voltage_Res	Voltage_Sam	Voltage_Res
2	0.002639	2	0.002599	2	0.002394
3	0.003598	3	0.003469	3	0.003541
4.5	0.006036	4	0.004801	4	0.005081
4.75	0.007608	5.25	0.007440	5.5	0.007379
5	0.01115	5.5	0.036726	5.75	0.037470
5.25	0.035132	X	X	X	X

80K	
Voltage_Res	Voltage_Sam
2	0.002593
3	0.003527
4	0.004662
5.75	0.007690
6	0.040504

Data for Field Maps

Joined Sample

X Values \ Y Values	0	2	4	6	8	10	12	14	16	18	20	22	24	26	28	30	32	34	36	38	40	42
0	0.1	0.1	0.2	0.2	0.2	0.2	0.2	0.2	0.2	0.2	0.2	0.2	0.2	0.2	0.2	0.1	0.1	0.1	0.1	0.1	0.1	0.1
2	0.1	0.2	0.2	0.2	0.2	0.2	0.2	0.4	0.4	0.4	0.4	0.2	0.2	0.2	0.2	0.2	0.2	0.1	0.1	0.1	0.1	0.1
4	0.1	0.2	0.2	0.2	0.4	0.4	0.4	0.4	0.4	0.4	0.4	0.4	0.4	0.4	0.2	0.2	0.2	0.2	0.1	0.1	0.1	0.1
6	0.2	0.2	0.4	0.4	0.4	0.4	0.4	0.5	0.5	0.5	0.5	0.4	0.4	0.4	0.4	0.2	0.2	0.2	0.1	0.1	0.1	0.1
8	0.2	0.2	0.4	0.4	0.4	0.5	0.5	0.5	0.5	0.5	0.5	0.5	0.5	0.4	0.4	0.4	0.2	0.2	0.2	0.1	0.1	0.1
10	0.2	0.4	0.4	0.5	0.5	0.5	0.6	0.6	0.6	0.6	0.6	0.5	0.5	0.5	0.4	0.4	0.2	0.2	0.2	0.2	0.1	0.1
12	0.4	0.4	0.5	0.5	0.5	0.6	0.6	0.8	0.6	0.6	0.6	0.6	0.6	0.5	0.5	0.4	0.4	0.2	0.2	0.2	0.1	0.1
14	0.4	0.4	0.5	0.5	0.6	0.6	0.8	0.8	0.8	0.8	0.8	0.6	0.6	0.6	0.5	0.5	0.4	0.2	0.2	0.2	0.1	0.1
16	0.4	0.5	0.5	0.6	0.6	0.8	0.8	0.9	0.9	0.8	0.8	0.8	0.6	0.6	0.5	0.5	0.4	0.4	0.2	0.2	0.1	0.1
18	0.4	0.5	0.6	0.6	0.8	0.8	0.9	0.9	0.9	0.9	0.9	0.8	0.8	0.6	0.6	0.5	0.4	0.4	0.2	0.2	0.1	0.1
20	0.4	0.5	0.6	0.6	0.8	0.9	0.9	0.9	0.9	0.9	0.9	0.9	0.8	0.6	0.6	0.5	0.4	0.4	0.2	0.2	0.1	0.1
22	0.4	0.5	0.6	0.6	0.8	0.9	0.9	0.9	1.1	1.1	0.9	0.9	0.8	0.8	0.6	0.5	0.4	0.4	0.2	0.2	0.1	0.1
24	0.4	0.5	0.6	0.6	0.8	0.9	0.9	0.9	1.1	1.1	0.9	0.9	0.8	0.8	0.6	0.5	0.4	0.4	0.2	0.2	0.1	0.1
26	0.4	0.5	0.6	0.6	0.8	0.8	0.9	0.9	0.9	0.9	0.9	0.9	0.8	0.6	0.6	0.5	0.4	0.4	0.2	0.2	0.1	0.1
28	0.4	0.5	0.5	0.6	0.8	0.8	0.9	0.9	0.9	0.9	0.9	0.8	0.8	0.6	0.5	0.5	0.4	0.2	0.2	0.1	0.1	0.1
30	0.4	0.4	0.5	0.6	0.6	0.8	0.8	0.9	0.8	0.9	0.8	0.8	0.6	0.6	0.5	0.4	0.4	0.2	0.2	0.1	0.1	0.1
32	0.2	0.4	0.4	0.5	0.6	0.6	0.8	0.8	0.8	0.8	0.8	0.6	0.6	0.5	0.5	0.4	0.2	0.2	0.2	0.1	0.1	0.1
34	0.2	0.4	0.4	0.5	0.5	0.6	0.6	0.6	0.6	0.6	0.6	0.5	0.5	0.5	0.4	0.4	0.2	0.2	0.1	0.1	0.1	0.1
36	0.2	0.2	0.4	0.4	0.4	0.5	0.5	0.5	0.5	0.5	0.5	0.5	0.5	0.4	0.4	0.2	0.2	0.1	0.1	0.1	0.1	0
38	0.1	0.2	0.2	0.2	0.4	0.4	0.5	0.5	0.5	0.5	0.4	0.4	0.4	0.2	0.2	0.2	0.1	0.1	0.1	0.1	0	0
40	0.1	0.1	0.2	0.2	0.2	0.2	0.4	0.4	0.4	0.4	0.4	0.2	0.2	0.2	0.2	0.1	0.1	0.1	0.1	0	0	0
42	0.1	0.1	0.1	0.1	0.2	0.2	0.2	0.2	0.2	0.2	0.2	0.2	0.2	0.2	0.1	0.1	0.1	0.1	0	0	0	0

Parent Sample

X Values \ Y Values	0	2	4	6	8	10	12	14	16	18	20	22	24	26	28	30	32	34	36	38	40	42
0	0.1	0.1	0.2	0.2	0.2	0.2	0.2	0.2	0.2	0.2	0.2	0.2	0.2	0.2	0.2	0.1	0.1	0.1	0.1	0.1	0.1	0.1
2	0.1	0.2	0.2	0.2	0.2	0.2	0.2	0.4	0.4	0.4	0.4	0.2	0.2	0.2	0.2	0.2	0.2	0.1	0.1	0.1	0.1	0.1
4	0.1	0.2	0.2	0.2	0.4	0.4	0.4	0.4	0.4	0.4	0.4	0.4	0.4	0.4	0.2	0.2	0.2	0.2	0.1	0.1	0.1	0.1
6	0.2	0.2	0.4	0.4	0.4	0.4	0.4	0.5	0.5	0.5	0.5	0.4	0.4	0.4	0.4	0.2	0.2	0.2	0.1	0.1	0.1	0.1
8	0.2	0.2	0.4	0.4	0.4	0.5	0.5	0.5	0.5	0.5	0.5	0.5	0.5	0.4	0.4	0.4	0.2	0.2	0.2	0.1	0.1	0.1
10	0.2	0.4	0.4	0.5	0.5	0.5	0.6	0.6	0.6	0.6	0.6	0.5	0.5	0.5	0.4	0.4	0.2	0.2	0.2	0.2	0.1	0.1
12	0.4	0.4	0.5	0.5	0.5	0.6	0.6	0.8	0.6	0.6	0.6	0.6	0.6	0.5	0.5	0.4	0.4	0.2	0.2	0.2	0.1	0.1
14	0.4	0.4	0.5	0.5	0.6	0.6	0.8	0.8	0.8	0.8	0.8	0.6	0.6	0.6	0.5	0.5	0.4	0.2	0.2	0.2	0.1	0.1
16	0.4	0.5	0.5	0.6	0.6	0.8	0.8	0.9	0.9	0.8	0.8	0.8	0.6	0.6	0.5	0.5	0.4	0.4	0.2	0.2	0.1	0.1
18	0.4	0.5	0.6	0.6	0.8	0.8	0.9	0.9	0.9	0.9	0.9	0.8	0.8	0.6	0.6	0.5	0.4	0.4	0.2	0.2	0.1	0.1
20	0.4	0.5	0.6	0.6	0.8	0.9	0.9	0.9	0.9	0.9	0.9	0.9	0.8	0.6	0.6	0.5	0.4	0.4	0.2	0.2	0.1	0.1
22	0.4	0.5	0.6	0.6	0.8	0.9	0.9	0.9	1.1	1.1	0.9	0.9	0.8	0.8	0.6	0.5	0.4	0.4	0.2	0.2	0.1	0.1
24	0.4	0.5	0.6	0.6	0.8	0.9	0.9	0.9	1.1	1.1	0.9	0.9	0.8	0.8	0.6	0.5	0.4	0.4	0.2	0.2	0.1	0.1
26	0.4	0.5	0.6	0.6	0.8	0.8	0.9	0.9	0.9	0.9	0.9	0.9	0.8	0.6	0.6	0.5	0.4	0.4	0.2	0.2	0.1	0.1
28	0.4	0.5	0.5	0.6	0.8	0.8	0.9	0.9	0.9	0.9	0.9	0.8	0.8	0.6	0.5	0.5	0.4	0.2	0.2	0.1	0.1	0.1
30	0.4	0.4	0.5	0.6	0.6	0.8	0.8	0.9	0.8	0.9	0.8	0.8	0.6	0.6	0.5	0.4	0.4	0.2	0.2	0.1	0.1	0.1
32	0.2	0.4	0.4	0.5	0.6	0.6	0.8	0.8	0.8	0.8	0.8	0.6	0.6	0.5	0.5	0.4	0.2	0.2	0.2	0.1	0.1	0.1
34	0.2	0.4	0.4	0.5	0.5	0.6	0.6	0.6	0.6	0.6	0.6	0.5	0.5	0.5	0.4	0.4	0.2	0.2	0.1	0.1	0.1	0.1
36	0.2	0.2	0.4	0.4	0.4	0.5	0.5	0.5	0.5	0.5	0.5	0.5	0.5	0.4	0.4	0.2	0.2	0.1	0.1	0.1	0.1	0
38	0.1	0.2	0.2	0.2	0.4	0.4	0.5	0.5	0.5	0.5	0.4	0.4	0.4	0.2	0.2	0.2	0.1	0.1	0.1	0.1	0	0
40	0.1	0.1	0.2	0.2	0.2	0.2	0.4	0.4	0.4	0.4	0.4	0.2	0.2	0.2	0.2	0.1	0.1	0.1	0.1	0	0	0
42	0.1	0.1	0.1	0.1	0.2	0.2	0.2	0.2	0.2	0.2	0.2	0.2	0.2	0.2	0.1	0.1	0.1	0.1	0	0	0	0

Voltage vs Temperature (Group 1)

Sample 1-A (Yb123)		Sample 1-B (75:25)		Sample 1-C (60:40	
Voltage	Temperature	Voltage	Temperature	Voltage	Temperature
0.002405	100.3043	0.002063	100.0385	0.009897	99.982864
0.002381	99.9515	0.002061	99.988152	0.009969	99.622833
0.00238	99.652214	0.00206	99.911507	0.009953	99.643211
0.002386	99.233086	0.002032	98.992455	0.009973	99.791664
0.002385	98.924667	0.00203	98.966675	0.009983	99.532593
0.002364	98.591187	0.002002	97.96534	0.00994	99.233849
0.002346	98.239304	0.002	97.8797	0.00993	98.895241
0.002329	97.931877	0.001979	97.214798	0.009875	98.58152
0.002322	97.606232	0.001969	96.882904	0.009844	98.294846
0.002322	97.224319	0.001967	96.805801	0.009855	97.904266
0.0023	96.94487	0.001964	96.779984	0.009775	97.691658
0.002288	96.578934	0.001961	96.642311	0.009729	97.324463
0.002279	96.245865	0.001958	96.60186	0.009679	97.018425
0.002271	95.941811	0.001956	96.458588	0.009655	96.751175
0.002257	95.621811	0.00195	96.434349	0.009595	96.548798
0.002246	95.277458	0.001949	96.271729	0.009542	96.193047
0.00223	94.95742	0.001945	96.148422	0.009505	95.908211
0.002211	94.673584	0.001941	96.062004	0.009462	95.708748
0.002195	94.304947	0.001938	96.059937	0.009432	95.386147
0.002181	93.980675	0.001935	95.891327	0.009406	95.170418
0.00216	93.656151	0.001931	95.777504	0.009375	94.901398
0.002143	93.388351	0.001928	95.726822	0.009353	94.705025
0.002126	93.057152	0.001926	95.606613	0.009314	94.468155
0.0021	92.637428	0.001922	95.5187	0.009263	94.178574
0.002071	92.335426	0.001918	95.423378	0.009239	93.935341
0.002041	92.073334	0.001916	95.37117	0.009188	93.694656
0.002015	91.683334	0.001912	95.286125	0.009136	93.50235
0.00199	91.344116	0.001908	95.206947	0.009121	93.309189
0.00196	91.01535	0.0019	95.129478	0.009047	93.020905
0.001918	90.708946	0.00189	94.988091	0.009014	92.826126
0.001866	90.386246	0.001886	94.789482	0.00895	92.572411
0.001745	90.091789	0.001882	94.721275	0.008892	92.418922
0.001248	89.717812	0.001878	94.666885	0.008797	92.199738
0.000432	89.467278	0.001874	94.565369	0.008671	91.918831
0.000146	89.130257	0.001871	94.440651	0.008546	91.687851
0.000109	88.77861	0.001865	94.428581	0.008249	91.489441
0.000102	88.464638	0.001861	94.24884	0.007468	91.242859
0.000096	88.150734	0.001856	94.141441	0.005176	91.020531
0.000095	87.845566	0.001852	94.110321	0.003095	90.901024
0.000092	87.485077	0.001849	93.972778	0.00272	90.695023
0.000091	87.187965	0.001843	93.914017	0.002638	90.443893

0.000089	86.860771	0.00184	93.846985	0.002607	90.261017
0.000089	86.5158	0.001836	93.657776	0.002549	89.99102
0.000087	86.242722	0.001832	93.560028	0.002489	89.767975
0.000086	85.839172	0.001826	93.478188	0.002452	89.547989
0.000086	85.535492	0.001821	93.376266	0.002402	89.355202
0.000086	85.21328	0.001814	93.34742	0.002421	89.128151
0.000085	84.941864	0.00181	93.222252	0.002416	88.960129
0.000085	84.577621	0.001807	93.153336	0.002405	88.742912
0.000084	84.29744	0.001801	92.990402	0.002382	88.503159
0.000084	83.937531	0.001795	92.952316	0.002377	88.30584
0.000083	83.651726	0.001789	92.761864	0.002413	88.141403
0.000082	83.364334	0.001784	92.658829	0.002403	87.882072
0.000081	82.981873	0.00178	92.644173	0.002405	87.664177
0.00008	82.774055	0.001772	92.494179	0.0024	87.517235
0.000079	82.386162	0.001766	92.347939	0.002416	87.302048
0.000079	82.038979	0.001758	92.256866	0.002385	87.03801
0.00008	81.740288	0.001752	92.161659	0.002368	86.831329
0.00008	81.435547	0.001746	92.118523	0.002368	86.650627
0.00008	81.165459	0.001738	91.972549	0.00235	86.430809
0.000081	80.797447	0.00173	91.867668	0.002357	86.21035
0.000081	80.557861	0.001721	91.728645	0.00237	86.009697
0.000079	80.188766	0.001711	91.729179	0.002357	85.789558
		0.001701	91.619347	0.002336	85.591644
		0.001691	91.438927	0.002325	85.37677
		0.001677	91.408722	0.002328	85.221451
		0.001661	91.2528	0.002329	84.950569
		0.001641	91.104836	0.002314	84.79364
		0.001613	90.99839	0.002346	84.599274
		0.001573	90.944817	0.002341	84.34063
		0.001504	90.816689	0.002338	84.148689
		0.001377	90.679512	0.002339	83.976662
		0.001143	90.574272	0.002329	83.731102
		0.00084	90.528946	0.002331	83.511482
		0.000645	90.35952	0.002309	83.343613
		0.000558	90.343544	0.002309	83.122017
		0.000507	90.117378	0.002257	82.94532
		0.000473	90.048775	0.002264	82.799881
		0.000441	89.99015	0.002263	82.503616
		0.000406	89.879913	0.002259	82.32457
		0.00036	89.792313	0.002257	82.104256
		0.000323	89.697701	0.002254	81.942429
		0.000312	89.532593	0.00226	81.712616
		0.000306	89.35733	0.002259	81.492706
		0.000302	89.25853	0.002259	81.266617
		0.0003	89.14682	0.002263	81.135895
		0.000299	89.086647	0.002249	80.909386

		0.000297	88.924118	0.002247	80.675453
		0.000298	88.810577	0.002252	80.472191
		0.000296	88.708183	0.002243	80.260422
		0.000296	88.577866	0.002235	80.054443
		0.000295	88.466232		
		0.000294	88.426544		
		0.000296	88.248688		
		0.000295	88.171585		
		0.000294	88.027344		
		0.000293	87.920135		
		0.000294	87.781227		
		0.000294	87.665703		
		0.000293	87.552498		
		0.000292	87.4757		
		0.000292	87.335686		
		0.00029	87.187698		
		0.000291	87.05117		
		0.000289	86.960152		
		0.00029	86.893524		
		0.00029	86.785416		
		0.000289	86.613007		
		0.000287	86.49855		
		0.000286	86.421898		
		0.000285	86.336708		
		0.000283	86.129631		
		0.000285	86.022858		
		0.000283	85.970108		
		0.000283	85.879578		
		0.000282	85.668106		
		0.000283	85.558197		
		0.000284	85.491165		
		0.000284	85.318596		
		0.000281	85.198372		
		0.000279	85.067535		
		0.000281	85.043243		
		0.00028	84.834763		
		0.000279	84.730156		
		0.000278	84.660759		
		0.000277	84.460426		
		0.000278	84.380707		
		0.000277	84.241226		
		0.000277	84.151314		
		0.000277	83.959473		
		0.000277	83.872513		
		0.000276	83.702599		
		0.000276	83.586449		

		0.000273	83.444679		
		0.000272	83.380272		
		0.000272	83.323364		
		0.000271	83.177887		
		0.000272	82.950577		
		0.000271	82.876801		
		0.000272	82.734444		
		0.000272	82.536903		
		0.000271	82.451538		
		0.000272	82.404228		
		0.00027	82.268547		
		0.00027	82.103157		
		0.00027	82.041054		
		0.000263	81.024475		
		0.000263	80.965286		

Voltage vs Temperature (Group 2)

Sample 2-B		Sample 2-A		Sample 2-C	
Voltage	Temperature	Voltage	Temperature	Voltage	Temperature
0.00833	99.74408	0.01208	99.50248	0.012467	99.607994
0.008321	99.461189	0.012077	99.715576	0.01245	99.519188
0.008317	99.419304	0.012076	99.633194	0.012443	99.181419
0.008296	99.119942	0.012053	99.380875	0.012419	99.23632
0.008258	98.79615	0.012016	98.990364	0.012397	98.916939
0.008219	98.452126	0.011967	98.647964	0.012373	98.546295
0.008177	98.054466	0.011915	98.270599	0.012318	98.140923
0.008135	97.774673	0.011861	97.852692	0.012268	97.870422
0.008092	97.360115	0.011807	97.514954	0.012216	97.509171
0.008046	97.019417	0.011752	97.135269	0.012157	97.105957
0.008	96.690628	0.011691	96.762444	0.012097	96.673958
0.007951	96.306999	0.011631	96.449669	0.012041	96.287735
0.007903	96.043892	0.011576	96.142136	0.011979	95.977043
0.007853	95.70742	0.01151	95.714859	0.011916	95.591118
0.007805	95.396355	0.011447	95.443069	0.011863	95.253799
0.007752	95.069901	0.011384	95.058792	0.011794	94.931473
0.007703	94.785027	0.011316	94.697502	0.011731	94.587547
0.007649	94.490845	0.011258	94.379143	0.011664	94.237213
0.007594	94.230988	0.011187	94.082581	0.0116	93.92086
0.007538	93.909607	0.011114	93.718292	0.011532	93.592194
0.00748	93.59156	0.011042	93.426079	0.01146	93.254448
0.00742	93.302628	0.010971	93.111328	0.011387	92.938805
0.007357	93.002899	0.010896	92.75473	0.011315	92.682793
0.00729	92.69529	0.010821	92.493736	0.011241	92.292496
0.007218	92.476959	0.010735	92.125229	0.01116	92.007553
0.007142	92.175758	0.01065	91.882294	0.011082	91.699898
0.007055	91.857849	0.010558	91.581802	0.010988	91.341347
0.00696	91.542755	0.010457	91.19532	0.010908	91.046387
0.00685	91.25251	0.01035	90.922569	0.010813	90.737724
0.00671	90.981155	0.010236	90.597313	0.010701	90.474213
0.006477	90.729012	0.010109	90.276711	0.010576	90.172699
0.00576	90.395355	0.009963	89.984489	0.01044	89.802063
0.003681	90.11245	0.009796	89.698311	0.010296	89.500252
0.001957	89.81218	0.009581	89.422089	0.010114	89.189537
0.001806	89.565163	0.009261	89.053833	0.009859	88.864815
0.001667	89.25621	0.008894	89.019119	0.009358	88.579498
0.001558	88.958328	0.008775	89.182693	0.00695	88.229546
0.001495	88.663376	0.008708	89.235153	0.001254	87.955154
0.00147	88.775108	0.007349	89.02256	0.000379	87.681206
0.00146	88.676926	0.002328	88.756248	0.000334	87.330894
0.001463	88.852432	0.00109	88.609383	0.000328	87.035248
0.001447	88.646637	0.000813	88.709381	0.000325	86.745361

0.001426	88.45504	0.000755	88.825073	0.000323	86.37384
0.001408	88.091713	0.000711	88.634613	0.000321	86.159065
0.001397	87.793922	0.00067	88.369789	0.000319	85.782318
0.001391	87.535591	0.000618	87.587898	0.000319	85.434448
0.001391	87.793282	0.000613	87.262505	0.000318	85.151253
0.001394	87.984245	0.000599	86.913414	0.000317	84.853775
0.001393	88.034927	0.000593	86.835724	0.000316	84.520195
0.001395	87.80735	0.000586	86.674225	0.000312	84.198532
0.001397	88.189949	0.000585	86.653656	0.000312	83.940002
0.001383	87.61618	0.00059	86.914848	0.000309	83.56002
0.001372	87.201561	0.000591	87.147659	0.00031	83.254898
0.001363	86.868599	0.000593	86.847862	0.000309	82.989319
0.001358	86.851021	0.000592	86.572937	0.000307	82.662094
0.001355	87.069786	0.000588	86.235474	0.000303	82.325424
0.001355	86.985741	0.000581	85.912292	0.000306	82.156631
0.001349	86.727692	0.000578	85.760902	0.000305	81.7892
0.001343	86.38842	0.000575	86.109108	0.000304	81.444618
0.001335	86.048592	0.000577	85.989799	0.000302	81.208717
0.00133	85.684967	0.000576	85.970016	0.000301	80.838501
0.001322	85.579605	0.000574	85.747887	0.000299	80.530807
0.001321	85.406815	0.000567	85.802856	0.000299	80.210564
0.001317	85.583237	0.000569	85.779625	0.000296	79.935883
0.001315	85.362259	0.000569	85.808899	0.000295	79.61599
0.001309	85.083427	0.000569	85.59549	0.000295	79.3246
0.001305	84.736038	0.000565	85.29628	0.000293	78.993698
0.001299	84.962181	0.000562	84.995552	0.000292	78.687576
0.001296	84.810631	0.000557	84.953041	0.000291	78.463943
0.001293	84.855827	0.000548	84.837196	0.000291	78.166298
0.00129	84.683693	0.000546	84.994156	0.000291	77.873718
0.001283	84.374199	0.00055	85.067978	0.000289	77.614174
0.001277	84.068283	0.00055	84.882835	0.000291	77.220901
0.001276	84.279694	0.000547	84.56691	0.000287	76.953117
0.001275	84.043205	0.000544	84.22699	0.000287	76.629227
0.001268	83.758667	0.000539	83.907631	0.000287	76.366798
0.001266	83.740395	0.000533	83.54557	0.000287	76.036919
0.001263	83.890709	0.000528	83.438416	0.000287	75.77063
0.001264	83.962425	0.000531	83.81385	0.000287	75.551491
0.001259	83.652847	0.000534	83.673439	0.000286	75.189041
0.001253	83.413307	0.000535	83.712616	0.000284	74.880074
0.001244	83.080803	0.000532	83.516754	0.000287	74.644135
0.001239	82.645515	0.000526	83.147011	0.000289	74.32531
0.001239	82.853981	0.000522	82.827179	0.000287	74.094269
0.001235	82.696968	0.000516	82.890251	0.000287	73.752716
0.001232	82.661026	0.000513	82.667892	0.000281	73.440079
0.00123	82.657722	0.000512	82.300751	0.000281	73.256035
0.001226	82.464218	0.00051	82.605095	0.000278	72.927536

0.00122	82.041374	0.000512	82.520805		
0.001213	81.859604	0.000514	82.760422		
0.001214	81.966179	0.000512	82.624329		
0.001215	82.266273	0.000512	82.325699		
0.001213	82.170273	0.000505	82.040634		
0.001209	81.953888	0.000504	81.722755		
0.001205	81.634445	0.000502	81.409233		
0.001197	81.209427	0.000504	81.597816		
0.001189	80.956421	0.000495	82.112106		
0.001184	80.792183	0.000487	81.607216		
0.001182	80.502892	0.000484	81.65715		
0.00118	80.734573	0.000488	81.680534		
0.001179	80.894714	0.000491	81.883354		
0.001176	80.700081	0.000491	82.155846		
0.001169	80.439575	0.00049	82.051201		
0.001164	80.033951	0.000487	81.816605		
0.00116	80.015846	0.000488	81.70237		
0.001158	79.771019	0.000489	81.731232		
0.001153	79.45713	0.00049	81.830963		
0.001152	79.758812	0.000487	81.588867		
0.001155	80.226906	0.000482	81.351219		
0.001157	80.182556	0.000478	81.229385		
0.001154	79.836411	0.000476	80.979675		
0.001146	79.488838	0.000476	80.666466		
0.001141	79.479256	0.000472	80.607506		
0.001138	79.305313	0.000467	80.395218		
0.001128	78.94619	0.000471	80.798576		
0.001123	78.578293	0.000475	80.910637		
0.001121	78.388847	0.000471	80.709076		
0.001122	78.813599	0.000465	80.390106		
0.001122	78.997963	0.000462	80.057281		
0.00112	78.791153	0.00046	79.70446		
0.001115	78.500473	0.000453	79.491966		
0.00111	78.262825	0.000455	79.64846		
0.001106	78.242859	0.000458	79.986084		
0.001101	77.947067	0.000461	80.037056		
0.001101	78.058815	0.00046	79.976166		
0.0011	78.002441	0.00046	79.957268		
0.001098	78.052834	0.000457	79.716736		
0.001095	77.774078	0.000451	79.617493		
0.001091	77.461678	0.000451	79.821022		
0.001081	77.166725	0.000452	79.56337		
0.001073	76.784744	0.00045	79.265076		
0.001065	76.435905	0.000444	78.991417		
0.001056	76.092979	0.000439	78.624512		
0.001049	75.760735	0.000434	78.379112		

0.001041	75.512558	0.000434	77.938118		
0.001032	75.084854	0.000431	77.671371		
0.001023	74.854279	0.000425	77.349396		
0.001021	74.430801	0.000424	76.997711		
0.001016	74.536507	0.00042	76.689873		
0.001002	73.846146	0.000413	76.413589		
0.000993	73.611053	0.00041	76.230087		
0.000985	73.197472	0.000403	75.798523		
0.000976	72.868614	0.0004	75.626816		
0.000968	72.577606	0.000394	75.270622		
0.000959	72.262375	0.00039	74.984634		
0.000951	71.954971	0.000384	74.718941		
0.000944	71.689041	0.000384	74.410385		
0.000935	71.431129	0.00038	74.167763		
0.000925	71.067467	0.000378	73.807396		
0.000915	70.761185	0.000375	73.540588		
0.000908	70.502563	0.000369	73.263443		
0.000901	70.304955	0.000364	72.96489		
0.000899	69.993027	0.000357	72.76413		
		0.000355	72.431297		
		0.00035	72.255051		
		0.000344	72.007149		
		0.000342	71.668297		
		0.000338	71.387253		
		0.000337	71.077789		
		0.000334	70.901443		
		0.000329	70.542038		
		0.000325	70.362503		
		0.000318	70.056496		
		0.000317	69.761215		
		0.000315	69.787071		
		0.000318	69.671066		

Voltage vs Temperature (Group 3)

Sample 3-B		Sample 3-A	
Voltage	Temperature	Voltage	Temperature
0.016354	99.98513	0.007408	99.758011
0.016341	100.03526	0.007369	99.942909
0.016336	99.921394	0.007427	99.800575
0.016379	99.88327	0.007387	99.95182
0.016343	99.839043	0.007355	99.681465
0.016336	99.815979	0.007259	99.79274
0.016339	99.700981	0.00721	99.349922
0.01635	99.657402	0.007208	99.107185
0.016358	99.608307	0.007201	98.718193
0.016344	99.54837	0.00714	98.34063
0.016362	99.490456	0.007135	98.094315
0.016333	99.44117	0.007116	97.770256
0.0163	99.353424	0.007133	97.435829
0.016273	99.343971	0.00709	97.116402
0.016277	99.266708	0.007055	96.840515
0.016269	99.19146	0.007034	96.484756
0.016283	99.211014	0.007001	96.193405
0.016301	99.075516	0.006977	95.909271
0.016293	99.077026	0.006951	95.64595
0.016276	98.944832	0.006938	95.358322
0.016252	98.882736	0.006903	95.016045
0.016261	98.799622	0.006889	94.774918
0.016239	98.783295	0.006877	94.517448
0.016257	98.720673	0.00682	94.209061
0.016227	98.693977	0.006796	93.90789
0.016218	98.568359	0.006741	93.71257
0.0162	98.502373	0.006717	93.39389
0.016233	98.445099	0.006668	93.162155
0.016214	98.456696	0.00662	92.815277
0.016194	98.32901	0.006606	92.56778
0.016212	98.298119	0.006556	92.260574
0.016208	98.16964	0.006507	91.984131
0.016195	98.139229	0.006492	91.689522
0.016176	98.108772	0.006435	91.539406
0.016184	97.985229	0.006402	91.166412
0.016201	97.951546	0.006329	90.913727
0.016177	97.911316	0.006149	90.639206
0.016144	97.755547	0.005853	90.38031
0.016145	97.779594	0.005385	90.12178
0.016141	97.599602	0.00491	89.893967
0.016157	97.575439	0.004504	89.545425
0.016116	97.553413	0.004134	89.303604
0.016118	97.480858	0.003791	89.067116
0.016104	97.386139	0.003473	88.762566
0.016066	97.346291	0.003162	88.521774
0.01603	97.226997	0.002891	88.232018

0.016051	97.093674	0.002657	88.012794
0.016012	97.018562	0.002453	87.75885
0.016019	97.021667	0.002254	87.423576
0.016031	96.845848	0.002093	87.255089
0.015998	96.782822	0.001911	86.916359
0.016022	96.717018	0.001777	86.675041
0.016	96.631012	0.001656	86.387711
0.015973	96.596695	0.001548	86.136093
0.015944	96.500282	0.00148	85.891426
0.015981	96.369514	0.001386	85.616051
0.015969	96.335602	0.001322	85.34259
0.015984	96.231598	0.00129	85.070869
0.01598	96.177826	0.001252	84.833557
0.01598	96.04554	0.001216	84.566811
0.015993	96.04808	0.001175	84.293182
0.015979	95.938828	0.001165	84.038963
0.015925	95.916199	0.001154	83.784431
0.015833	95.733078	0.001144	83.593399
0.015817	95.631813	0.001118	83.262924
0.01581	95.548874	0.001137	82.969452
0.01579	95.456779	0.001112	82.755623
0.015797	95.388412	0.001111	82.535049
0.01575	95.36982	0.001112	82.312935
0.015746	95.282722	0.001126	82.046959
0.015703	95.076637	0.00114	81.711731
0.01571	94.963837	0.001093	81.457771
0.015693	94.916695	0.001076	81.196396
0.015711	94.823936	0.001086	80.917877
0.015708	94.745049	0.001121	80.670486
0.01569	94.649956	0.001125	80.514587
0.015669	94.542419	0.001122	80.26873
0.015653	94.559502	0.001108	79.987038
0.015643	94.444969	0.001097	79.716721
0.015635	94.286438	0.001086	79.420517
0.01559	94.211349	0.001083	79.124825
0.015583	94.10556	0.001058	78.899773
0.01556	93.982414	0.0011	78.645515
0.015541	93.887672	0.001075	78.376106
0.015518	93.784752	0.001062	78.202194
0.015518	93.728798	0.001079	77.900787
0.015471	93.620316	0.001071	77.68454
0.01545	93.532021	0.001083	77.470047
0.015453	93.431557	0.001096	77.131683
0.015436	93.336662	0.001089	76.845207
0.015439	93.209755	0.001116	76.625732
0.015436	93.158623	0.001062	76.326073
0.015453	93.018204	0.001062	76.139725
0.015409	92.930634	0.001097	76.173805
0.015344	92.925346	0.001068	75.802513
0.01533	92.780281	0.0011	75.569183

0.015286	92.64975	0.001105	75.231453
0.015261	92.590134	0.001067	75.033272
0.015246	92.440804	0.001033	74.719322
0.015251	92.400711	0.001062	74.533348
0.015227	92.253395	0.001046	74.292427
0.0152	92.162056	0.001053	73.945435
0.015184	92.083916	0.001056	73.721382
0.01517	92.011292	0.001068	73.509811
0.015119	91.839996	0.001104	73.243439
0.0151	91.758965	0.001115	73.100502
0.01505	91.646698	0.001103	72.735497
0.01499	91.534843	0.001092	72.53231
0.014937	91.491707	0.001076	72.301994
0.014869	91.383354	0.001065	72.030899
0.014808	91.23262	0.001038	71.723251
0.014679	91.121895	0.001013	71.542381
0.014383	91.004639	0.001018	71.246933
0.013788	90.977051	0.000995	71.0839
0.01276	90.818932	0.001028	70.763596
0.01178	90.754951	0.001046	70.544357
0.011311	90.577637	0.001018	70.667709
0.010965	90.47583	0.001046	70.574806
0.010576	90.437393		
0.010152	90.281502		
0.009726	90.154892		
0.009377	90.077339		
0.00918	89.947884		
0.009024	89.84391		
0.00883	89.720299		
0.008649	89.723633		
0.008473	89.531296		
0.008282	89.409805		
0.008072	89.280701		
0.007882	89.278557		
0.00769	89.091667		
0.007519	88.997993		
0.007286	88.885414		
0.007103	88.808609		
0.006926	88.621368		
0.006751	88.506035		
0.006607	88.375801		
0.00644	88.274811		
0.006268	88.172264		
0.006078	88.031883		
0.005953	87.953041		
0.00576	87.806732		
0.005599	87.788643		
0.00545	87.702461		
0.005316	87.536705		
0.005137	87.333664		

0.005027	87.250359		
0.004878	87.151207		
0.004796	86.996231		
0.004654	86.84613		
0.004505	86.9618		
0.004409	86.841759		
0.004291	86.667824		
0.004176	86.523621		
0.004034	86.49456		
0.00397	86.312027		
0.003811	86.156548		
0.003768	86.104836		
0.003662	85.940872		
0.003542	85.790833		
0.003475	85.7621		
0.003385	85.56456		
0.003288	85.490578		
0.003184	85.33168		
0.003105	85.186424		
0.003014	85.090561		
0.002958	84.993073		
0.002867	84.830833		
0.002815	84.715324		
0.00274	84.661728		
0.002697	84.470009		
0.002639	84.384888		
0.002566	84.226387		
0.002541	84.123573		
0.002476	84.01384		
0.002433	83.844818		
0.002381	83.711906		
0.002343	83.666534		
0.002303	83.451454		
0.002235	83.364555		
0.002193	83.223015		
0.002184	83.087029		
0.002146	82.961807		
0.002136	82.815865		
0.002103	82.684273		
0.002087	82.558746		
0.002064	82.431168		
0.002034	82.29216		
0.002028	82.17318		
0.001976	82.037399		
0.001942	81.965164		
0.001934	81.852432		
0.001909	81.646187		
0.001885	81.515984		
0.001884	81.435326		
0.00189	81.274345		

0.001866	81.167419		
0.001894	80.991867		
0.001863	80.865845		
0.001847	80.727211		
0.001829	80.626762		
0.001841	80.491661		
0.001833	80.383652		
0.001818	80.215721		
0.001827	80.017754		
0.001816	80.017395		